CENTRO FEDERAL DE EDUCAÇÃO TECNÓLOGICA DE MINAS GERAIS
Directorate of Research and Postgraduate Studies
Mechanical Engineering Postgraduate Program

MASTER'S THESIS

EDER PEREIRA RESENDE SOARES

INTERNAL COMBUSTION ENGINE NUMERICAL SIMULATION OPERATING WITH GASOHOL (E25) AND PROVIDED WITH A STRATIFIED TORCH IGNITION SYSTEM

Advisor: Prof. Dr. Fernando Antônio Rodrigues Filho

Research line: Energy Efficiency

Belo Horizonte
2024

EDER PEREIRA RESENDE SOARES

INTERNAL COMBUSTION ENGINE NUMERICAL SIMULATION OPERATING WITH GASOHOL (E25) AND PROVIDED WITH A STRATIFIED TORCH IGNITION SYSTEM

Thesis presented to the Graduate Program in Mechanical Engineering from the “Centro Federal de Educação Tecnológica de Minas Gerais" as a partial requirement for obtaining a master’s degree in Mechanical Engineering.

Advisor: Prof. Dr. Fernando Antônio Rodrigues Filho

Research Line: Energy Efficiency

Belo Horizonte
2024

Eder Pereira Resende Soares

INTERNAL COMBUSTION ENGINE NUMERICAL SIMULATION OPERATING WITH GASOHOL (E25) AND PROVIDED WITH A STRATIFIED TORCH IGNITION SYSTEM

Dissertação apresentada ao Programa de Pós-graduação em Engenharia Mecânica do Centro Federal de Educação Tecnológica de Minas Gerais como requisito parcial para a obtenção do título de Mestre em Engenharia Mecânica.

Linha de Pesquisa: Eficiência Energética

Belo Horizonte, 05 / Abril / 2024

Resultado: **APROVADO**

Banca Examinadora:

Prof. Dr. Fernando Antonio Rodrigues Filho - Orientador
CEFET-MG

Prof. Dr. Hélder Giostri Alves de Almeida
IBMEC

Prof. Dr. José Eduardo Mautone Barros
UFMG

Prof. Dr. José Guilherme Coelho Baeta
UFMG

Soares, Eder Pereira Resende
S676i Internal combustion engine numerical simulation operating with gasohol (E25) and provided with a stratified torch ignition system / Eder Pereira Resende Soares. – 2024.
124 f. : il., gráfs., tabs., fotos.

Dissertação apresentada ao Programa de Pós-Graduação em Engenharia Mecânica do Centro Federal de Educação Tecnológica de Minas Gerais.
Orientador: Fernando Antônio Rodrigues Filho.
Banca examinadora: Fernando Antônio Rodrigues Filho, Hélder Giostri Alves de Almeida, José Eduardo Mautone Barros e José Guilherme Coelho Baeta.
Bibliografia: f. 100-103.
Dissertação (mestrado) – Centro Federal de Educação Tecnológica de Minas Gerais.

1. Motores de combustão interna – Teses. 2. Automóveis – Modelos – Teses. 3. Engenharia automotiva – Simulação – Teses. 4. Dinâmica dos fluidos – Teses. I. Rodrigues Filho, Fernando Antônio. II. Centro Federal de Educação Tecnológica de Minas Gerais. III. Título.

CDD 621.43

Elaboração da ficha catalográfica pela bibliotecária Jane Marangon Duarte, CRB 6ª 1592 / Cefet/MG

ACKNOWLEDGMENT

First of all, I thank God for all his blessings, because without Him I can do nothing, and for giving me the opportunity to carry out this work. To Him and my Lord, Jesus Christ, His Son, be all Glory!

To my mother Irenilda Maria Pereira Resende and my father Ivan Resende Soares for always supporting me unconditionally in every way, in good and bad times with a lot of effort. Of everything I achieved, a large portion of the worthiness is theirs.

To my siblings Haniel Pereira Resende Soares and Giovanna Pereira Resende Soares for their companionship and help in many ways.

To my other relatives and friends who have always supported and encouraged me.

To CEFET-MG, of which I was proudly part as a student and as a worker.

To the Graduate Program in Mechanical Engineering and all its professors for providing the facilities, equipment, and knowledge that made this work possible.

Special thanks to CEFET-MG together with Fundação CEFET Minas for acquiring and making available the GT-POWER software, and for providing grants, without which this work would not have been possible.

To the adviser professor and great friend, Dr. Fernando Antônio Rodrigues Filho for the knowledge imparted, for the work guidance, for the many dedicated hours and for providing the experimental data that were essential for the calibration of the models developed in this work.

To the CTM of UFMG for the contributions that, even if for a short period of time, were very important for the accomplishment of this work. Especially to Professor Dr. José Guilherme Coelho Baeta and colleagues in the project I was part of: Augusto, Bárbara, Gabriel, Hiago, Lucas, Mateus, Pedro, Rafael, Wender and Yara.

To my friend and research partner Marcelo Suman Silva Assis for his help and guidance in using GT-POWER software.

Thank you to everyone who in one way or another contributed to the completion of this work.

AGRADECIMENTOS

Agradeço, primeiramente a Deus por todas as suas bênçãos, porque sem Ele nada posso fazer, e por ter me dado a oportunidade de realizar este trabalho. A Ele e ao meu Senhor, Jesus Cristo, Seu filho, seja toda a Glória!

À minha mãe Irenilda Maria Pereira Resende e ao meu pai Ivan Resende Soares por estarem sempre me apoiando incondicionalmente de todas as formas, nos bons e nos maus momentos com muito esforço. De tudo que conquistei, uma grande parcela do mérito é deles.

Aos meus irmãos Haniel Pereira Resende Soares e Giovanna Pereira Resende Soares pelo companheirismo e pela ajuda prestada de muitas formas.

Aos meus demais familiares e amigos que sempre me apoiaram e incentivaram.

Ao CEFET-MG, do qual orgulhosamente fiz parte como aluno e como servidor.

Ao Programa de Pós-graduação em Engenharia Mecânica e a todos seus os docentes pela disponibilização das instalações, equipamentos e conhecimentos que possibilitaram a realização deste trabalho.

Em especial ao CEFET-MG em conjunto com a Fundação CEFET Minas pela aquisição e disponibilização do software GT-POWER, e pelo fornecimento de bolsas, sem os quais a realização deste trabalho não seria possível.

Ao professor orientador, e grande amigo, Dr. Fernando Antônio Rodrigues Filho pelos conhecimentos transmitidos, pela orientação no trabalho, pelas muitas horas dedicadas e pela disponibilização dos dados experimentais que foram fundamentais para a calibração dos modelos desenvolvidos neste trabalho.

Ao CTM da UFMG pelas contribuições que, ainda que por um breve espaço de tempo, foram muito importantes para a realização deste trabalho. Em especial ao professor Dr. José Guilherme Coelho Baeta e aos colegas no projeto do qual fiz parte: Augusto, Bárbara, Gabriel, Hiago, Lucas, Mateus, Pedro, Rafael, Wender e Yara.

Ao meu amigo e companheiro de pesquisa Marcelo Suman Silva Assis pela ajuda e orientação no uso do software GT-POWER.

Agradeço a todos que de alguma maneira contribuíram para a realização deste trabalho.

Whatsoever comes to your hand to do, do it with your might; because there is
no work, no device, or project, or knowledge, or wisdom
in the place of the dead where you go.

Ecclesiastes 9:10

LIST OF FIGURES

LIST OF TABLES

LIST OF ABBREVIATIONS

BL	Baseline
BDC	Bottom Dead Center
BMEP	Mean Effective Shaft Pressure
BSFC	Brake specific fuel consumption
CA	Crank Angle
CO	Carbon Monoxide
CO2	Carbon Dioxide
CoV IMEP	Covariance of IMEP
C_{DE} / DEM	Dilution Effect Multiplier
C_{TFS} / TFSM	Turbulent Flame Speed Multiplier
C_{TLS} / TLSM	Taylor Length Scale Multiplier
C_{FKG} / FKGM	Flame Kernel Growth Multiplier
DI	Direct Injection
EGR	Exchange Gas Recirculation
EV	Electrical Vehicles
FMEP	Mean Effective Friction Pressure
$FMEP_{const}$	Constant pressure term
HC	Hydrocarbons
HRR	Heat Release Rate
IC	Internal Combustion
IMEP	Indicated Mean Effective Pressure
ISFC	Indicated specific fuel consumption
MBF	Mass Burned Fraction
MEP	Mean Effective Pressure
NO	Nitrogen oxide
NO_2	Nitrogen dioxide
NO_X	Nitrogen oxides in General
PC	Pre-Chamber
PCIS	Pre-Chamber Iignition System
P_{ind}	Pressure Indicated
PMEP	Mean Effective Pumping Pressure
SFC	Specific fuel consumption
SI	Spark Ignition
TDC	Top Dead Center

PFI	Port Fuel Injection
TJI	Turbulent Jet Ignition
TPA	Three Pressure Analysis
WOT	Wide Open Throttle

LIST OF SYMBOLS

α	Temperature Exponent
A_e	Surface area at flame front
A/F(r)	Actual air/fuel mass ratio
A/F(s)	Stoichiometric air/fuel mass ratio
B_m	Maximum Laminar Speed
B_ϕ	Laminar Speed Roll of Value
B_S	Average speed factor
β	Pressure Exponent
B	Cylinder bore [m]
$\forall_d$	Displaced volume [m^3]
$\forall_r$	Volume of fluid in the cylinder before combustion [m^3]
f	Engine frequency [rev/s]
h_c	Convective coefficient [w/ m^2.K]
L_i	Integral length scale
λ	Lambda factor
λ_{TML}	Taylor microscale length
M_e	Entrained mass
M_b	Burned mass
μ_u	Unburned zone dynamic viscosity
η_{fi}	Fuel conversion efficiency
ϕ	Mixture leanness
ϕ'	Equivalent ratio
ϕ'_m	Equivalent ratio at Maximum Speed
P	Pressure
$P_{Cyl,\,max}$	Maximum Cylinder Pressure [bar];
P_i	Instantaneous pressure in the cylinder [kPa]
P_m	Fluid pressure in the cylinder in motoring [kPa]
P_{ref}	Reference Pressure (101325 Pa)
ρ_u	Unburned density
P_r	Fluid pressure in the cylinder before combustion [kPa]
R_f	Flame radius
Re_t	Turbulent Reynolds number

S_L	Laminar Flame Speed
$\bar{S}p$	Average piston speed [m/s]
S_T	Turbulent Flame Speed
T	Cylinder temperature [K]
t	Time
τ	Time constant
T_r	Temperature of the fluid in the cylinder before combustion [K]
T_{ref}	Reference Temperature (298 K)
T_u	Unburned gas Temperature
u'	Turbulent intensity
V_{cc}	Volume of the Combustion Chamber [m^3]
V_d	Displaced Volume [m^3]

ABSTRACT

The transport sector currently faces significant challenges related to polluting gas emissions and their environmental impacts. Replacing internal combustion engines with electric propulsion systems is widely promoted as a sustainable solution to address these challenges. However, it is important to highlight that the electricity generation sector is the main responsible for greenhouse gas emissions in the world, being responsible for around 45% of emissions. A complete electrification of the fleet could worsen this situation. One approach to tackling this problem is the development of more efficient and less polluting engines. One of the promising technologies is the pre-chamber ignition system, which can improve the combustion process of internal combustion engines, increasing their fuel conversion efficiency and reducing the emission of polluting gases. In this context, the objective of this work was to analyze the operation of a Ford SIGMA 1.6 engine, with and without ignition pre-chamber, using gasohol (E25) as fuel. For this, one-dimensional numerical simulations were carried out with the GT-POWER software. These simulations allowed the calibration and validation of numerical models, based on experimental data obtained in dynamometric tests. Predictive and non-predictive models were created, which were validated with experimental data and subsequently used to evaluate the performance of the system using the pre-chamber in different operating conditions. The models presented consistent results, with errors of less than 5% in relation to experimental data. The results showed gains in fuel conversion efficiency and, consequently, a reduction in pollutant emissions, in relation to the spark ignition engine. The predictive models created also allowed changing the pre-chamber geometry parameters such as volume and orifice diameter, allowing the study of the influence of these pre-chamber geometric parameters on fuel conversion efficiency. Similarly, the proposed model also allows changing geometric parameters of the engine in order to minimize specific fuel consumption. It was also observed that, although reducing the diameter of the pre-chamber hole produces an increase in power and a reduction in specific fuel consumption, this reduction cannot be done exaggeratedly, as in these cases it can cause opposite effects. worsening engine performance.

Key-words: Internal combustion engine, GT-POWER, predictive simulation, turbulent jet ignition

RESUMO

O setor dos transportes enfrenta atualmente desafios significativos relacionados com as emissões de gases poluentes e os seus impactos ambientais. A substituição de motores de combustão interna por sistemas de propulsão elétrica é amplamente promovida como uma solução sustentável para enfrentar esses desafios. No entanto, é importante destacar que o setor de geração de energia elétrica é o principal responsável pelas emissões de gases de efeito estufa no mundo, sendo responsável por cerca de 45% das emissões. Uma eletrificação completa da frota poderia agravar esta situação. Uma abordagem para enfrentar esse problema é o desenvolvimento de motores mais eficientes e menos poluentes. Uma das tecnologias promissoras é o sistema de ignição por pré-câmara, que pode melhorar o processo de combustão dos motores de combustão interna, aumentando sua eficiência de conversão de combustível e reduzindo a emissão de gases poluentes. Neste contexto, o objetivo deste trabalho foi analisar o funcionamento de um motor Ford SIGMA 1.6, com e sem pré-câmara de ignição, utilizando gasolina (E25) como combustível. Para isso, foram realizadas simulações numéricas unidimensionais com o software GT-POWER. Essas simulações permitiram a calibração e validação de modelos numéricos, a partir de dados experimentais obtidos em testes de bancada dinamométrica. Modelos preditivos e não preditivos foram criados, os quais foram validados com dados experimentais e posteriormente utilizados para avaliar o desempenho do sistema com o uso de pré-câmara em diferentes condições de operação. Os modelos apresentaram resultados consistentes, com erros inferiores a 5% em relação aos dados experimentais. Os resultados evidenciaram ganhos na eficiência de conversão de combustível e, consequentemente, redução na emissão de poluentes, em relação ao motor de ignição por centelha. Os modelos preditivos criados permitiram ainda alterar os parâmetros da geometria da pré-câmara tais como volume e diâmetro de orifício, permitindo o estudo da influência desses parâmetros geométricos da pré-câmara na eficiência de conversão de combustível. Analogamente, o modelo proposto também permitiu alterar parâmetros geométricos do motor visando minimizar o consumo específico de combustível. Observou-se ainda que, apesar de a redução do diâmetros do furo da pré-câmara produz um aumento da potência e redução do consumo específico de combustível, mas que essa redução não pode ser feita de forma exagerada, pois nesses casos pode causar efeitos contrários de piora do desempenho do motor.

Palavras-chave: Motor de combustão, GT-POWER, simulação preditiva, ignição por jato turbulento

CONTENTS

1 INTRODUCTION

The purpose of internal combustion engines is to convert heat into mechanical work. They are widely used by the automotive industry for their robustness and high power-to-weight ratio, and this is clearly evident by the fact that there are about two billion internal combustion engines in use today (HEYWOOD, 2018). Spark-ignition (SI) and diesel engines are significant sources of air pollutants. The spark-ignition engine exhaust gases contain oxides of nitrogen (nitric oxide, NO, and small amounts of nitrogen dioxide, NO_2) collectively known as NO_x, carbon monoxide (CO), and organic compounds, which are unreacted or partially reacted fuel hydrocarbons (HC). (HEYWOOD, 2018). The increase in pollutants released into the atmosphere has generated more and more environmental concerns, and this, combined with the rising cost of fuel, has made it necessary to reduce the amount of pollutants and fuel consumption by internal combustion engines. Different strategies and technologies have been developed to meet these two needs, pre-chamer ignition systems, non-conventional cycles (Miller and Atikson), turbochargers, variable valve timing, direct injection (DI), lean mixtures, controlled auto-ignition (CAI), with special attention for biofuels, (RODRIGUES FILHO et al., 2016) In fact, combustion engines are the biggest consumers of fossil fuels, according to (Reitz et al., 2020) being responsible for consuming about 70% of the fuels derived from petroleum, as can be seen in the Figure 1.1.

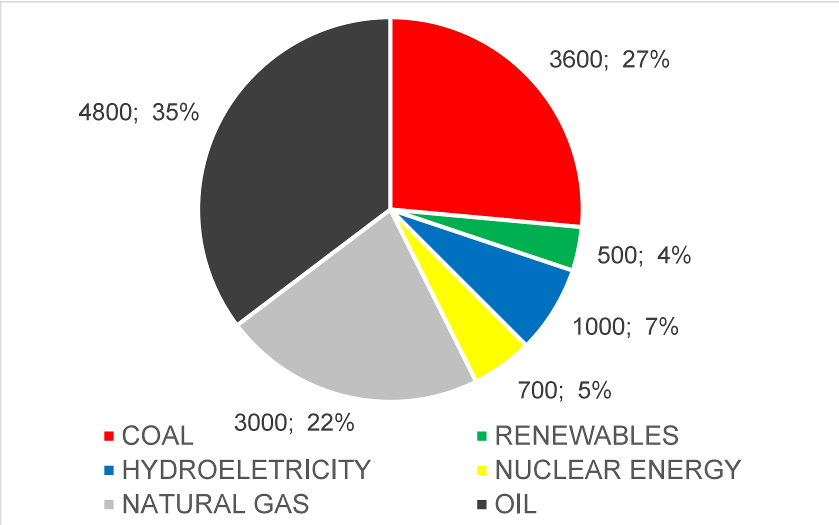

Figure 1.1 – World energy consumption by source (millions of petroleum equivalent) in the last 25 years. Source: Reitz et al., 2020 - Adapted

Regulations of CO_2 emissions and pollutants are becoming more stringent, which increases the interest in technologies that can promote its reduction while increasing fuel conversion efficiency without compromising performance. In order to achieve these goals, studies have been conducted on new spark control systems, advanced combustion technologies, and alternative fuels.(Hua et al., 2020) and (CRUZ et al., 2016a).

The electrification of vehicles is another alternative to replacing petroleum derivatives in the transport sector. As reported by Anfavea (National Association of Automobile Manufacturers), 34,990 electric vehicles (including hybrid-electric versions) were licensed in Brazil in 2021. This number represents 2.15% of the total number of flex-fuel vehicles licensed in 2021 (1,624,348 according to ANFAVEA, 2022). The low market share of electrical vehicles (EV) may be a result of their high price, low autonomy of electric vehicles compared to internal combustion vehicles, and the lack of charging stations in highways and cities associated with the long charging time. Other aspects such as emissions during battery production and the scarcity of noble metals to meet global demand are other obstacles that could prevent electric vehicles from replacing combustion vehicles. (MALAQUIAS, 2019).

The pollutant emissions level due to the use of EV is influenced by the country's energy matrix, with oil as the dominant source in Africa, Europe, and America and coal as the leading source in Asia and the Pacific. (BP GROUP, 2021). The relevance of the transport sector in greenhouse gas emissions can be seen in Figure 1.2. Based on information published by (Reitz et al., 2020) the transport sector contributes about 10% of all greenhouse gases released into the atmosphere, while the energy sector, for example, is responsible for more than 40% of these emissions.

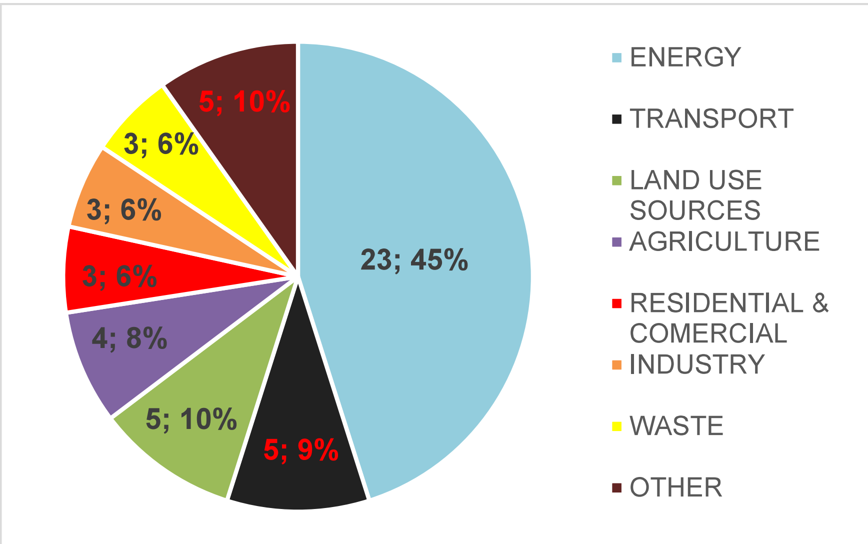

Figure 1.2 - Global warming potential in billion tons of CO_2 equivalent by sector. Source: Reitz et al., 2020 - Adapted

In recent years, internal combustion engines have come under strong criticism, driven by environmental policies and agreements, such as the Kyoto protocol, attributing to them their responsibility for the emission of greenhouse gases (GHG) and the use of non-renewable fuels, characteristics of its use. Among the gases resulting from the combustion process, carbon dioxide (CO2) contributes to the intensification of the greenhouse effect that raises the planet's average temperature, causing climate change. (MALAQUIAS, 2019).

One solution to reducing CO_2 emissions in the transport sector is the use of ethanol as a substitute for fossil fuels as it can be produced from renewable sources. The production of ethanol, like gasoline, emits CO_2 into the atmosphere during the planting of the raw material and the production of the fuel (HILOIDHARI, 2021). However, unlike fossil fuels, during the planting phase sugar cane and other plants used to produce ethanol absorb CO_2 from the atmosphere through photosynthesis and can therefore be considered a clean fuel as it has emissions of CO_2 equivalents close to 0 gCO_2/km when considering the entire ethanol cycle. (EMBRAPA, 2023) and (INMETRO, 2019)

Electrification of the fleet in Brazil, as a solution to reducing greenhouse gas emissions, would require the implementation of an entire new energy distribution infrastructure and vehicle charging points. Furthermore, Brazil has an advantage in the use of biofuels because, in addition to being one of the world's largest ethanol producers, the country also has an entire fuel distribution and sales infrastructure with almost 300 distribution centers and more than 40,000 points of sale. of fuels in which ethanol can be found for sale. (ANP, 2023)

Among the main goals in studying the use of the pre-chamber in internal combustion engines is its potential to reduce specific fuel consumption and emissions, with special attention to nitrogen oxides, due to the lower in-cylinder gas temperature. Pre-chamber ignition system (PCIS) also produces higher heat release and combustion rates, lower engine cyclic variation, extend the lean mixture formation limit and decreases the in-cylinder gas temperature and combustion duration in comparison with traditional engines.

The use of a pre-chamber ignition system (PCIS) produces some desirable effects on the combustion process. The decrease of in-cylinder temperature associated with a shorter combustion duration makes the engine less prone to knock, hence allowing the use of higher compression ratio that contributes to achieve higher fuel conversion efficiency. Due to the turbulence generated by ignition systems with pre-chambers and the consequent homogenization of the air-fuel mixture contained in the main combustion chamber, the use of pre-ignition chambers promotes faster combustion than the traditional spark system if considered the same air-fuel ratio. Chen et. al. (2022) and (ROSO, 2019).

1.1 MAIN GOALS

This work aims at the development, calibration, and validation of 1D mathematical model to evaluate the performance, specific fuel consumption and combustion parameters of Stratified Torch Ignition (STI) Engine fueled with gasohol (E25).

1.2 SPECIFIC OBJECTIVES

To achieve the main goal, the following specific objectives were established:

1 - Obtaining engine data, necessary for building the model.

2 - Construction of a 1D mathematical model in the GT-Power software that represents the combustion system coupled with and without pre-chamber.

3 - Calibration of the simulated the baseline and the STI engine model, based on experimental data.

4 - Engine simulation for different volume and diameter ranges of pre-chamber.

5 - Model validation and Results analysis.

2 LITERATURE REVIEW

In this chapter, the concepts necessary for the development of this work are discussed. This bibliographic review is divided into two parts. In the first part, the basic concepts about the functioning of internal combustion engines are described. The second part presents the state of art of the pre-chamber ignition system (PCIS)

2.1 FUNDAMENTAL CONCEPTS

The fundamental concepts about the internal combustion engines covered include the operation of four-stroke spark ignition engines, the theoretical and real cycles that govern them, the processes of air-fuel mixture formation and the formation of vehicle emissions. In addition, combustion processes and their possible abnormalities are mentioned, providing a concise overview of the principles of the combustion engine.

2.1.1 FOUR STROKE SPARK-IGNITION ENGINES

There are many different types of internal combustion engines. They can be classified by application, basic engine configuration, working cycle, valve location, fuel, method of mixture preparation, method of ignition, and combustion chamber design among other important features. Most vehicular reciprocating engines operate on what is known as the four-stroke cycle. Each cylinder requires four strokes of its piston — two revolutions of the crankshaft — to complete the sequence of events that produces one power stroke. The four-stroke engine was initially described in 1862 by French engineer Alphonse Beau de Rochas but is commonly called the Otto cycle engine, in reference to the German scientist Nikolaus Otto who patented and ran his prototype in 1876. (Heywood, 2018). The operation of this type of motor is illustrated in Figure 2.1.

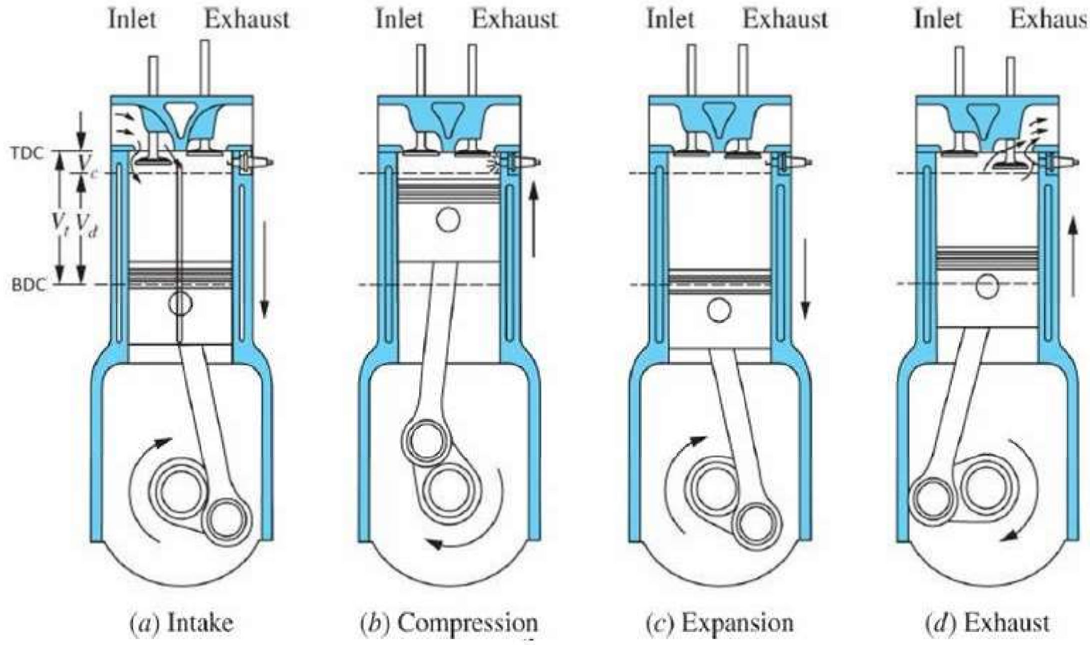

Figure 2.1 - The four-stroke operating cycle. (Heywood, 2018)

(a) An intake stroke, which starts with the piston moving from the top dead center (TDC) toward de bottom dead center (BDC), which draws fresh air or fuel-air mixture into the cylinder. To increase the mass inducted, the inlet valve opens shortly before the stroke starts and closes after it ends.

(b) A compression stroke, which starts with the piston at BDC and ends at TDC, when the mixture inside the cylinder is compressed to a small fraction of its initial volume. Toward the end of the compression stroke, combustion is initiated, and the cylinder pressure rises more rapidly.

(c) A power stroke, or expansion stroke, starts with the piston at TDC and ends at BDC as the high-temperature, high-pressure gases push the piston down and force the crank to rotate. About five times as much work is done on the piston during the power stroke as the piston had to do during compression. As the piston approaches BDC, the exhaust valve opens to initiate the exhaust process and drop the cylinder pressure to close to the exhaust system pressure.

(d) An exhaust stroke, where, as the piston moves from BDC to TDC, the remaining burned gases exit the cylinder: first, because the cylinder pressure may be significantly higher than the exhaust pressure; then as these gases are swept out by the piston as it moves toward TDC. As the piston approaches TDC the inlet valve opens and just after TDC the exhaust valve closes, and the cycle then starts again. (Heywood, 2018)

2.1.2 THEORETICAL AND REAL CYCLES FOR SPARK-IGNITION ENGINES

Theoretical cycles are simplified representations of real cycles, and they are used to represent it more easily and to simplify calculations related to the operation of engines. The theoretical Otto cycle consists of four processes: Isentropic compression, heat-addition at constant volume, isentropic expansion, and heat rejection at constant volume. It is important to notice, that in the theoretical cycles the combustion process is replaced by a heat transfer process at constant volume and the working fluid is air, which behaves like an ideal gas with constant specific heat. Figure 2.2 (a) demonstrates the real PV diagrams (pressure x volume) of an otto engine compared with an theoretical Otto cycle, showed in Figure 2.2 (b).

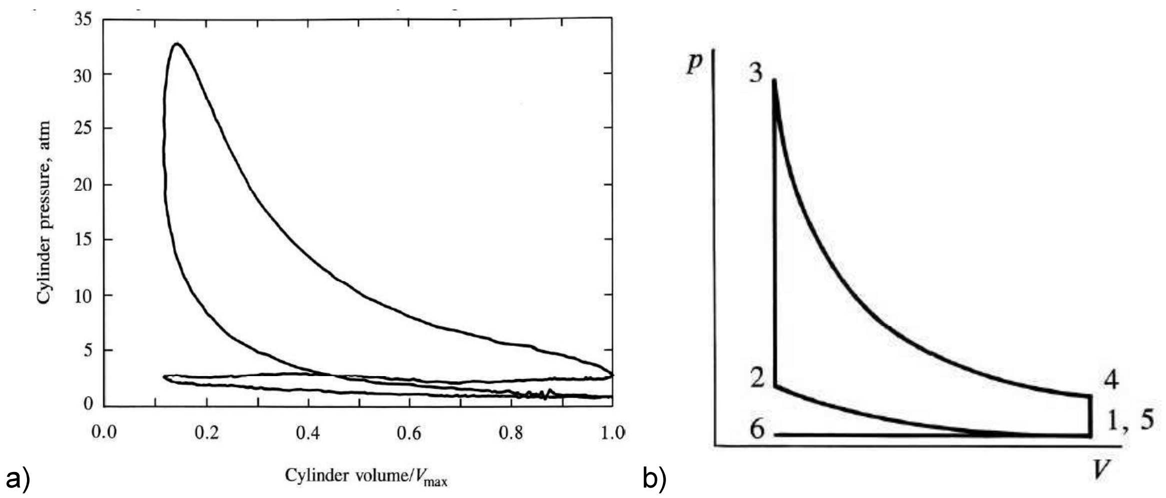

Figure 2.2 – a) Real PV diagram; b) Theoretical Diagram - Adapted from (Heywood, 2018)

2.1.3 FUEL

Fuel is a chemical substance that, when reacting with an oxidant, undergoes a chemical reaction called combustion, in which a certain amount of energy is released in the form of heat. The fuels commonly used in automotive vehicles are gasoline and diesel oil, which are derived from petroleum. Among the alternative fuels to petroleum derivatives, there are alcohols, mainly ethanol and methanol, natural gas, hydrogen, and biodiesel, each with different characteristics that make them better depending on the application. Baeta (2006)

2.1.3.1 ETHANOL

According to Baeta (2006), ethyl alcohol is a chemical compound of the alcohol family with the basic formula C_2H_5OH. Ethanol can be obtained by fermenting vegetables rich in sugars, such as sugarcane in Brazil. Currently, the largest producers and consumers of ethanol in the world are the USA and Brazil. In the USA, ethanol is produced in anhydrous form from corn, being used mainly in the mixture with gasoline up to a percentage of 15% by volume (E15) for vehicles exclusively powered by gasohol. In Brazil, ethanol is produced from sugar cane and is used in two ways. In the form of anhydrous ethanol mixed with gasoline, with percentages of up to 27% in volume (E27). It is also produced on a large scale in the form of hydrated ethanol, containing 96% ethyl alcohol and 4% water by volume, used in multi-fuel vehicles (PETROBRAS, 2021). The main advantages of using ethanol are the fact that it is a renewable fuel that can be obtained from numerous sources, has a high-octane number that results in a high resistance to the occurrence of knock, allowing the use of higher compression ratios, and less pollutant emissions when compared with gasohol. Ethanol also has a high latent heat of vaporization that results in the cooling of the inlet and compression process, in the case of using a PFI injection system, leading the engine to be less prone to knock. The main disadvantages of ethanol are its lower heating value, compared to gasoline, its greater amount of aldehydes in the exhaust gases and might cause greater corrosion in some engine parts and systems. (Sandoval, 2018).

The complete combustion of ethanol reacting with air can be described as shown in the Equation 2.1:

$$C_2H_5OH + 3O_2 + 11{,}28N_2 = 2CO_2 + 3H_2O + 11{,}28N_2 \qquad (2.1)$$

2.1.3.2 GASOLINE

Gasoline is the main fuels used in internal combustion engines applied to light vehicles and is a mixture of compounds, mainly hydrocarbons extracted from petroleum. Its average molecular composition is represented by C8H15, and its molecular weight is equal to 111 kg/kmol. Gasoline can also be represented by the iso-octane hydrocarbon C8H18 since its structural and thermodynamic characteristics are very close to those of gasoline. However, some chemical characteristics of iso-octane are different, such as the octane number, which in gasoline is around 90 and iso-octane is 100, and the air/fuel mass ratio, which for gasoline is around of 14.6:1 and for iso-octane it is 15.1:1. Since the best approximation in terms of octane number and air/fuel mass ratio for gasoline is achieved with C8H15, it was decided to use this hydrocarbon to represent gasoline. Baeta (2006), (RODRIGUES FILHO, 2014).

The complete combustion of gasoline reacting with air can be described as shown in the Equation 2.2:

$$C_8H_{18} + 12{,}5O_2 + 47N_2 = 8CO_2 + 9H_2O + 47N_2 \qquad (2.2)$$

2.1.4 AIR-FUEL MIXTURE

The air/fuel mixture is created by the fuel injection, which can take place directly in the cylinder (DI) or through the intake port (PFI), and which is controlled by the engine injection module through solenoid valves, which controls the injection time and whose activation frequency is dependent on the engine load. There are two types of direct injection systems: low-pressure direct injection, which takes place at the end of the intake stroke, and high-pressure direct injection, which takes place during compression, shortly before the ignition of the mixture of air/fuel. The latter provides the formation of the stratified mixture, which is the spatial variation of the lambda factor in the combustion chamber. When using passive pre-chambers, the fuel injection can be indirect (PFI) or low pressure direct, so that there is enough time for the air to mix with the fuel before ignition, and the resulting mixture can be either rich, stoichiometric, or lean. The mixture is stoichiometric if the amount of oxygen present is equal to the theoretical amount necessary for the complete combustion of the oxidizer, obtaining as a combustion product carbon dioxide (CO_2) water (H_2O) and inert gases present in the intake air. The mixture is considered lean when the amount of fuel is less than that required for stoichiometric combustion and rich when the amount of fuel is greater. So rich mixtures work with a lack of oxygen and lean mixtures with excess. For pure ethanol, for example, the stoichiometric amount of air required for combustion is 9.0 kg of air for every kg of fuel. (RODRIGUES FILHO, 2014). Due to the variation in the composition of the A/F mixture between different engines and in their different regimes, a factor, known as Lambda (λ), is defined, obtained from the ratio between the values of the actual and the stoichiometric air/fuel mass ratio, according to the equation 2.3. (HEYWOOD, 2018).

$$\lambda = \frac{\left({}^{A}/_{F}\right)_r}{\left({}^{A}/_{F}\right)_s} \tag{2.3}$$

λ: lambda factor;
A/F(r): actual air/fuel mass ratio;
A/F(s): stoichiometric air/fuel mass ratio;

The indicated power, the specific fuel consumption (SFC) and emissions of the engines are directly influenced by the lambda factor. As can be seen in Figure 2.3 the maximum power (P_{ind}) occurs with slightly rich mixtures, and the lowest specific consumption point (SFC) is obtained with slightly lean mixtures.

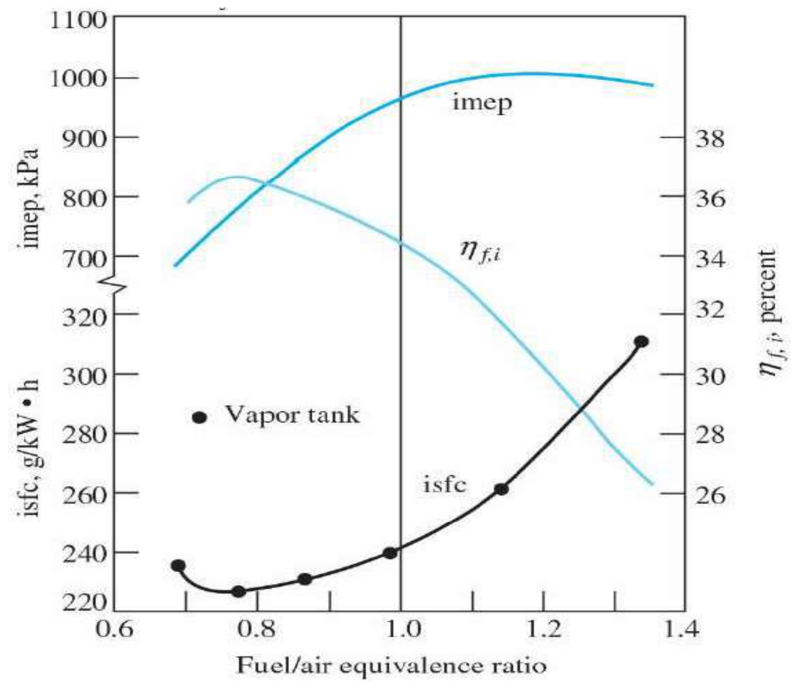

Figure 2.3 - Effect of the fuel/air equivalence ratio on indicated mean effective pressure, specific fuel consumption, and fuel conversion efficiency – (HEYWOOD, 2018).

2.1.5 THE FORMATION OF VEHICULAR EMISSIONS

It has been mentioned before that ideally, combustion produces only carbon dioxide, water vapor, and nitrogen, which would leave the engine inert. However, in practice, engines emit other gases caused by combustion that does not take place in an ideal manner. Thus, the exhaust gases of spark ignition engines contain nitrogen oxides, carbon monoxide and organic compounds, which are mainly hydrocarbons unburned (HEYWOOD, 2018).

As well as the power and consumption of engines, one of the most important variables in pollutant emissions is the lambda factor. As can be seen in the Figure 2.4, for richer mixtures there is an increase in unburned hydrocarbon and carbon monoxide emissions and mixtures closer to stoichiometric tend to provide an increase in nitrogen oxide emissions. For very lean mixtures there is an increase in unburned hydrocarbon emissions.

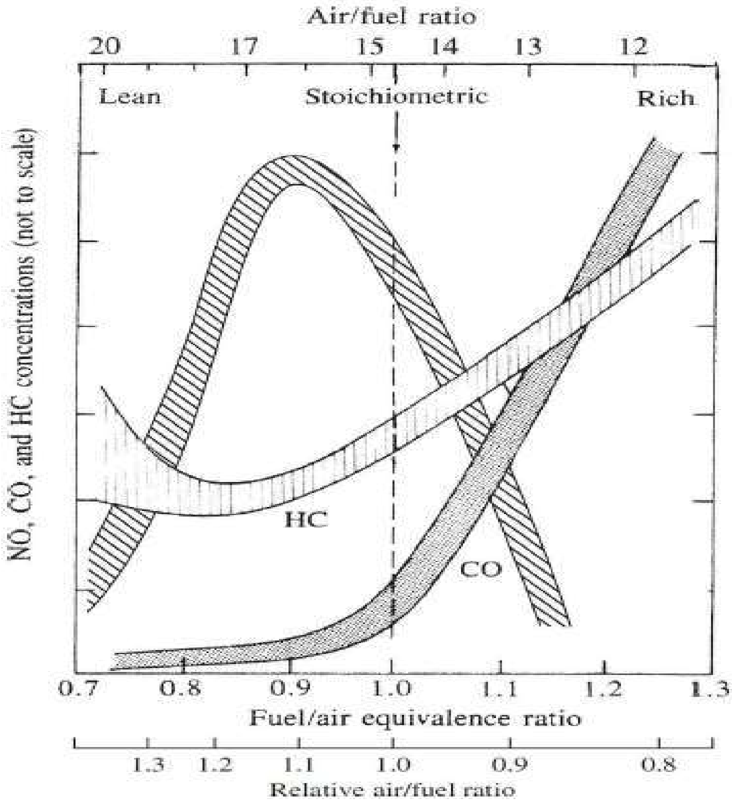

Figure 2.4 – Variation of HC, CO, and NO concentration in the exhaust engine with relative air-fuel ratio and fuel/air equivalence ratio – (HEYWOOD, 2018).

The increase in cylinder pressure forces some of the gas into crevices of small volumes connected to the combustion chamber, volumes between the piston, rings, and cylinder wall. Most of this gas in the crevices is not burned and escapes from the combustion process because the entrance of these slits is too narrow for the entrance of the flame. This un-burned gas, which leaves these crevices during expansion and exhaustion processes, is the main source of hydrocarbon emissions. Another source is the extinction of flames on the walls of the combustion chamber due to low temperatures. An additional source of hydrocarbons is believed to be engine oil left in a thin film on the cylinder liner. This oil layer absorbs and desorbs the hydrocarbon components of the fuel, before and after. combustion respectively, thus allowing a fraction of the fuel to escape primary combustion unburned process. The mechanisms for CO emissions formation are largely similar to those for HC emissions. The main difference lies in the fact that, unlike the hydrocarbons that leave the engine without being burned, carbon dioxide is the product of incomplete combustion of the fuel, either due to lack of sufficient time for combustion or due to the extinction of the flame front. The formation of nitrogen oxides is endothermic and happens mainly because of the high temperatures inside the cylinder. Under these high temperatures and pressures, nitrogen reacts with oxygen molecules to form nitrogen monoxide and nitrogen dioxide. (HEYWOOD, 2018).

2.1.6 COMBUSTION AND ABNORMALITIES OF COMBUSTION

Once the process of admitting the mixture of air and fuel in the internal combustion engines of spark ignition is finished, the upward movement of the piston begins, thus compressing the mixture in the cylinder. Near the end of the compression stroke, the ignition system provides an electrical spark promoting the start of combustion, which generates a flame front that rapidly grows towards the cylinder walls. This electrical spark is provided by a spark plug installed directly in the combustion chamber (SI). (Sandoval, 2018)

In the normal process of combustion on a SI engine, the mixture is ignited by the electrical spark and forms a well-defined flame front. This flame front separates the burned and unburned mixture portion and travels from the spark plug electrodes to the other end of the combustion chamber. If the temperature at any point in the cylinder reaches the ignition temperature value for a sufficient time, abnormal ignition reactions will occur, and they are called surface ignition or self-ignition. Abnormal combustion in SI engines reveals itself in several ways and can occur for different reasons, such as low-quality fuels, very high pressures, higher than normal temperatures or even geometric design parameters and materials of the engine. These abnormal combustion phenomena are worrisome because, when severe, they can cause catastrophic failure of the engine. Nevertheless, even if they are not intense, they are unwanted mainly because of the strong noise generated. Knock is the name given to the noise which is transmitted through the engine structure when spontaneous ignition occurs. (HEYWOOD, 2018). Figure 2.5 shows the in-cylinder pressure with normal combustion (a), occurrence of low-intensity knock and (b), and occurrence of high-intensity knock (c). It is observed that the pressure peak in the second Figure 2.5 (b) is higher and occurs earlier than in the normal engine cycle.

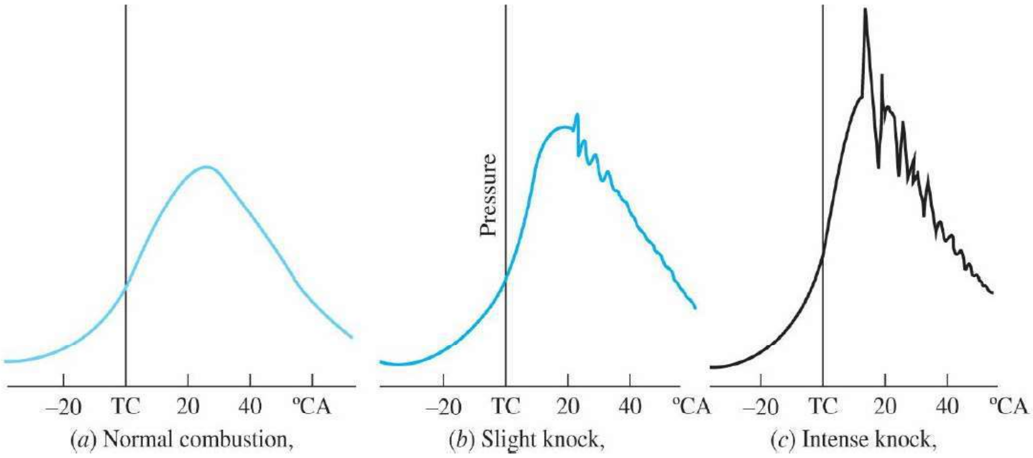

Figure 2.5 – Cylinder with normal combustion (a), low-intensity knock and (b), high-intensity knock (c) – (HEYWOOD, 2018)

2.1.7 ENGINE PERFORMANCE PARAMETERS

The main performance parameters of internal combustion engines are presented below. These parameters are fundamental for evaluating the efficiency and power of an internal combustion engine.

2.1.7.1 MEAN EFFECTIVE PRESSURE

Some parameters are generally used in evaluating the performance of internal combustion engines. Among them, the most common are the power and torque produced by the engine. However, these parameters are very dependent on the size of the engine and, therefore, are not the most suitable for comparing the performance of different engines. Thus, the Mean Effective Pressure (MEP) is a more appropriate parameter to compare engine performance, Specific fuel consumption (SFC) and emissions.

The Mean Effective Pressure (MEP) is an engine performance measure obtained by dividing the work per cycle by the cylinder volume displaced by cycle. This parameter has unity of pressure hypothetical pressure, on PV diagram that would produce the same cycle work if it were kept constant, as shown in Figure 2.6. It is an important engine load parameter, so it is used to compare the performance, emissions, and combustion parameters of different engines.

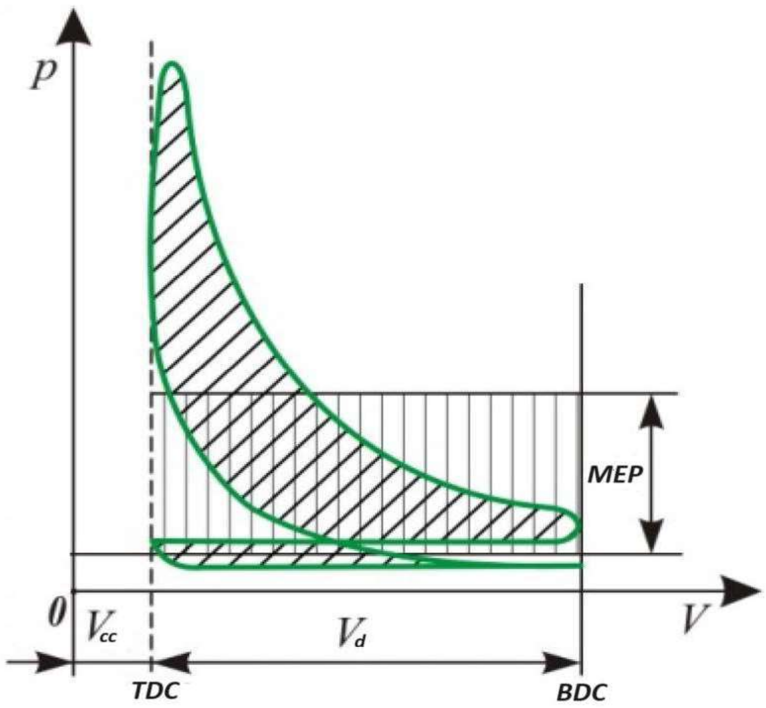

Figure 2.6 – Representation of Engine Mean Effective Pressure. Source: Jankowski and Kowalski, 2015 - (Adapted)

IMEP – Indicated Mean Effective Pressure, considers the cycle work extracted from the from the work fluid inside the cylinder. The IMEP calculation can be done using equation 2.4

$$IMEP = \frac{W_{c,i}}{V_d} \tag{2.4}$$

BMEP – Brake Mean effective pressure, considers the passive engine friction losses, thus relating to shaft work. The BMEP is obtained by subtracting the work related to friction from the work resulting of the working fluid.

PMEP – Pumping Mean Effective Pressure, represents the pumping work performed by the piston in the intake and exhaust processes.

FMEP – Friction Mean Effective Pressure, indicates the friction losses in the engine, and constitutes the average pressure produced in the expansion phase, which would be necessary to have a mechanical friction work produced by the engine per cycle. Thus, these Mean Effective Pressures are related in the Equation 2.5 (HEYWOOD, 2018):

$$\text{IMEP} = \text{FMEP} + \text{PMEP} + \text{BMEP} \tag{2.5}$$

2.1.7.2 ENGINE EFFICIENCY

The mechanical efficiency of an internal combustion engine is determined by the ratio between the shaft work done (W_b) and the work indicated (W_i). This parameter is influenced by pumping work in the intake and exhaust processes, which affects shaft work. Mechanical efficiency is also affected by engine speed and load, as well as by the mechanical design of the components, which can increase losses resulting from friction between moving parts. At low loads, the pumping work is more significant, resulting in lower mechanical efficiency due to higher friction losses. However, as the engine load increases, the indicated power increases more sharply in relation to the friction losses, since the butterfly valve opening increases, reducing the pumping losses. Therefore, there is an increase in the mechanical efficiency of the engine, accompanied by a reduction in specific fuel consumption. The mechanical efficiency is calculated according to the Equation 2.6.

$$\eta_m = \frac{W_b}{W_i} \tag{2.6}$$

The volumetric efficiency of an internal combustion engine is determined by the capacity of the intake system to admit atmospheric air or air/fuel mixture into the cylinder. This parameter is calculated as the ratio between the mass flow rate of air admitted to the cylinder and the volumetric displacement rate produced by the reciprocating movement of the piston. Mechanical components such as air filter, intake duct, butterfly valve, intake manifold and intake valves influence the volumetric efficiency by reducing the mass flow of air due to the pressure drop imposed by the flow in these components. The volumetric efficiency also depends on the reference temperature, the specific mass of the admitted air and the engine speed. The volumetric efficiency of 4-stroke engines is calculated according to the Equation 2.7.

$$\eta_v = \frac{2 \text{ x } 60 \text{ x } m_a}{\rho_a \text{ x } V_d \text{ x N}} \tag{2.7}$$

Where:

m_a = Air mass flow into the cylinder [kg/s];

ρ_a = Specific gravity [kg/m^3];

V_d = Displaced volume in the Cylinder [m^3];

N = Engine rotation [rpm];

The theoretical thermal efficiency of an internal combustion engine is determined by the ratio between the work produced and the heat supplied. Higher compression ratio can increase the thermal efficiency of the engine. The compression ratio C_r is calculated as the ratio between the maximum and minimum volume of the cylinder, which occurs respectively with the piston at the Bottom Dead Center (BDC) and Top Dead Center (TDC). In practice, the increase of the volumetric compression ratio is limited by the appearance of knock, a phenomenon undesirable for combustion in internal combustion engines. The theoretical thermal efficiency is calculated according to the Equation 2.8.

$$\eta_t = 1 - \frac{1}{{C_r}^{\gamma-1}} \tag{2.8}$$

During the combustion process, not all fuel molecules react completely, resulting in a small fraction of unburned or partially oxidized fuel after the flame front has ended. Combustion efficiency is calculated as the ratio between the energy released during the combustion process and the energy supplied in the fuel per cycle. The energy released in combustion is determined by the difference in enthalpy of formation between the products before combustion and the reactants after burning. Fuel conversion efficiency measures the engine's ability to convert fuel energy into brake power (HEYWOOD, 2018). Combustion efficiency is calculated according to the Equation 2.9.

$$\eta_c = \frac{h_p - h_r}{m_f.LHV} \tag{2.9}$$

Where:

h_p = Enthalpy of products [kJ];

h_r = Enthalpy of reactants [kJ];

m_f = Fuel input mass per cycle [kg];

LHV = Lower Heating Value [kJ/kg];

2.1.8 COMBUSTION PARAMERES

In conventional spark ignition engines, ignition is triggered when a minimum portion of the air/fuel mixture reacts after being exposed to an electrical spark, whose temperature varies between 3000 and 6000 ºC. The crucial factor for the initiation of combustion lies not in temperature, but in molecular excitation and ionization. If the ignition energy is insufficient, combustion will not occur, except for a small portion of fuel in direct contact with the electric spark.

Due to the non-instantaneous nature of combustion, but rather its duration over a finite time interval, it begins at the end of the compression time, preceding the moment at which the piston reaches Top Dead Center. Once initiated, combustion propagates through conduction, diffusion, radiation, and convection of heat, resulting in the heating and ignition of the remaining portion of the unburned mixture, as well as an increase in pressure within the combustion chamber.

Thus, the conduction and diffusion of heat from the fresh mixture to the burned mixture plays a crucial role in the combustion process. The flame propagation speed is intrinsically linked to the properties and conditions of the mixture. In the absence of any directed flow within the combustion chamber, the flame front will spread uniformly in all directions, consequently assuming a spherical geometry (RODRIGUES FILHO, 2014); (HEYWOOD, 2018).

Measuring gas pressure in the cylinder in relation to the angular position of the crankshaft, together with calculating the volume available in the cylinder, makes it possible to determine crucial parameters for combustion analysis. Among the prominent combustion parameters are the mass burned fraction (MBF), as seen in the Figure 2.7, the heat release rate (HRR), the IMEP, as mentioned previously, and the covariance of the IMEP (Cov IMEP). The variation in the pressure curve from cycle to cycle is a phenomenon known as cyclic variability, whose quantification is inferred by the IMEP covariance, represented by the ratio between the standard deviation and the mean IMEP. The IMEP covariance serves as an indicator of combustion stability, and it is desirable that its value is less than 3.5% (HEYWOOD, 2018).

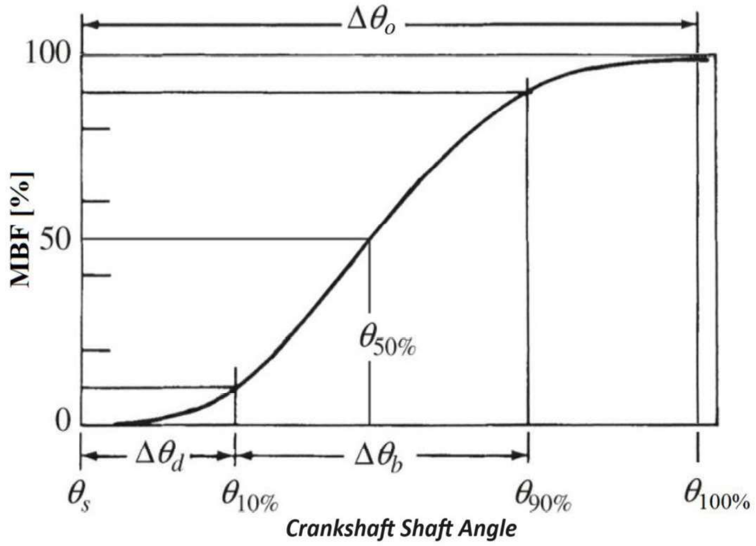

Figure 2.7 – Typical MBF curve of an engine. Source: (HEYWOOD, 2018) (Adapted)

Where:

$\Delta\ \theta_o$ = Angular displacement from zero to 100% of mass burned;

$\Delta\ \theta_b$ = Angular displacement from 10% to 90% of mass burned (MBF 10 - 90);

$\Delta\ \theta_d$ = Angular displacement of 10% of mass burned;

θ_s = Combustion start angle;

$\theta_{10\%}$ = Angle of combustion where 10% of the mass is burned;

$\theta_{50\%}$ = Angle of combustion where 50% of the mass is burned;

$\theta_{90\%}$ = Angle of combustion where 90% of the mass is burned;

$\theta_{100\%}$ = Angle of combustion where 100% of the mass is burned.

The mass burned fraction allows us to analyze important combustion parameters, such as the beginning, speed, and end of combustion, among which the following stand out:

Combustion starts: Due to the enormous variability of the ignition process, the start of combustion is considered when 5% of the fuel mass has been burned, MBF 5. Alternatively, the start of combustion can be considered at MBF 10.

End of combustion: Analogous to the ignition process, the flame extinguishing process is also characterized by high variability. Thus, the end of combustion is considered when 90% of the fuel mass has been consumed, MBF 90.

Burn angle: Called fast burn angle, it corresponds to the angular displacement of the engine during the combustion process, disregarding the initial and final 10% of the burning process. In this way, the fast burn angle is obtained by subtracting MBF10 from MBF 90, being identified by the acronym MBF10-90. The MBF10-90 is an inference of the speed of the combustion process (HEYWOOD, 2018).

2.1.9 PRE-CHAMBER IGNITION SYSTEM

The pre-ignition chamber system consists of using a combustion pre-chamber instead of the conventional spark plug to initiate ignition in the main chamber. In this system, the spark plug, which is installed in the pre-chamber, produces the spark that starts combustion, the flame expands and is then expelled through one or more orifices that connect the pre-chamber and the main chamber. Through these orifices, the combustion products in the pre-chamber are expelled at high speed, causing ignition in the main chamber.

There are two possible types of prechambers: active and passive. In the passive chamber type, the mixture present inside the main chamber is compressed and part of it is admitted into the pre-chamber. A Fuel injection can be done in the intake port (Port Fuel Injection - PFI) or directly into the main chamber (Direct Injection - DI).

In the case of the active pre-chamber there is an injector installed in the pre-chamber and there may or may not be a fuel injector in the main chamber. In this method it is possible to work with a stratified mixture, as it is possible to choose to operate with a rich or stoichiometric mixture in the pre-chamber and a lean mixture in the main chamber, in addition to the possibility of performing multiple injections in the pre-chamber.

There is also another classification of pre-chambers that refer to the speed at which combustion products are expelled through their orifices. The speed of the jet leaving the pre-chamber towards the main chamber can be greater than the speed of sound propagation (supersonic), less (subsonic) or equal (sonic). If the jet is subsonic, the ignition system is then designated as Torch Ignition. When the jet reaches supersonic speeds, the system is called Turbulent Jet Ignition (TJI) or just Jet Ignition. (CRUZ et al., 2016b, HUA et al., 2016b, HUA et al., 2021).

2.2 SIMULATION OF INTERNAL COMBUSTION ENGINES

Simulations on internal combustion engines are a way to study their most important parameters and optimize their design, generating less polluting and more efficient engines. Through one-dimensional modeling we can evaluate engine performance, combustion efficiency and emissions in a simplified way, whether through predictive or non-predictive models.

2.2.1 INITIAL CONSIDERATIONS

One-dimensional modeling in internal combustion engines is a computational approach that allows analyzing the behavior of internal combustion engines performance and combustions parameters, fuel conversion efficiency and emissions by solving the conservation equations of mass, linear momentum, and energy. In this type of simulation, the characteristics of the engine are represented by means of networks of pipes and control volumes, where the equations that describe the behavior thermofluiddynamic of the flow are solved in only one spatial direction. For the discretization of the problem, the entire domain is divided into several volumes, where each discretized unit is represented by a volume and each engine's conduit and tube divided into several volumes, where the scalar quantities are considered uniform within each volume and the vector quantities are given in the limits of the volume. This discretization strategy is called a staggered grid and is illustrated in Figure 2.6.

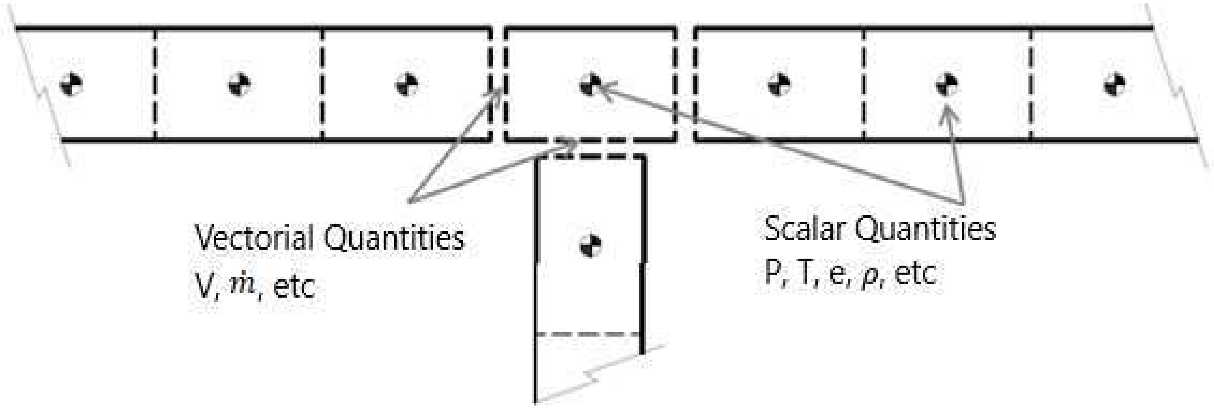

Figure 2.8 – Stepped grid approach in the one-dimensional simulation on *GT-SUITE* Source: Gamma Tecnhologies (2016).

By means of one-dimensional simulations, since the fuel addition data, heat transfer, and friction are accounted for, it is possible to simulate the transport of mass, moment, and energy of all components found in the operation of an engine and also to predict the behavior of thermodynamic cycles and performance. The spatial discretization in the flow direction is due to the numerical modeling of the intake and exhaust ducts, by interconnecting blocks that represent the characteristics of the implemented duct. As stated in the GT-SUITE manual of the GT-Power software, it is indicated as a discretization that the intake ducts are up to 40% of the piston diameter and 55% for the exhaust ducts, due to the influence of temperature and pressure at the speed of sound. For high rotations, above 6000 rpm or for acoustic analysis, the discretization values must be reduced by half. (GAMMA TECHNOLOGIES, 2022).

Combustion process modeling can be characterized by transferring a defined amount of a mixture of unburned fuel and air to a zone of burned gases within the combustion chamber. At each time interval, the air-fuel mixture is transferred from the unburned zone to the burned zone. This mass transfer between these two zones results in the release of chemical energy in the chamber, generating an increase in pressure and temperature inside the combustion chamber.

GT-POWER's combustion models can be predictive or non-predictive. A non-predictive combustion model imposes a combustion rate as the user inputs on the software the in-cylinder pressure curve, obtained previously by means of experiments. In this way, the combustion rate is not affected by factors such as the residual fraction of gases and the ignition time. On the other hand, a predictive combustion model calculates the combustion rate considering the combustion chamber geometry, spark plug location, ignition and injection timing, gas exchange and thermodynamic properties of the fuel. However, it is important to highlight that even predictive models require further validation based on experimental data. In both predictive and non-predictive engine models, when calibrated based on experimental data, it is recommended that model errors be less than 5.0% for all operational cases studied. (GAMMA TECHNOLOGIES, 2022), (SANTOS,2023)

2.2.2 SIMULATION WITH NON-PREDICTIVE MODELS

There are two main models applied for non-predictive simulation of combustion engines in GT Power. These models are the Wiebe combustion model and the Three Pressure Analysis (TPA) model.

The Wiebe combustion model is a non-predictive model used for simulation in SI engines that impose the combustion rate using the Wiebe function, approximating the combustion rate of the simulated case to the typical form of the combustion rate of an SI engine. This combustion model is convenient for cases where the simulation time must be shorter, because instead of using the entire pressure-pressure curve inside the combustion chamber, only combustion rate parameters such as MBF10, MBF50, MBF90, and Wiebe exponent must be provided by the user (GAMMA TECHNOLOGIES, 2016).

Another non-predictive combustion model is the Three Pressure Analysis (TPA), where the burning rate is calculated from three pressures – pressure in the combustion chamber, pressure in the intake, and pressure in the exhaust – This approach requires more detailed information about valves and ports. The methodology for simulating combustion applying the TPA model is given as follows. For the first cycle, any burning rate is assumed, and for subsequent cycles the simulation pauses at the start of each cycle where the burn rate is calculated by applying the in-cylinder conditions for that point, along with the experimentally measured pressure curve. The heat transfer rate is obtained from the result of the previous cycle. The simulation then continues, and the previously calculated burn rate is imposed during the cycle. Finally, the cycles repeat until steady-state convergence is reached. Both methods

– combustion model by Wiebe and *Three Pressure Analysis* – analyze the measured cylinder pressure and automatically generate a burn profile object containing the calculated burn rate. However, if measured cylinder pressures and boundary conditions are available, the TPA model is the recommended method of implementing a nonpredictive combustion model. (GAMMA TECHNOLOGIES, 2022).

2.2.3 SIMULATION WITH PREDICTIVE MODELS

Predictive models increase the complexity of computational calculations, demanding higher computational power and longer simulation time compared to non-predictive models. These combustion models calculate the combustion rate by considering combustion chamber geometry, spark plug location, ignition and injection timing, gas exchange, and thermodynamic properties of the fuel. (GAMMA TECHNOLOGIES, 2016b).

The Spark-Ignition Turbulent Flame Model on GT Power is a predictive model used for simulation in SI engines that calculates the combustion rate based on the cylinder's geometry, spark locations and timing, air motion, and fuel properties. Unless the head and piston have simple dome and cup geometries, it is necessary to set the shape of the combustion chamber. There are four attributes in the model template which should be used for calibration, which are indicated in red in the equations below. These attributes are C_{DE}, C_{TFS}, C_{TLS} and C_{FKG} they are defined in the program according to the Equation2.10 and Equation 2.11 that are presented below. After building the model these four attributes need to be adjusted and calibrated so that the model matches the experimental data. Laminar Flame Speed. The laminar flame speed is calculated by the following equation as mentioned earlier.

$$S_L = \left(B_m + B_\phi(\phi' - \phi'_m)^2\right)\left(\frac{T_u}{T_{ref}}\right)^\alpha \left(\frac{P}{P_{ref}}\right)^\beta f(Dilution) \tag{2.10}$$

$$f(Dilution) = \begin{cases} 1 - 2{,}06(Dilution)^{0{,}77*C_{DE}} & Model\,Version < v\,74 \\ 1 - 0{,}75 * \; C_{DE}\left(1 - (1 - 0{,}75 * \; C_{DE} * Dilution\,)\right)^7 & Model\,Version \geq v\,75 \end{cases} \tag{2.11}$$

Where:

S_L = Laminar Flame Speed [m/s];

B_m = Maximum Laminar Speed [m/s];

B_ϕ = Laminar Speed Roll-of Value [m/s];

ϕ' = Equivalent ratio;

ϕ'_m = Equivalent ratio at Maximum Speed;

T_u = Unburned gas Temperature [K];

T_{ref} = Reference Temperature [298 K];

α = Temperature Exponent;

β = Pressure Exponent;

$Dilution$ = Residual mass fraction in unburned zone.

P = Pressure [kPa];

P_{ref} = Reference Pressure [101325 Pa];

The unburned mixture of fuel and air is entrained into the flame front through the flame area at a rate proportional to the sum of the turbulent and laminar flame speeds. The burn rate is proportional to the amount of unburned mixture behind the flame front, (Me - Mb), divided by a time constant, t. The effects of turbulent intensity and length scale can be modified using the Turbulent Flame Speed Multiplier (C_{TFS}) and Taylor Length Scale Multiplier (C_{TLS}). Additionally, the Flame Kernel Growth Multiplier (C_{FKG}) can be used to adjust the initial growth rate of the flame kernel (GAMMA TECHNOLOGIES, 2022).

$$\frac{dM_e}{d_t} = \rho_u A_e (S_T + S_L) \tag{2.12}$$

$$\frac{dM_b}{d_t} = \frac{(M_e + M_b)}{\tau} \tag{2.13}$$

$$\tau = \frac{\lambda_{TML}}{S_L} \tag{2.14}$$

$$S_T = C_{TFS}\, u' \left(1 - \frac{1}{1 + C_{FKG}\left(\frac{R_f}{L_i}\right)^2} \right) \tag{2.15}$$

$$\lambda_{TML} = \frac{C_{TLS} L_i}{\sqrt{Re_t}} \tag{2.16}$$

$$Re_t = \frac{\rho_u\, u' L_i}{\mu_u} \tag{2.17}$$

Where:

M_e = Entering mass [kg];

M_b = Burned mass [kg];

ρ_u = Unburned density [kg/m^3];

A_e = Surface area at flame front [m^2];

τ = Time constant [s];

t = Time [s];

λ_{TML} = Taylor microscale length;

S_T = Turbulent Flame Speed [m/s];

u' = Turbulent intensity;

R_f = Flame radius [m];

L_i = Integral length scale;

Re_t = Turbulent Reynolds number;

μ_u = Unburned zone dynamic viscosity [N.s/m^2].

2.2.4 HEAT TRANSFER MODELS

Engine operation is characterized by thermal exchanges, being those more significant in the pistons during the compression and combustion strokes, although they also occur during the expansion and discharge strokes. The heat exchange between the combustion gases and the cylinder walls, which at first seems irrelevant, proves to be fundamental for the correct understanding and correlation of the combustion process of internal combustion engines. Because it is an extremely complex and dynamic process, which involves large variations in pressure and temperature inside the cylinder, as well as in the piston speed, one of the best ways to calculate heat exchange in cylinders is by using empirical equations.

The convection heat transfer model used by simulation software for internal combustion engines was developed by WOSCHNI (1967) and, like several other models in the area of heat transfer, it is a model that was obtained empirically through experiments. Therefore, the constants of this equation have been modified over the years to adapt to the evolution of engines and for their implementation in computational codes. The modified Woschni equation applied to the heat transfer model in GT-POWER is called WoschniGT and is given by Equation 2.18.

$$h_c = 3{,}01426 \frac{p^{0{,}8}}{B^{0{,}2} T^{0{,}50}} \left[C_1 \bar{S}_p + C_2 \frac{\forall_d T_r}{P_r \forall_r} (p_i - p_m) \right]^{0{,}8} \qquad (2.18)$$

Where

h_c = Convective coefficient [W/m^2.K];

B = cylinder bore [m];

P = Cylinder pressure [kPa];

P_i = Instantaneous pressure in the cylinder [kPa];

P_m = Fluid pressure in the cylinder in motoring [kPa];

P_r = Fluid pressure in the cylinder before combustion [kPa];

T = Cylinder temperature [K];

T_r = Temperature of the fluid in the cylinder before combustion [K];

$\forall_d$ = Displaced volume [m^3];

$\forall_r$ = Volume of fluid in the cylinder before combustion [m^3];

$\bar{S}$p = Average piston speed [m/s];

Constants C_1 and C_2 are from the WoschiniGT model, with constant C_1 given by Equation 2.19 and constant C_2 equal to 0.00324 for the period of combustion and expansion and 0 for the time of compression, intake and exhaustion.

$$C_1 = 2{,}28 + 3{,}9.Min\left[\frac{\dot{m}}{m_{cyl} \times f}, 1\right] \quad (2.19)$$

Where

$\dot{m}$ = Instantaneous mass flow rate, summed over valves and orifices through which flow is currently entering cylinder [kg/s];

m_{cyl} = Instantaneous cylinder mass [kg].

f = Engine frequency [rev/s].

The heat transfer model used by GT-Power requires input of cylinder wall, piston and head temperatures. As these temperatures were not measured in the experiment, the “default” values suggested by GT-Power were used, being 450K for the cylinder wall, 590K for the piston and 550K for the cylinder head. (GAMMA TECHNOLOGIES, 2022).

2.2.5 FRICTION MODEL

The friction model used in GT Power is based on the friction model proposed by Chen-Flyn, which defines the friction conditions of the moving parts according to the pressure inside the cylinder and is modeled according to Equation 2.20.

$$FMEP = FMEP_{const} + A * P_{Cyl,\,max} + B_S.\, C_{p,\,m} + C_{cp,\,m}{}^2 \tag{2.20}$$

Where:

$FMEP$ = friction mean effective pressure [bar];

$FMEP_{const}$ = constant pressure term, recommended values [0.3 – 0.5bar];

A = Peak pressure factor, recommended values [0.004 – 0.006 dimensionless];

$P_{Cyl,\,max}$ = Maximum Cylinder Pressure [bar];

B_S = Average speed factor, recommended values [0.08 – 0.010 bar/(m/s)];

C = Average speed factor squared, recommended values [0.0006 – 0.0012 bar/(m/s²)];

$C_{p,\,m}$ = Average speed of the cylinder [m/s].

The “A” term influences friction regardless of the load on the cylinder, due to perimeter friction and existing boundary conditions of the sleeve with the piston. The term “B” acts on friction proportional to the average velocity of the piston, representing hydrodynamic friction. The “C” term acts proportionally to the square of the average piston velocity, representing the turbulent dissipation forces. (HEYWOOD, 1988) presents an alternative to Equation 3.1 for SI engines, where the FMEP is calculated for the WOT condition for engines from 845cm³ to 2,000cm³ of volumetric displacement, considering only the rotation N [rpm], given by Equation 2.21.

$$FMEP = 0{,}97 + 0{,}15\left(\frac{N}{1000}\right) + 0{,}005\left(\frac{N}{1000}\right)^2 \tag{2.21}$$

Although it does not directly consider the load, the Equation 2.16 also considers the constant friction, independent of the rotation, the hydrodynamic friction proportional to the average piston speed and the turbulent dissipation proportional to the square of the average piston speed.

Auxiliary losses such as water pumps, radiator fans, etc. can also be combined in the model, although they can be modeled separately if specifically known. There are recommended values in the GT-Power handbook that are suitable for approximating the friction of an engine. However, when possible, the experimental determination of the FMEP for the simulated engine contributes to improve the specified values for the Chen-Flynn model. (GAMMA TECHNOLOGIES, 2022).

2.3 STATE OF ART

This section aims to summarize what is available in the scientific literature, with a focus on pre chamber of Ignition systems and highlighting the impact that the adoption of this ignition system has on the performance parameters of the engine, such as fuel conversion efficiency, specific fuel consumption, in the levels of pollutant emissions (NOx, CO_2, CO, HC) and also in the limit of lean operation and in the propensity to Knock.

2.3.1 INFLUENCE OF PRE-CHAMBER GEOMETRY

The pre-chamber design is one of the most important steps for the good performance of a TJI system in an internal combustion engine. Pre-chamber parameters such as the number of holes, the diameter of the holes, the volume, the ratio between the volume of the pre-chamber and the combustion chamber significantly impact the operation of the TJI and, consequently, the operation of the engine. According to Tang et al. (2022), among the geometric variables of the pre-chambers, the one that has the greatest influence on the operation of the engine and on the parameters of performance is the diameter of the interconnection holes between the pre-chamber and the main chamber. For this reason, most researchers who study the use of pre chambers analyze the influence of this parameter on engine’s performance, either through numerical simulations or in experimental analyses. To help the reader understand this section, the initial part of this section will provide an overview of the work done by several researchers and what results they obtained after varying the diameters and number of holes studied. In the following sections, the other results obtained by them will be shown under the influence of the variation of other parameters, such as the volume of the pre-chamber, the materials used in its manufacture, the air-fuel ratio, the type of fuel used, the loads and engine speeds and the compression ratios adopted.

Were experimentally studied by Zhou et. al. (2022), the effects of different configurations (one-hole, two-hole and three-hole) and diameters of holes (2 to 6mm) in the active pre-chamber. The engine used was the single-cylinder gasoline research engine Ricardo E6, four stroke, with a 3,6 cm^3 prechamber, with represents 7,2% of the main combustion chamber. The compression rate was 10:1. Very small diameters led to flame extinction and, consequently, the main chamber ignition retardation, while very large diameter holes produced low-velocity jets. Thus, the intermediate diameters of 3 to 4 mm were able to increase the peak rate of heat release in order to increase the flame velocity without causing the phenomenon of knock. The inclined triple hole configuration with different diameters showed the best result, as it showed good jet penetration as in the single and vertical hole configuration, but there was also good flame propagation as in the inclined double hole, thus leading to low levels of flame. NOx, lower specific fuel consumption and lambda from 1.4 to 1.7. However, the impoverishment of the mixture causes an increase in the CoV IMEP, which can be seen in Figure 2.7 with the increase in emissions of carbon monoxide and unburned hydrocarbons. The Figure 2.7 show the results of the study with different hole configurations.

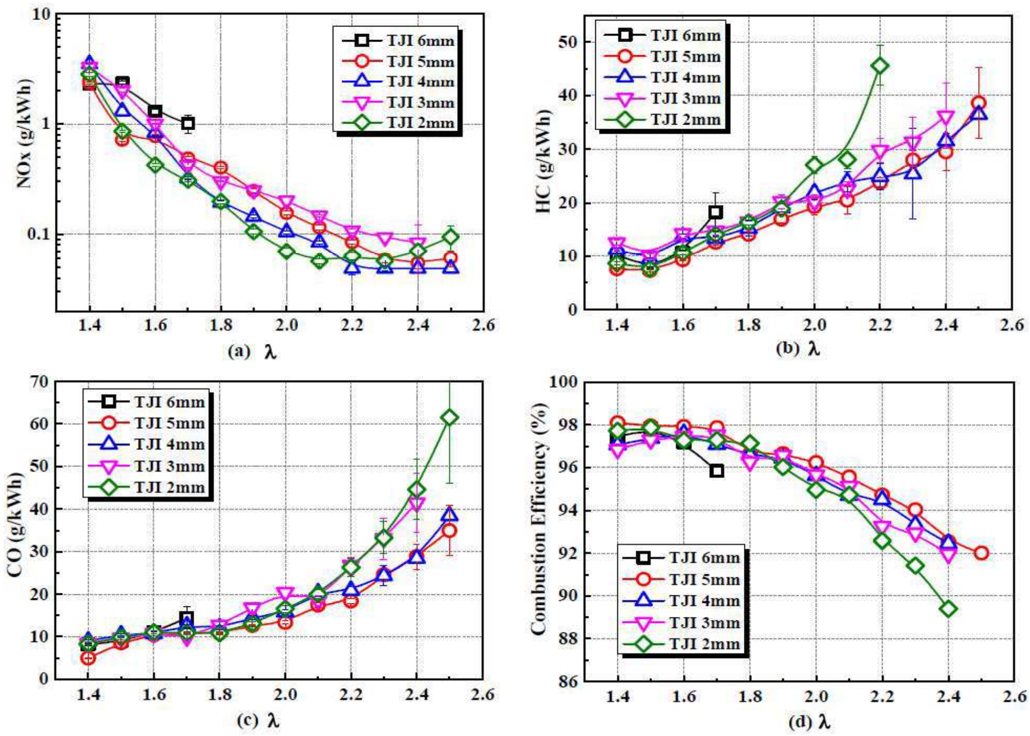

Figure 2.9 – TJI results with different hole configurations under lean-burn conditions. Emissions of: NOx (a), Hydrocarbons (b), CO2 (c) and combustion efficiency (d) Zhou et. al. (2022)

In a study by Chinnathambi et al. (2021), different pre-chamber hole configurations were compared to determine their effects on combustion efficiency. The experimental setup used was a rapid compression machine, where the prechamber is installed in a test section and this section is connecter in a hydraulic and a pneumatic section. Both active and passive pre-chambers were analyzed in this study, and the configurations studied included single holes (1.85 mm and 2.26 mm diameters), double holes (1.57 mm diameters with converging and diverging exit in the main chamber), and a configuration called no hole. The compression ratio used was 11.2, and methane was used as fuel. The results showed that both in the passive and active configurations, the single holes of diameter 1.85 mm and the double-diverging holes resulted in greater penetration and scattering in the main chamber, with the divergent double producing the best results. The combustion rate was measured for the passive pre-chamber, and the holes with the best initiation speeds and complete burning were the single holes and the divergent double. For the active configuration, results varied by hole and system global lambda, with the fastest speeds observed for the diverging holes. It was concluded that the initiation speed depends on the pre-chamber lambda and not on the configuration of the holes, and that the rate of pressure increase does not necessarily indicate combustion efficiency in the passive configuration, but is a reflection of the duration of burning in the main chamber

The study conducted by Qial et al. (2017) aimed to determine the impoverishment limits of a hydrogen gas and air mixture for a TJI system with an active pre-chamber. The study utilized a cylindrical pre-chamber with 101,4 cm^3 and a rectangular main chamber with various nozzle angle configurations and different spark plug positions. The volume ratio between the prechamber and the main chamber is 1:100. The results showed that the impoverishment limits were close, but pre-chambers with multiple holes had greater ability to operate with leaner mixtures, near the flammability limit. The ignition delay in the main chamber was attributed to the distance of the spark from the pre-chamber nozzle, with greater distance generating more turbulent jets and penetration. The best performing configuration (nominated Multi Jet) was the pre-chamber with multiple angled holes and the spark generated by the spark plug in the position furthest from the pre-chamber nozzle. Figure 2.8 shows that the ignition probability was, in general, higher for the multiple-hole configurations.

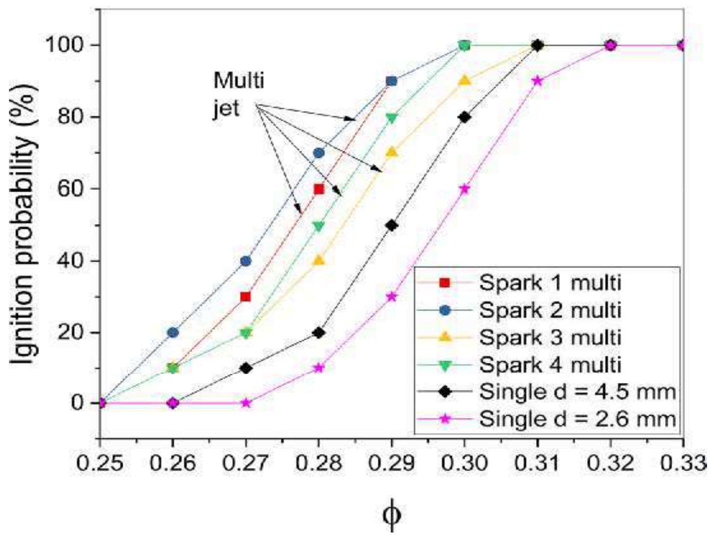

Figure 2.10 - Ignition probability as a function of mixture leanness (ϕ) and pre-chamber settings: Source Qial et al. (2017) ϕ

The effect of geometry in a passive prechamber was studied by Silva et. al. (2020) using the CFD CONVERGE simulation software. A Volvo D13C500 engine was used as a base and the fuel adopted was methane. In the simulation, only one engine cylinder was used, resulting in a total volume of 2.1 L and a compression ratio of 11.5:1. The total volume of the pre-chamber varied from 5.40 to 5.03 cm^3 (6.8% of main chamber volume) due to the variation in the throat diameter An air fuel mixture of $\lambda = 3$ was established for both chambers and the engine speed was 1200 rpm throughout the test. In the study, the diameter of the prechamber throat (from 3.3 to 5.3 mm), the diameter of the holes (from 1.15 to 1.56 mm) and the length of the holes (from 1 to 2 mm) of the pre-chamber were varied, the latter having the least impact on the effective pressure difference and on the time between the extinction of the jet and its re-ignition in the main chamber. The result obtained in relation to the diameter of the holes was a higher pressure peak in the main chamber for the holes of smaller diameter and also higher heat release rate. The study showed also that the configuration with narrow throat emitted three times less CO and two times less OH due to the faster combustion.

Vera-Tudela et al. (2021) conducted a study to analyze the influence of the hole diameter in a TJI engine using pure methane as fuel. The study was conducted in a constant volume combustion chamber, with a volume of 187 cm^3 and a pre-chamber volume of 3.6 cm^3 (1,9% of the main chamber). Xenon lights were placed in transparent areas of the combustion chamber, and high-speed cameras were used to capture images of the flame front. Algorithms in Matlab were used to obtain the flame's position and propagation rate. Pressure and heat release rate were measured with sensors in both the pre-chamber and the main chamber. Prechamber holes of 2 or 4 mm in diameter were used for comparison. The total added heat was the same for both nozzle configuration, and the larger hole produced torch ignition. Was also analyzed the dwell time (time between the fuel injection and the spark) and shorter dwell times resulted in greater turbulence in the pre-chamber, leading to a higher pressure peak in the pre-chamber and a higher flame propagation speed. The study concluded that a higher flame propagation speed resulted in a greater pressure increase in the pre-chamber. The Figure 2.9 shows the results and it can be seen that a smaller orifice diameter restricts the flow of hot gases from the pre-chamber to the main chamber and causes a higher pressure peak inside the pre-chamber (a). This phenomenon results in higher velocities, pressures (a) and higher heat release rate (HRR) in the main combustion chamber (b)

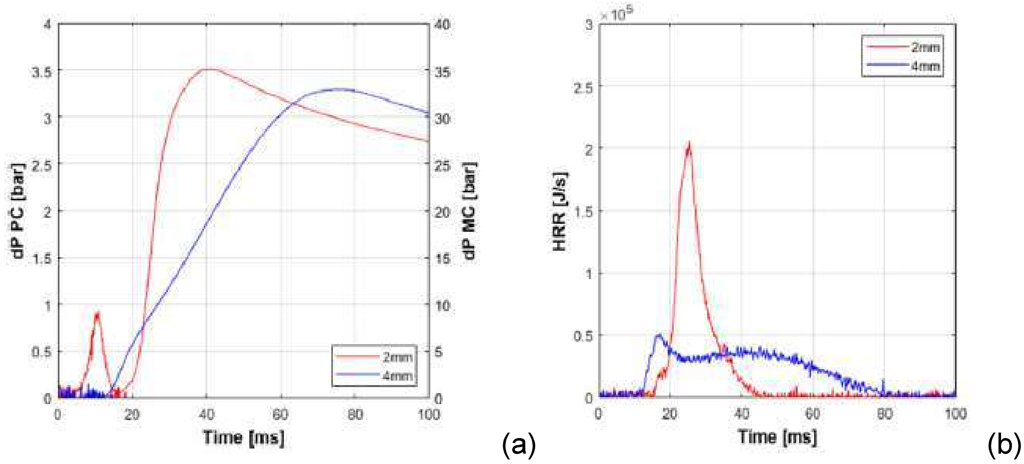

Figure 2.11 – Comparison of pressure in the pre-chamber with the main chamber (a) and heat release rate (HRR) (b) for the cases of nozzle diameters of 2mm and 4mm. Source: Vera-Tudela et. al. (2021)

Hua et al. (2020) and Hua et al. (2021) conducted experiments using a 0.5 L single-cylinder engine with direct injection and a pre-chamber volume of 1.5 cm³ (3% of the main chamber) to investigate the effects of pre-chamber design and ignition method on engine performance and emissions. The engine was operated at 1500 rpm with a compression ratio of 10:1 and inlet pressure of 1 bar. The ignition method and pre-chamber holes were varied, and test conditions were divided into groups with different pre-chamber volumes and numbers of holes. Results showed that pre-chamber volumes and number of holes increased IMEP and reduced fuel consumption and emissions. Dual ignition had the highest IMEP, while the 7-hole pre-chamber had the lowest. The 1-hole pre-chamber had the lowest cyclic variation. The angle of MBF 10-90 was measured, and the order of fastest to slowest burns were: one-hole pre-chamber, 7-hole pre-chamber, dual ignition, and single ignition. For medium loads, dual ignition had lower specific consumption and higher IMEP, followed by one-hole TJI. The single-hole TJI and dual ignition had very low cyclic variability. In the study carried out by Vera-Tudela et. al. (2021), and in the research carried out by Hua et al. (2021) and Onofrio et al. (2021), it was shown that the leaner case presented a higher combustion efficiency in with 80% of the added heat was returned as opposed to only 50% in the case of the stoichiometric mixture, which showed a reduction in fuel consumption of the order of 8%, a decrease of about 92% in NOx emissions, improvements in combustion speed and lower HC emissions.

A study was carried out by Onofrio et al. in an engine Scania D13, 2.1L and six cylinders adapted to work as a SI engine and a TJI engine with a pre-chamber of 2.44% of the main chamber volume. In this study, the engine operating point was 1500 rpm and the PME was of

10 bar 5 bar or 20 bar. The goal was to select an ideal hole-diameter from three options: 1.4 mm, 1.6 mm and 2.0 mm. To study and analyze the combustion, the cylinder pressure and the heat rate release were obtained by a 0-D simulation model. The results showed that the intermediate diameter (1.6 mm) allows a better balance regarding the combustion efficiency, the CoV IMEP, the combustion speed and less emissions of NOx and HC. In the study, it was possible to verify that the relationship between NOx and HC emissions is inverse: as NOx levels decline, HC levels increase, and vice versa. As can be seen on Figure 2.10, using pre-chamber allows working with leaner air/fuel mixture, however very lean mixtures cause lower pressure peaks and lower heat release rates.

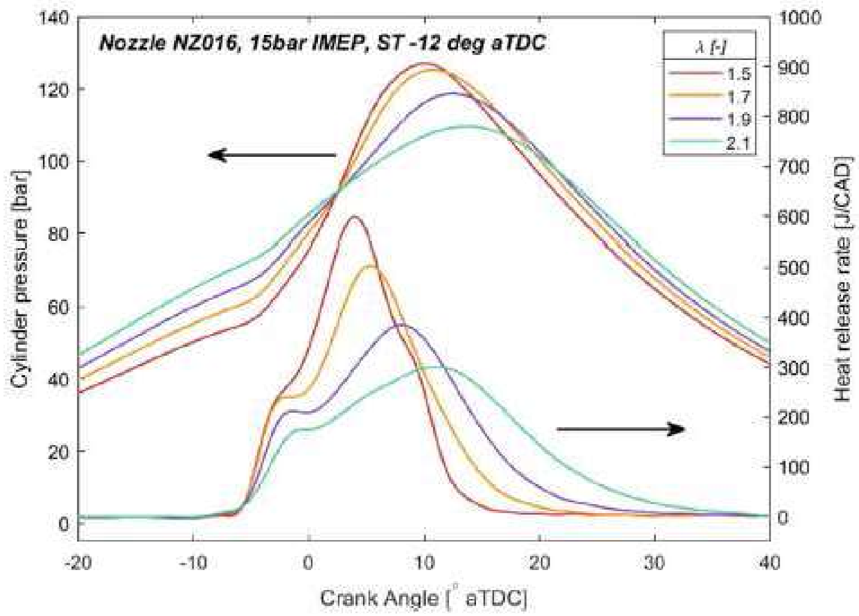

Figure 2.12 - Cylinder Pressure and Heat Rate Release. Source Onofrio et al. (2021)

Benajes et al. (2019) conducted a study on TJI with a passive pre-chamber, with the objective of designing, implementing, and evaluating the pre-chamber to validate a model that can help in the design of such systems. The pre-chamber was installed in a single-cylinder research engine and tests were performed with and without the pre-chamber. The pre-chamber was designed using a 1D Wave Action Model based on the experimental bench and cylinder parameters. The tests were performed at 4500 rpm and 12.5 bar IMEP, which is a medium-high load condition. The pre-chamber was located on top of the cylinder and used indirect injection (PFI), while direct injection (DI) was used when the engine was tested without the pre-chamber (SI). A pre-chamber layout has been added with ducts connecting it to the main chamber, which represent the pre-chamber holes. A heat release rate (HRR) profile generated through the Wiebe function was imposed on the main chamber due to the lack of experimental data at that time. The diameters of the pre-chamber holes ranged from 0.4 mm to 0.9 mm with 6 levels. The volume ranged from 400 mm³ to 1000 mm³ (1.33% to 3.33% of the main chamber) with levels, keeping the number of holes at 6 and the stoichiometric condition. As evaluation criteria, the amount of fuel present in the pre-chamber at the time of combustion and the pressure gradient between the main chamber and the pre-chamber at the time of ejection were used. Two pre-chamber models were chosen, one called pre-chamber 1, with a nozzle diameter of 0.7 mm and a volume of 600 mm³ (2.0% of the main chamber), and another called pre-chamber 2, with a diameter of 0.5 mm and a volume of 900 mm³ (3.0% of the main chamber). Comparing the pre-chambers with the spark-ignition engine, there was a significant increase in maximum pressure, a faster and more stable burn and as a consequence an increase in thermal efficiency. The comparison between the spark ignition engine and the one with the pre-chambers can be seen in Figure 2.11. Comparing the prechambers with 0.7mm against 0.4mm, the first presented a higher peak pressure value and greater tolerance to lambda. This result was attributed to a smaller value of the nozzle diameter, which makes the pre-chamber scavenging process difficult, resulting in a lower mass of fuel available for combustion and higher values of burned gases present in it. In the entire operating range, both pre-chambers present higher values of NOx emissions, which were formed due to the high flame temperatures. In addition, there was no reduction in HC and CO emissions.

A computational evaluation to study the energy conversion and the combustion process of lean mixtures in TJI passive pre-chamber systems was carried out by Benajes et al. (2020). For that, numerical tools were used (0D, 1D and CFD models) previously validated in a four-stroke turbocharged single-cylinder research engine, using gasoline and 13.4:1 compression ratio and stoichiometric lambda, in which analyzes are also performed of methods to verify combustion and energy conversion o in lean mixtures with lambda equal to 2. Different pre-chambers were used in the work, with different amounts (4, 6 and 10 holes), hole diameter (normalized diameters in relation to to the diameter of the first pre-chamber, in the ratios of 0.6; 1 and 1.6), different volumes of pre-chambers (volumes normalized in relation to the volume of the first pre-chamber, in the ratios of 0.7; 1 and 1.3) and the ratio of the pre-chamber area to its volume (1.2 1/m; 2.2 1/m; 3.9 1/m; 4.1 1/m and 4.4 1/m). It is important to emphasize that the values of the diameter of the holes and the volume of the pre-chamber 1 are not mentioned in the work. The first analysis performed is regarding the residual gases that remain in the pre-chamber after combustion. They led to a decrease in the laminar velocity of the generated flame and reduced the tolerance of using external EGR in the system. The cleaning (scavenging) of the pre-chamber is an important point and it was concluded that it is controlled by the force that the piston imposes on the mixture in the compression time of the engine, and if the ratio of area and volume of the pre-chamber is kept constant then the amount of residual gas in it remains constant. It was also found that large pre-chamber volumes combined with small holes worsen the pre-chamber scavenging process.

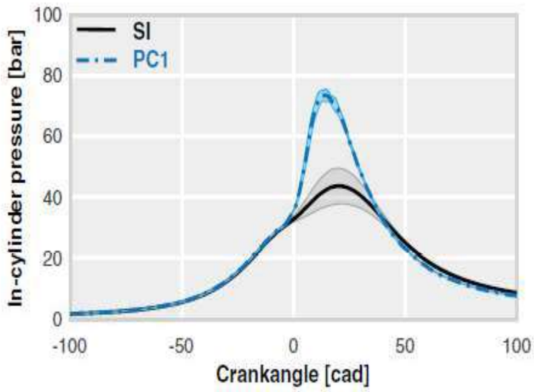

(a)

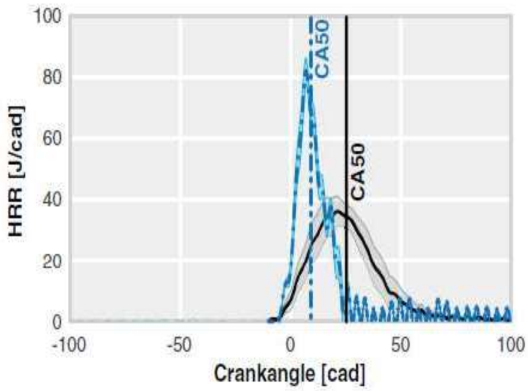

(b)

Figure 2.13 – Comparison of the pressure inside the cylinder (a) and heat release rate (b) of the engine with and without pre-chamber. Source Benajes et al. (2020).

An experimental study carried out by Tang et al. (2022) aimed to apply advanced observation techniques to guide the design and analyze the combustion in a TJI engine with an active pre-chamber. The techniques used were chemiluminescence and simultaneous laser-induced fluorescence (PLIF). The pre-chambers design consists of 3 different geometries, which maintain the orifice area and vary the ratio between the pre-chamber volume and the cylinder volume. In addition, one of the PCs uses a larger throat diameter than the other two (5.3 mm compared to 3.3 mm). The pre-chambers have 12 holes arranged in two different rows (top and bottom). From what was observed by these imaging techniques, it was observed that, in thin-throat pre-chambers, the performance is not so sensitive to the volume of the PC, and those with greater volume present only a greater variation in pressure in the pre-chamber while combustion in the main chamber remains practically the same. Furthermore, as previously mentioned, it was found that the most relevant dimension is the throat diameter, in which a larger diameter presents a slower penetration in addition to producing a smaller peak pressure variation. Finally, different jet characteristics were observed between the lower and upper prechamber columns due to local pressure differences. A pre-chamber with a smaller throat diameter result in a greater pressure gradient between the lower and upper rows of holes.

(Duan et al., 2021) proposed an experimental investigation of Turbulent Jet Ignition different from what is usually found in the literature. According to the authors, other works focus on "optimal points" of operation to demonstrate those predicted by the TJI, including the reduction of fuel consumption and pollutant emissions. In this analysis, the analysis was directed to situations of low load or low engine speed, because these conditions are critical for pre-chamber operation due to a greater tendency to combustion instability. Tests were performed on a 1.5 L turbocharged, direct injection engine with a compression ratio of 11.0:1. The 1.3 mL passive pre-chamber (3% of the volume of the main chamber in TDC) was mounted on the underside of the M8 sail. The PC is made up of four holes, each 1.5 mm in diameter, with a jet angle equal to 140°. An important data from Maserati concerns the thermal conductivity in the pre-chamber, which must be greater than 150 W/m.K to avoid overheating and structural damage to the engine.

The use of pre-chamber provided advancement of combustion phasing by 7.1° CA, reduction of specific fuel consumption by 24 g/kWh accompanied by a slight increase in maximum pressure in the combustion chamber and reduction in abnormal combustion propensity. At 2000 rpm and partial loads (BMEP between 0.8 and 1.6 MPa), the thermal efficiency of the PC equipped engine increased from 0.8 MPa (peak SI: 36.9% at 0.8 MPa; peak PC: 37.5% at 1.2 MPa). Below this BMEP, the pumping and thermal losses were higher. Higher loads improved combustion phasing and fuel consumption. In all BMEPs, the use of a pre-chamber reduced the duration of combustion. At lower loads, there was a slight increase in fuel consumption, higher NOX formation (up to 15%) and less HC formation (up to 36%). At idle, the use of the pre-chamber resulted in the worst combustion stability, as the low temperature prevented the proper propagation of the flame front, even causing its extinguishing in extreme cases. To overcome this negative point, it was found that the delay in injection timing, to a certain extent, minimized the IMEP covariance, although it did not reach the spark ignition threshold.

Several important geometric parameters were studied by Maserati and published in a patent specification document (Maserati, 2019). According to the study, the main objective of adopting the combustion pre-chamber in the engine is not to burn lean mixtures, as in the case of several known systems, but to increase the engine's resistance to knock. The increase in knock resistance, for example in the case of a supercharged engine, allows the engine to be configured with a higher compression ratio by more than 15% compared to a conventional engine. With respect to the holes, they preferably have a diameter of the order of 0.8 to 1.8 mm distributed around the surface of the pre-combustion chamber and may also include a hole concentric with the axis of said pre-chamber. The diameters of 1.8 mm and with concentric hole showed better values of fuel conversion efficiency and a better cleaning process (scavenging) of the burned gases. The axis of each hole is inclined with respect to the axis of the pre-chamber by an angle that can be between 0 and 80 degrees. According to Benajes et al. (2020), the cleaning (scavenging) of the pre-chamber is an important point and it was concluded that it is controlled by the force that the piston imposes on the mixture in the compression time of the engine, and if the area and volume ratio of the prechamber is kept constant then the amount of residual gas in it remains constant. It was also found that large pre-chamber volumes combined with small holes make the cleaning process worse. The reduced volume of the combustion pre-chamber (about 3% of the volume of the main chamber) adopted in the engine according to the invention makes it possible to minimize thermal losses due to the increase in the heat transfer surface. The increase in thermal losses is more than offset by the increase in compression ratio obtained due to the increase in knock resistance.

The pre-chamber volume in the turbulent jet ignition (TJI) process directly impacts the flame propagation velocity and also the knock tendency. Chen et. al. (2022) explored the effects of TJI in a stoichiometric operating regime and a slightly leaner mixture (lambda from 1.0 to 1.2) in a single-cylinder engine with a high compression ratio through optical access, evaluating a pre-chamber of 1805 mm^3 and another of 855 mm^3 (1.7% and 3.7% of the dead volume of the main chamber, respectively). The studies showed that the higher volume passive pre-chamber produced higher peak values of heat release rate (3.6 bar/deg versus 1.4 bar/deg) and higher combustion speed compared to the lower one. However, due to pumping losses and heat dissipation (due to the larger area of the pre-chamber), a lower IMEP value was verified for the pre-chamber of greater volume (6.2 bar against 5.75 bar). Compared to a conventional SI engine, the TJI resulted in lower levels of combustion instability and higher thermal efficiency due to higher flame speed in lean operating regime.

The main information in terms of prechamber geometry, collected from the authors studied, are summarized in Table 2.1. The values indicated after the arrows represent the best values among those studied.

Table 2.1 – Summary of important geometric parameters about the use of pre-chamber of Combustion. Source: Author

NV = Normalized Volume		CR: Compression Ratio			PC: Pre-Chamber		
ND = Normalized Diameter		SFC: Specific Fuel Consumtion			Tested Values → Best Result		
Author	A = Active P = Passive	D. Throat (mm)	D. Holes (mm)	Nº Holes	Vol. PC (cm3)	% Vol. PC	CR
Zhou et al. (2022)	A	...	2, 3, 4, 5, 6 → 3 & 4	1 to 3 → 3	3.6	...	...
Chen et al. (2022)	P	...	1.5	6	0.885, 1.885 → 1.885	1.7, 3.7 → 3.7	13:01
Silva et al. (2020)	P	3.3, 4.3, 5.3 → 5.3	1.15, 1.37, 1.56 → 1.15	12	5.03 to 5.4 → 5.4	around 3.4 %	11.5:1
Hua et al. (2021)	A	...	1.5, 4 → 4	1 to 7 → 1	3.6, 6.0 → 3.6	...	10.0:1
Benajes et al. (2019)	P	...	0.7, 0.5 → 0.7	6	0.6, 0.9 → 0.6	0.140, 0.22 → 0.148	13.4:1
Huan et al. (2021)	P	...	1.5	4	1.3	3	11.0:1
Chinnathambi et al (2021)	A e P	...	1.85, 1.57, 1.26	...	...	2.15	11.2:1
Benajes et al. (2020)	P	...	ND	4, 6, 10	NV	...	13.4:1
Vera-Tudela et al. (2021)	P	...	2 to 4 → 2	1	3.6	1.9	...
Tang et Al. (2021)	A	5.3, 3.3 → 3.3	...	12	...	...	...
Onofrio et al. (2021)	A	...	1,4 to 2 → 1.6	6	4.67	2.4	12.1:1
Hua et al. (2020)	P	...	1.5 to 4 → 4	1, 7 → 1	1.5	0.3	10.0:1
Qial et al. (2017)	A	...	2.6, 4.5, 6.35 → 2.6	1, 3 → 3	101.4	1.0	...
Maserati (2019)	P	...	0,8 to 1.8	...	...	3.0	...

2.3.2 INFLUENCE OF FUEL AND COMPRESSION RATIO

Bureshaid et al. (2019a) and Bureshaid et al. (2019b) carried out experiments on a single-cylinder research engine with optical access with a compression ratio of 8.4:1 to analyze the effects of using hydrated ethanol (E90W10), anhydrous ethanol and gasoline in the TJI system with active pre-chamber and passive and also to determine the levels of pollutant emissions and the combustion process. The experiments were carried out in the fully open throttle valve (WOT) condition and at 1200 rpm. The pre-chamber used has 6 holes of 1.25 mm each and a volume of 1 cm^3, representing 1.27% of the dead volume of the main chamber. The results indicated that ethanol produces less cyclic variability, with a CoV IMEP of 2%, while gasoline obtained a CoV IMEP of 3.5%, both for an injection of 0.3 mg/pulse. As the pre-chamber pressure with ethanol was higher compared to that fueled by gasoline, the propagation distance of the jet between its extinction and reappearance was greater for ethanol compared to gasoline. For the configuration with passive pre-chamber, there was a slight increase in the maximum lambda factor (maximum excess air considering a CoV IMEP of up to 5%) for all fuels. Compared to the SI system, the TJI system with passive pre-chamber enabled an increase in lambda from 1.1 to 1.2 by injecting gasoline into the main chamber. For anhydrous ethanol, lambda increased from 1.25 to 1.35 and for hydrated ethanol the variation was from 1.25 to 1.3. These increases can be explained by the combustion at multiple points and by the increase in combustion speed provided by the TJI system. For the configuration with active pre-chamber, it was found that NOx emissions were reduced with increasing lambda due to lower combustion temperature, with gasoline being the fuel that produced the highest NOx emission, followed by hydrated ethanol and anhydrous ethanol. In the case of HC emissions, anhydrous ethanol produced lower emission values in the entire lambda range (1.2 to 2.2). For lambda of 1.2, anhydrous ethanol resulted in 360 ppm of HC emissions, which is lower than that of hydrated ethanol (415 ppm) and gasoline (490 ppm). This lower value was due to the higher flame speed and shorter duration of combustion produced by anhydrous ethanol.

A survey was carried out by Kheyrollahi et al. (2021) regarding the influence of the compression ratio in a 0.662 L four-cylinder engine equipped with a combustion pre-chamber, engine speed of 1500 rpm and three compression ratios were used: 11.5, 13.5 and 16. The engine load varied between the values of 25%, 50%, 75%, 94% and 100%. The results showed that the lean limit of the mixture increased at all engine loads when the pre-chamber was used. It was still possible to verify that the temperature of the exhaust gases decreased with the increase of the compression ratio, as can be seen in Figure 2.12. According to the authors, this phenomenon occurs as a result of the shorter ignition delays and duration of combustion and the significantly leaner mixture, which results in better thermal efficiency as heat losses decrease. In addition, the CoV was reduced by up to 1% with the use of the pre-chamber, while the thermal efficiency and the specific fuel consumption improved by up to 9% and 11%, respectively, with the help of an increase in the compression ratio. In this same scenario, with regard to pollutant emissions, it was possible to verify that there was a reduction in CO levels at all engine loads, while NOx levels reduced especially at low loads.

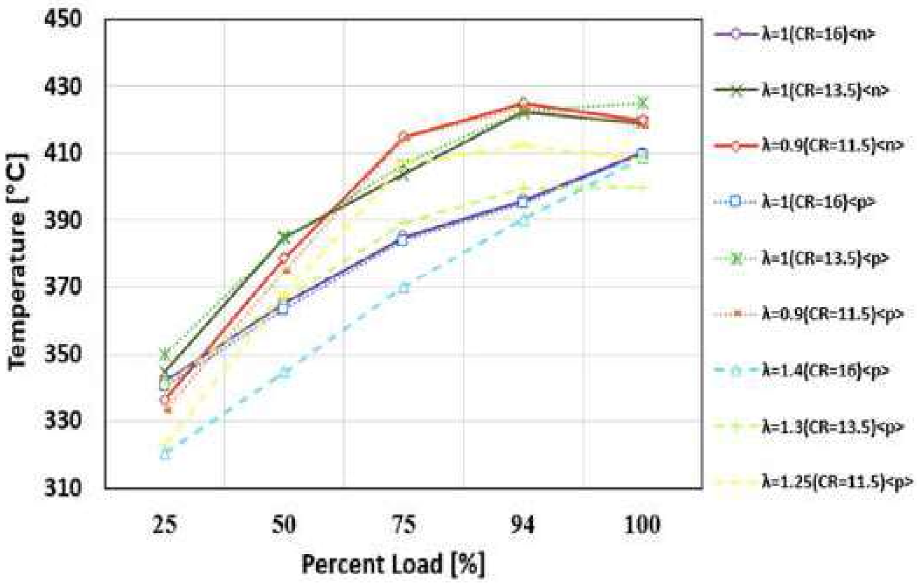

Figure 2.14 – Exhaust gas temperature as a function of load, compression ratio and lambda factor. Source Kheirollahi et al. (2021)

Sens and Binder (2019) studied the use of passive and active pre-chamber compared to conventional SI engines. The experiments were carried out in a single-cylinder research engine at 1500 rpm and 2000 rpm, 6 bar and 16 bar BMEP, 0.9 to 2.2 lambda and with a compression ratio of 10:1 and 12:1. The results showed that the use of the passive pre-chamber produced a reduction in combustion duration of up to 30% compared to the SI system, with the peak of heat release being advanced by about 5° CA. In addition, increasing the compression ratio from 10:1 to 12:1 reduced specific fuel consumption by up to 1.2% at 200 rpm and 16 bar BMEP and 3.2% at 1500 rpm. and 6 bar BMEP. These decreases in specific consumption are explained by the decrease in combustion duration and by the advance of the release peak, factors that compensate for the greater heat loss to the walls in the pre-chamber system, compared to the SI engine.

2.3.3 FINAL CONSIDERATIONS ON THE LITERATURE REVIEW

Regarding the diameter of the pre-chamber hole, Zhou et al. (2022) found that very small and very large diameters led to problems, but intermediate diameters of 2 to 4 mm improved peak heat release rate and flame velocity without causing knock. In their study, a smaller diameter of 1.85 mm resulted in greater penetration and flame spread in the main chamber. Silva et al. (2020) found that smaller diameter holes (1.15 to 1.56 mm) produced higher pressure peaks in the main chamber. Vera-Tudela et al. (2021) verified that a 4 mm diameter hole in the passive pre-chamber was unable to extinguish the flame. Onofrio et al. (2021) studied the influence of pre-chamber hole diameter on efficiency, CoV IMEP, speed of combustion, and emissions. They found that an intermediate diameter of 1.6 mm and a lambda of approximately 1.7 provided a better balance of these factors. Thus, it can be concluded from these studies that smaller hole diameters produce greater penetration and flame spread with consequent higher peak pressure in the main chamber. Also, larger diameters are not able to extinguish the TJI jet as it passes through the pre-chamber holes, which causes greater engine heating and can lead to self-ignition and other problems due to overheating.

The performance of pre-chamber holes is influenced by their orientation and arrangement. Multiple holes more effectively distribute the turbulent jet in the main chamber, increasing the combustion rate. The inclined triple hole configuration with different diameters shows the best result. Diverging holes in the pre-chamber produce higher jet velocities, penetration, and scattering in the main chamber. The probability of ignition in lean mixtures is higher in pre-chambers with multiple angled holes. Residual gases remaining in the pre-chamber after combustion lead to decreased flame velocity and reduced tolerance of external EGR use. The cleaning of the pre-chamber is important and is influenced by the force the piston imposes on the mixture and the number and arrangement of holes. A small number of holes or holes with narrow diameters make cleaning the pre-chamber difficult.

Choosing the type of fuel used in the TJI system is also a topic of important analysis. Bureshaid et al. (2019a) found that hydrated ethanol produces lower cyclic variability compared to gasoline. As the pre-chamber pressure with ethanol was higher compared to that fueled by gasoline, the propagation distance of the jet between its extinction and reappearance was greater for ethanol compared to gasoline. Bureshaid et al. (2019b) concluded that in relation to the impoverishment threshold (with CoV IMEP of up to 5%), anhydrous ethanol provided an increase in lambda from 1.25 to 1.35 and for hydrated ethanol the variation was from 1.25 to 1 .3 compared to gasoline. For lambda of 1.2, anhydrous ethanol resulted in 360 ppm of HC emissions, which is lower than that of hydrated ethanol (415 ppm) and gasoline (490 ppm). This lower value was due to the higher flame speed and shorter duration of combustion produced by anhydrous ethanol.

3 METHODOLOGY

This chapter aims to present the technical specifications of the engine, the computational models created, the calibration and validation of the 1D mathematical models developed in GT-Power and the experimental operational points considered for analysis of performance and combustion parameters.

3.1 SIMULATED ENGINE DATA

The engine used for the creation of the model in the GT-POWER software was the Ford Sigma 1.6 16V four-stroke and four-cylinder in-line, represented by Figure 3.1. Engine performance was characterized for IMEP [bar], specific fuel consumption (BSFC), [g/kWh]. Torque [N.m], power [kW] and air and fuel flow were also analyzed and are presented in annex 2. The most important characteristics of the engine are presented in Table 3.1. The environmental conditions during the experimental tests, which serve as a reference for the simulations, were a temperature of 27 °C and an absolute pressure of 0.92 bar, and the fuel used was E25 gasohol.

The ratio between the volumes of the main chamber and the pre-chamber of 7.3%. This volumetric fraction corresponds to a volume of 2.912 cm^3 or the volume of the pre-chamber to be used in the Ford Sigma 1.6 16V engine. The interconnection holes between the pre-chamber and the main chamber must have a minimum diameter, so that the flame does not extinguish when passing through its interior. Various configurations regarding the arrangement and number of interconnecting holes can be used. For cases of more than one interconnection hole, the diameter of the equivalent holes can be calculated, depending on the cross-sectional area and wetted perimeter. For this work, an interconnection configuration equipped with one central hole of 6 millimeters was adopted as used by Rodrigues Filho, 2014. The Table 3.1 shows the motor data used in this work.

All experimental data cited and used in this work to calibrate the mathematical models were obtained from Rodrigues Filho, 2014. The scope of this work was limited to mathematical modeling.

Figure 3.1 – Ford Sigma Engine 1.6 16V (Source: Avelar 2018)

Table 3.1 - Used Engine data - Source: (Rodrigues Filho, 2014). Adapted

Displacement	1596 cm³
Number of cylinders:	4 in Line
Valves per cylinder	4 Valves
Weight	76 kg
Block, cylinder head, pistons and crankcase material	Aluminum
Bore x Stroke	79 x 81,4 mm
Compression ratio:	11:1
Intake Valve Lift	7.55mm
Eexhaust Valve Lift	6.35mm
Intake Valve Diameter	30.1mm
Exhaust Valve Diameter	24.1mm
Maximum power	Gasohol: 110 cv / 6250 rpm; Ethanol: 115 cv / 5500 rpm
Maximum torque	Gasohol: 154,9 kgfm / 4250 rpm Ethanol: 158,8 kgfm / 4250 rpm

3.1.2 GEOMETRIC DATA OF ENGINE AIR DUCTS

The dimensional geometric data of the engine intake and exhaust manifolds, which serve as input for the creation of the model, are presented in the Table 3.2.

Table 3.2 - Engine's geometric data (Source: Avelar 2018. Adapted)

Part	Diameter	Length	Material
Intake Manifold	69mm	210mm	Plastic
Intake Manifold - Plenum	90mm	365mm	Plastic
Intake Manifold - Primary	40mm	230mm	Plastic
Exhaust Manifold - Primary	40mm	200mm	Steel
Discharge Collector	42mm	3800mm	Steel

3.1.3 VALVE OPENING CURVE

The lifting curve of the intake and exhaust valves as a function of the angular position of the engine shaft is shown in the figure Figure 3.2. The zero in the figure corresponds to the compression top dead center of cylinder 1.

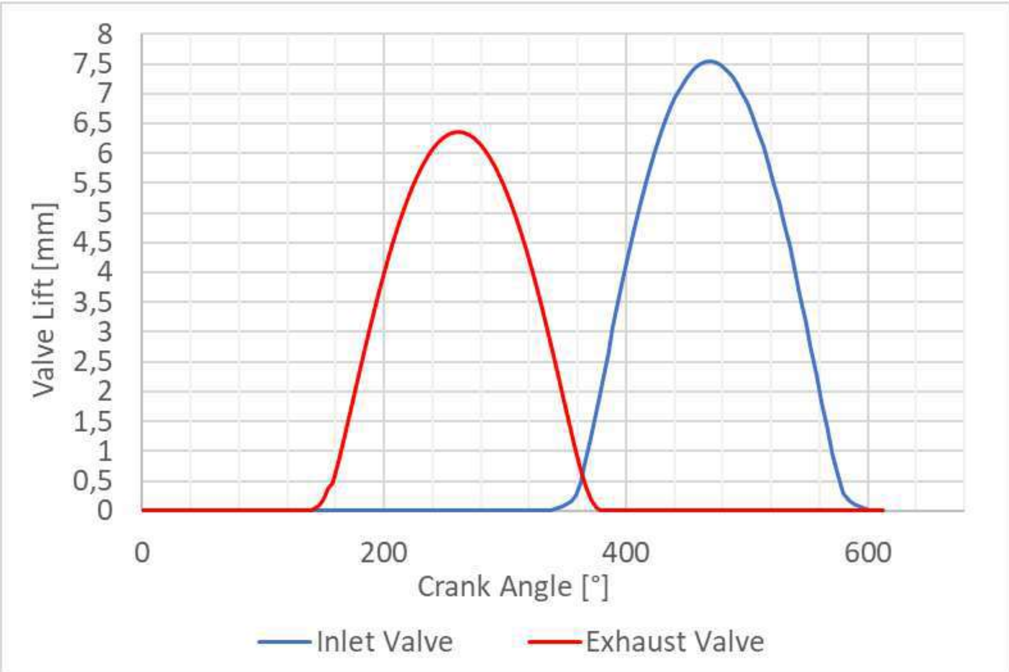

Figure 3.2 - Valve lifting curve. (Source: Avelar, 2018. Adapted)

3.2 ANALYZED OPERATION POINTS

The engine's operating points that were simulated are shown in the Table 3.3. For each lambda value at a constant speed of 2500 rpm, four different engine loads were simulated. The first line of the Table 3.3 refers to the baseline engine, without the pre-chamber, and the remaining lines refer to engine data using the pre-chamber.

Table 3.3 - Simulated operating points. Source: Author

2500 rpm			
Lambda - λ	28 - IMEP [bar]	38 - IMEP [bar]	47 - IMEP [bar]
1.0 - (Baseline)	3.66	5.19	6.17
1.0 - (Torch)	4.45	5.42	-
1.1 - (Torch)	4.23	5.65	-
1.2 - (Torch)	4.52	5.79	-
1.3 - (Torch)	4.13	5.54	-

3.3 CALIBRATION METHODOLOGY

Numerical model calibration should be performed using experimental data to minimize mismatch with numerical results. For these adjustments, some multipliers of the flow, friction in mechanical parts and heat transfer functions can be used to obtain a correlation between the models. The greater the amount of experimentally measured data, the better the adjustments obtained. To calibrate the model in terms of performance, were used the specific fuel consumption (SFC) and indicated mean effective pressure (IMEP), as well as torque, power, air, and fuel mas flow [kg/h] were also analyzed.

The complete geometry of the intake and exhaust ducts, engine cylinder and engine valve lifts were implemented, as well as combustion data acquired in the TPA Model, such as the burn rate by Wiebe exponents, the MBF 50, the MBF 10-90 and the fraction of fuel burned. In Figure 3.3, the blocks used in GT-Power for engine modeling can be seen.

3.4 MODELS CREATED IN GT POWER

In this work, two types of models were created: predictive and non-predictive. Finally, in the predictive models some geometric changes were made. These templates are described in this section.

The models were created and drawn manually in the GT Power interface itself, where the software provides standardized templates for all sections and components of the engine, and based on their dimensions and characteristics, the models that best represent the engine studied were created.

3.4.1 NON-PREDICTIVE MODEL WITHOUT PRE-CHAMBER

Based on the geometric data of the engine and intake and discharge ducts, as well as roughness and transfer characteristics of heat from the materials of these parts, the first model of the engine was built. This first model is based on the baseline spark ignition engine without pre-chamber. The Figure 3.3 shows this first model that was developed in the software.

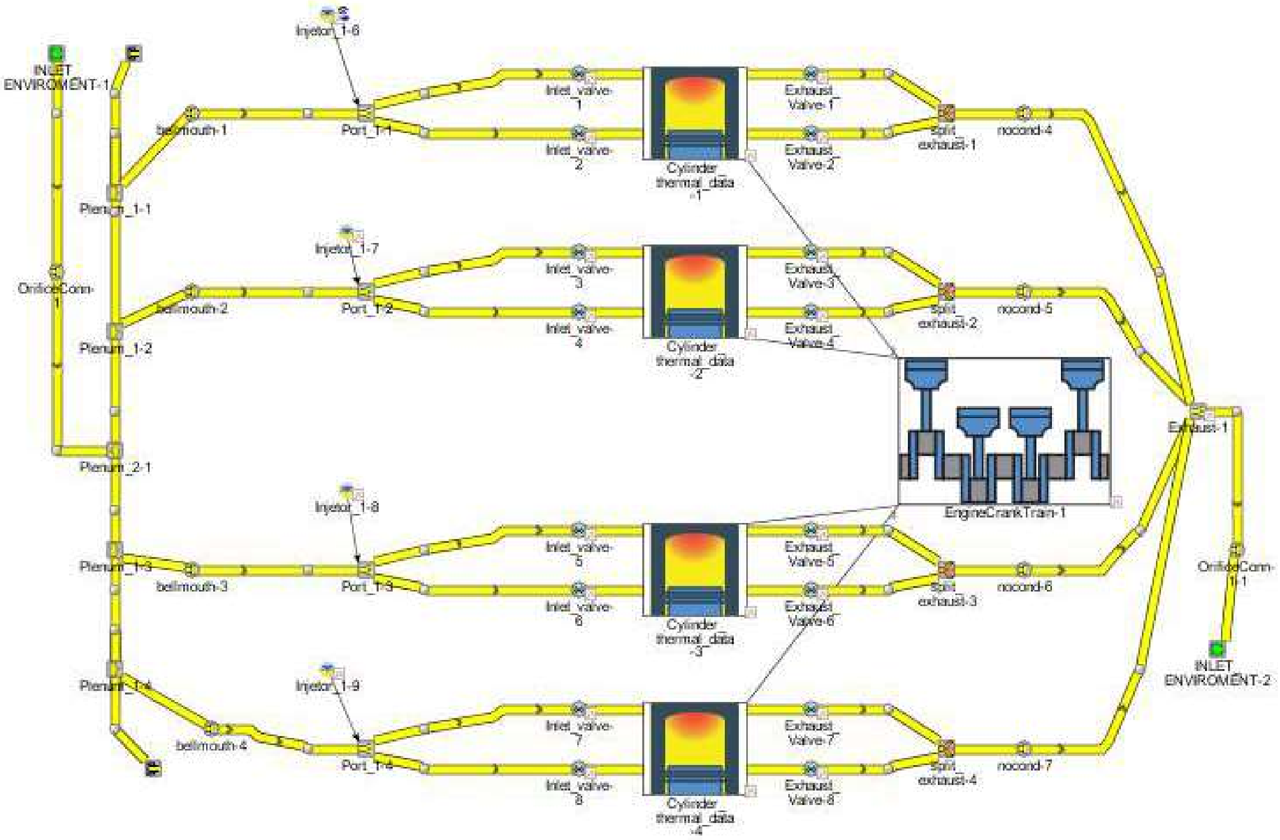

Figure 3.3 – Non-predictive model without pre-chamber. Source: Author

Based on experimental data, combustion was modeled in a non-predictive way. After that, the model must go through the calibration step, where the mass and fuel airflow rate, and injection timing are iteratively calibrated so the simulation will only converge if the simulated data reaches the measured results with a maximum tolerance of 5%. Figure 3.4 schematically represents the calibration process. It is calibration methodology was the same used for the adjustment of all other built models.

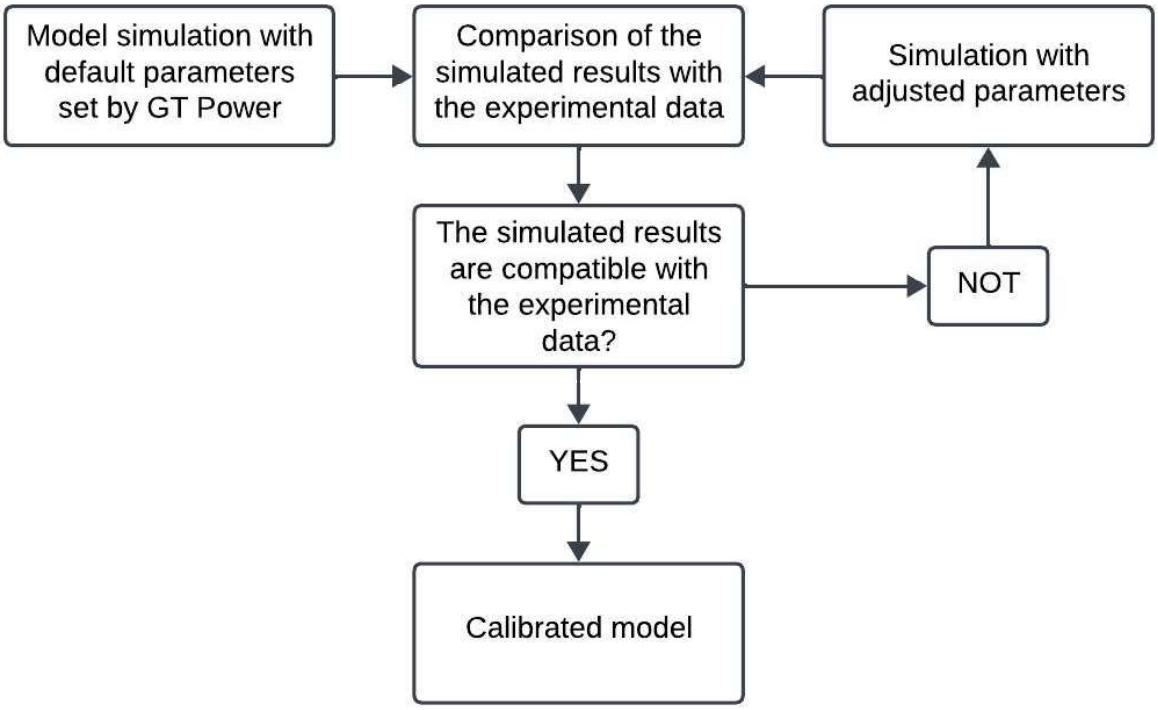

Figure 3.4 - Calibration process of simulated models. Source: Author

Due to the simplifications necessary for the implementation of the model and adequacy of the materials available in the library, multiplier coefficients that act in the calculation of friction and heat transfer from the fluid to the wall are available to adapt the model to the actual conditions observed. As these equations used in computational models come from empirical models, these multipliers are a way for the model to be adjusted, within certain ranges, to new experimental data entered by the. These calibrated multipliers are shown in the Table 3.4.

Table 3.4 - Multipliers of friction and heat transfer models. Source: Author

Multiplier	Object value
Heat transfer multiplier in the exhaust manifold	0,99
Intake manifold friction multiplier	1,0
Heat Transfer Multiplier in the exhaust manifold	1,0
Exhaust Manifold Friction Multiplier	1.03
Cylinder Convection Multiplier	0,89
Inlet Valve Lift Multiplier	1,0
Exhaust Valve Lift Multiplier	1,0
Inlet Valve Flow Area Multiplier	1,0
Exhaust Valve Flow Area Multiplier	1,0
Radiation Multiplier in the cylinder	1,0
Constant part of FMEP [bar]	0,3
Peak Cylinder Pressure Factor	0,004
Mean Piston Speed Factor [bar/(m/s)]	0,09
Mean Piston Speed Squared Factor [bar/(m/s)^2]	0,001
Wiebe Exponent	2,0

The developed model was calibrated, and Figure 3.5 shows the P x V diagram of the cycle obtained with experimental data in blue and numerical data in orange for the baseline engine under conditions of 2500 rpm and IMEP of 3.6 bar. Figure 3.6 shows the gas pressure curve in the cylinder obtained with experimental data in blue and numerical data in orange for the baseline engine under conditions of 2500 rpm and IMEP of 3.6 bar.

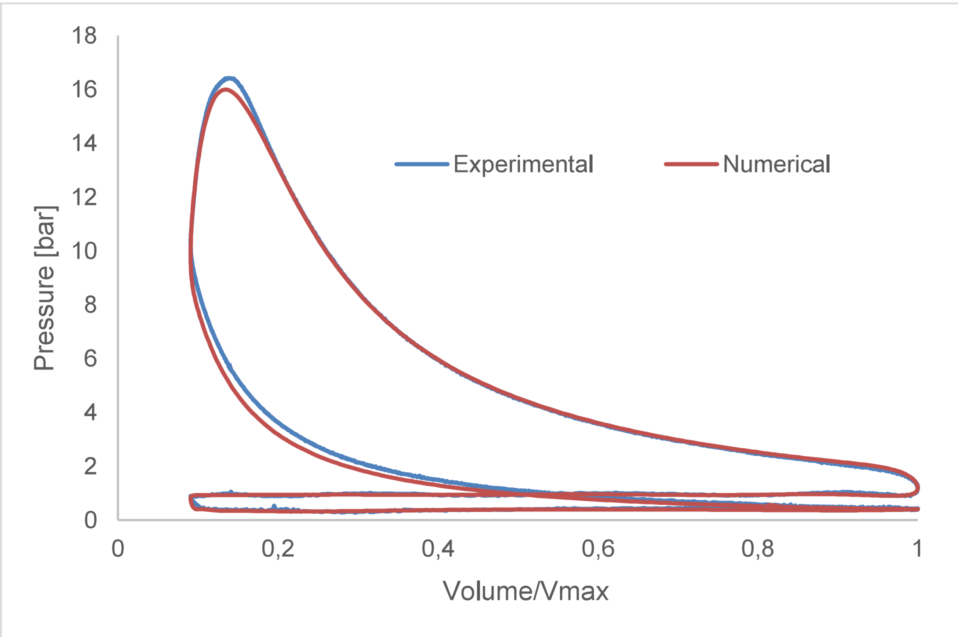

Figure 3.5 - P x V for 2500 rpm and IMEP of 3.66 bar. Source: Author

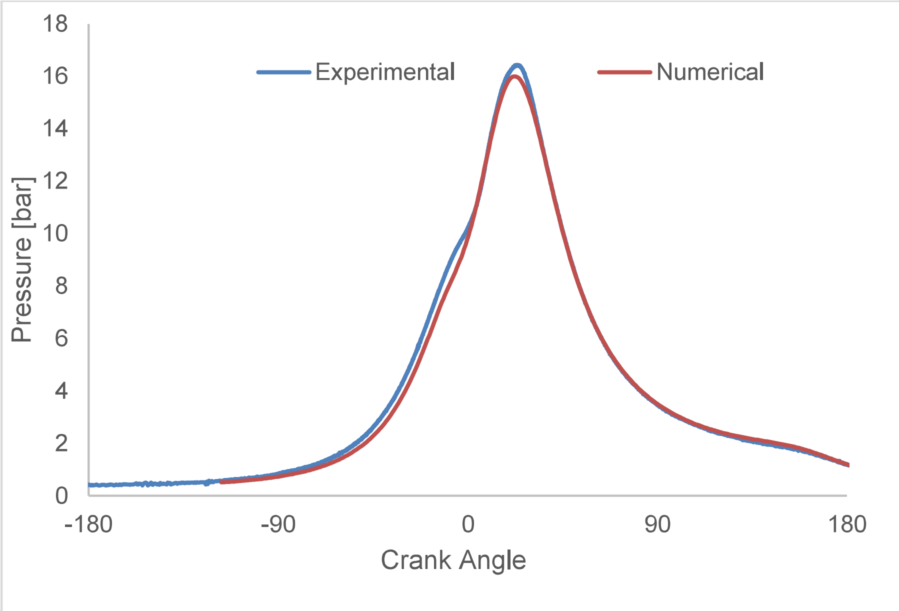

Figure 3.6 - In cylinder pressure for 2500 rpm and IMEP of 3.66 bar. Source: Author

The Table 3.5 shows the experimental and numerical values of power, torque, air, and fuel mass flow [kg/h], specific consumption and IMEP and their respective errors after model calibration for the baseline engine under conditions of 2500 rpm and IMEP of 3.66 bar.

Table 3.5 - Comparison between numerical and experimental data. Source: Author

	Numerical	Experimental	Error
Power [kW]	11.14	11.52	3.30%
Torque [N.m]	42.55	43.98	3.25%
BSFC [g/kW.h]	322.4	332	2.89%
Fuel Flow [kg/h]	3.35	3.41	1.76%
Airflow [kg/h]	43.85	45.3	3.20%
IMEP [bar]	3.79	3.66	3.55%

3.4.2 NON-PREDICTIVE MODEL WITH PRE-CHAMBER

The second model elaborated was based on the previous model, with the same characteristics and geometric data. The main difference, in this case, it is due to the use of the pre-chamber of combustion to replace the spark plug in the engine's original system. The Figure 3.7 shows this second model developed.

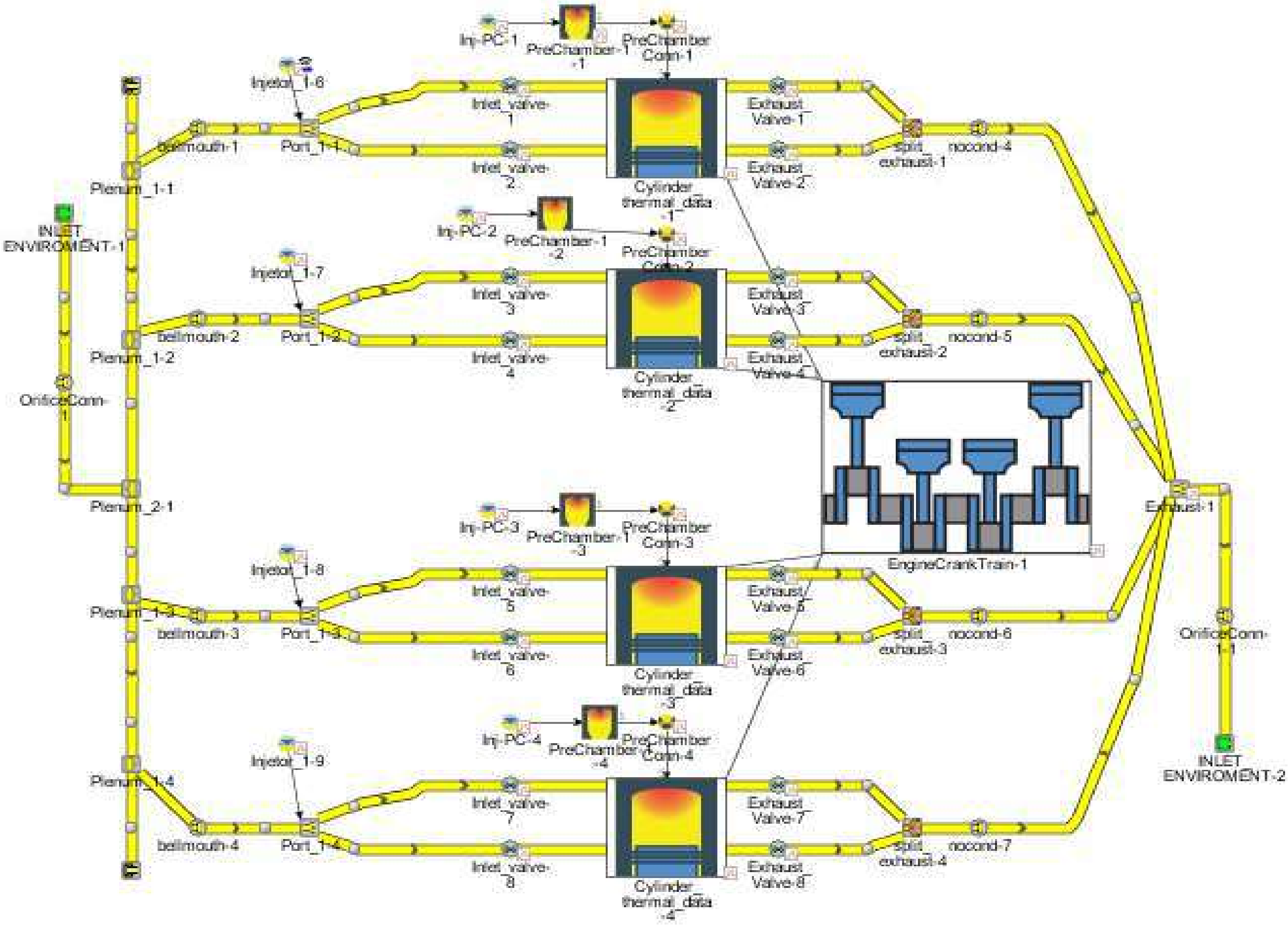

Figure 3.7 - Non-predictive model with pre-chamber. Source: Author

It is possible to notice the presence of pre-chambers at the top of all cylinders, as well as the presence of a fuel injector for each pre-chamber. This, like the first model, is a non-predictive model and has been calibrated in the same way as the above based on experimental data, and the models and results obtained will be presented in the next chapter. Non-predictive simulation refers to a form of simulation that does not aim to predict the actual behavior of a system, but to reproduce its operation under a known condition. It is important to emphasize that non-predictive simulation should not be confused with low-quality or inaccurate simulation. Although it does not provide exact quantitative results, non-predictive simulation can be a valuable tool for understanding and qualitatively analyzing complex systems, especially when detailed data or knowledge is limited.

3.4.3 PREDICTIVE MODELS WITH PRE-CHAMBER

The third built model was also based on the geometric data of the engine, intake and discharge ducts, roughness characteristics and heat transfer of the materials. This model also has a pre-combustion chamber like the second model. The main difference of this one is that this is a predictive model, that is, this model is built based on specific technical information of the engine in question, such as geometric specifications, flow characteristics and experimental data and through mathematical modeling the predictive model is capable to predict the operation of the engine under conditions different from the experimental ones. Presenting the model figure would be redundant, as visually it would be the same as the one shown in the previous Figure 3.7. The difference is in the mathematical equation behind it, which is able to predict the burning in the combustion chamber.

The same calibration methodology was used to adjust the predictive model, however as shown in the predictive combustion modeling section, to calibrate the combustion in the pre-chamber, it is necessary to use four multipliers, described below:

TFSM - Turbulent Flame Speed Multiplier: This multiplier is used to modify the calculated turbulent flame velocity and influences the total duration of combustion. Higher values increase the burning rate.

TLSM - Taylor Length Scale Multiplier: This multiplier is used to modify the calculated value of the combustion time constant of the air/fuel mixture drawn into the flame zone, changing the thickness of the region that limits the burned mixture from the unburned one. This multiplier mainly influences the final part of the combustion curve and is relatively insensitive.

FKGM - Flame Kernel Growth Multiplier: This multiplier is used to modify the calculated value of the flame front growth rate and influences the ignition delay. Larger values shorten the delay, advancing the transition from laminar combustion to turbulent combustion, having its greatest effect on ignition advancement.

DEM - Dilution Exponent Multiplier: This multiplier is used to modify the effect of waste dilution and EGR on laminar flame velocity. Increasing this value reduces the dilution effect on the laminar flame velocity and increases the burn rate. The greatest effect of this parameter is shown in the ratio of residual gases, mainly in conditions of partial loads.

The Table 3.6 shows the calibrated parameters referring to the predictive combustion model, as well as the minimum and maximum values given by default by the software. The predictive models and the results obtained will also be presented in the next chapter.

Table 3.6 - Calibrated parameters of predictive combustion model. Source: Author

	Def. Min.	Def. Max.	Adjusted
TLSM	0.5	2	1.5
TFSM	0.5	2	0.5
FKGM	0.1	1	0.33
DEM	0.7	1.6	1.0

3.4.4 PREDICTIVE MODELS WITH VARIATIONS IN PRE-CHAMBER GEOMETRY

As previously mentioned, based on the created predictive model, it becomes possible to predict the engine performance by changing some parameters of its operation or geometric characteristics. In other words, a well-calibrated model can predict the engine operation in other conditions not experimentally tested. For this purpose, a last category of models was created in which some geometric characteristics of the pre-chamber of combustion were changed based on the already calibrated model. The geometric parameters changed were the pre-chamber's volume and the diameter communicating it with the main chamber.

Figure 3.8 illustrates the methodology used in this part. In the first column, the volume of the pre-chamber used in the tests was kept constant (7.3% of the main chamber volume) and with the effect of diameter variations (4mm, 5mm, 6mm, 7mm and 8mm respectively) of the pre-chamber orifices. In the second part, the diameter of the interconnection orifice of the experimentally tested prechamber (6mm) was kept constant and the volume of the prechamber was varied (6.5%, 7.0%, 7.3%, 8.0 % and 8.5% of the main chamber volume, respectively). This entire methodology was applied, after validating the model for the pre-chamber with its experimentally tested geometric configuration.

Two predictive models were simulated with variations in prechamber orifice diameter and prechamber volume. They are "model 28 with prechamber and lambda 1.10" and "model 38 with prechamber and lambda 1.10", among all the cases presented in figure 3.8.

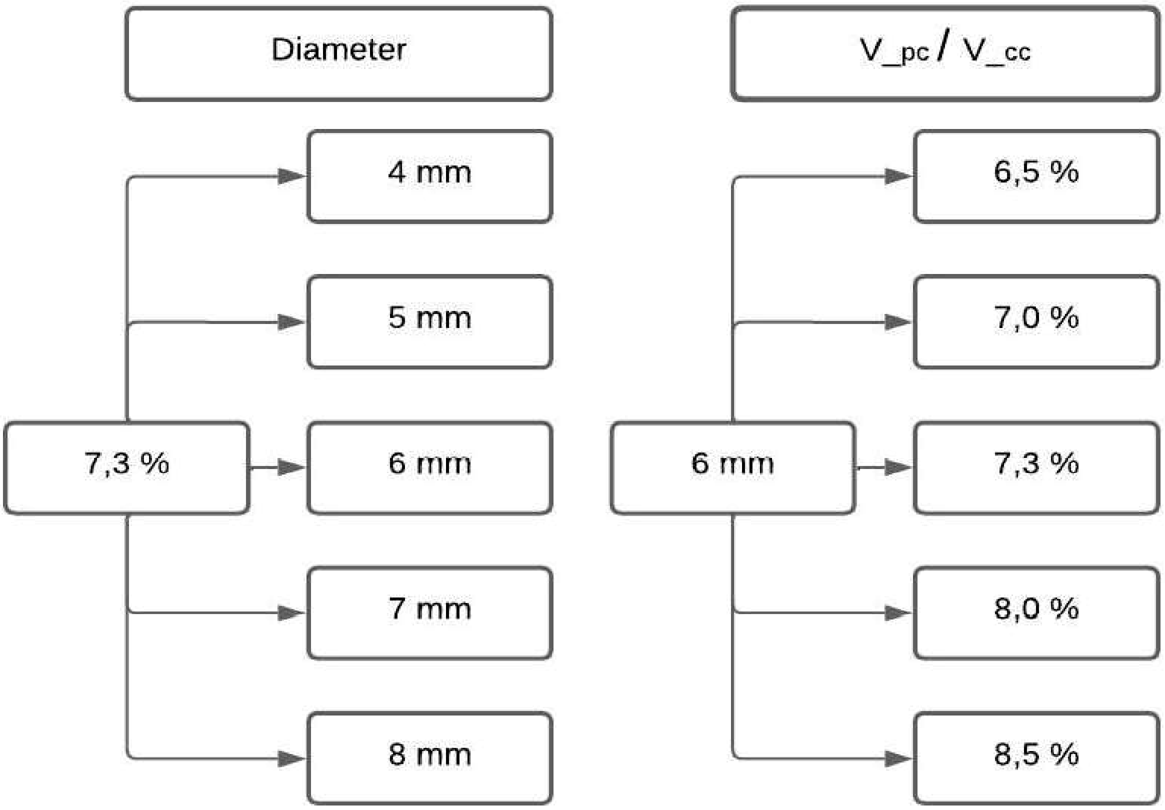

Figure 3.8 – Variations in the diameter and volume of the pre-chambers. Source: Author

It is worth mentioning that the central line of the Figure 3.8 – where the volume corresponds to 7.3% and the diameter is 6 mm – is the reference case and the other values in the other lines are the simulated variations.

3.5 FINAL CONSIDERATIONS ABOUT THE NUMERICAL MODEL

A one-dimensional model of the proposed engine was built, using the GT-Power computational program, operating with E25, with and without pre-chamber, predictive and non-predictive. Based on experimental data, its calibration was carried out for all the requested operating conditions with numerical error always below 5%. Thus, the numerical results obtained from the implemented model can be considered satisfactory.

4 RESULTS

In this chapter, numerical results obtained from specific fuel consumption, IMEP are presented. Numerical results are compared with experimental results at various loads, air/fuel ratio variations and geometric variations in the pre-combustion chamber. All pressure curves, and detailed result values of non-predictive simulation, for all cases compared to experimental data, are shown in Annex 1.

4.1 PERFORMANCE AND RESULTS ANALYSIS FOR NON-PREDICTIVE MODELS

This topic presents the simulated results obtained for all experimental operating conditions with the non-predictive models, as shown in Figure 3.3. The Figure 4.1 shows the comparison of simulated IMEP values with experimental data for all 11 simulated cases at 2500 rpm. This type of comparison is fundamental, as it allows evaluating the accuracy of the simulation model in replicating real conditions observed experimentally.

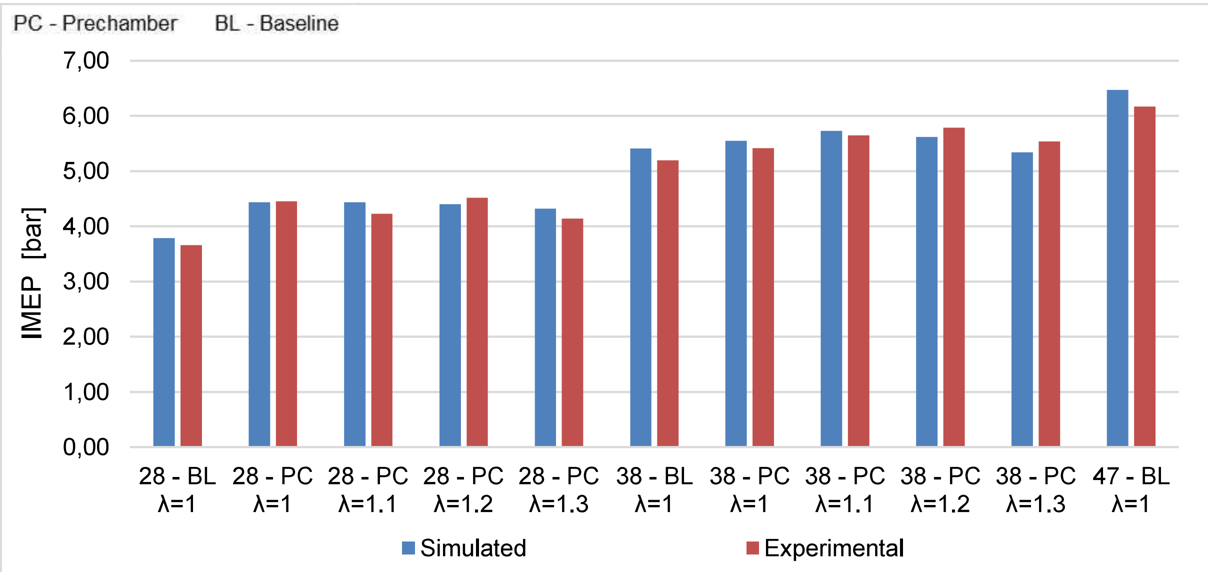

Figure 4.1 – Comparison of simulated IMEP values with experimental data at 2500 rpm.

Source: Author

The proximity of the simulated IMEP values to the experimental data indicates the accuracy of the model. A significant difference could suggest the need for adjustments to the simulation model, such as improving theoretical assumptions, reviewing boundary conditions or calibrating specific engine parameters.

The Figure 4.2 shows the percentage error values between the simulated and experimental IMEP values results for all 11 simulated cases. This figure shows graphically that the errors between the simulation and experimental data are less than 5.0%, which shows the accuracy of the models.

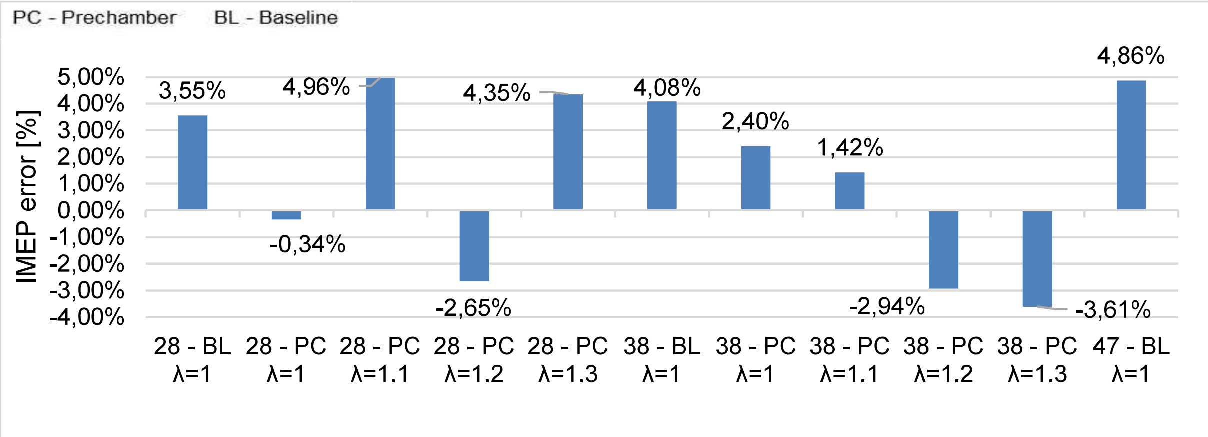

Figure 4.2 – Percentage error between the simulated and experimental IMEP values at 2500 rpm. Source: Author

The Figure 4.3 shows the comparison of simulated BSFC values with experimental data for all 11 simulated cases.

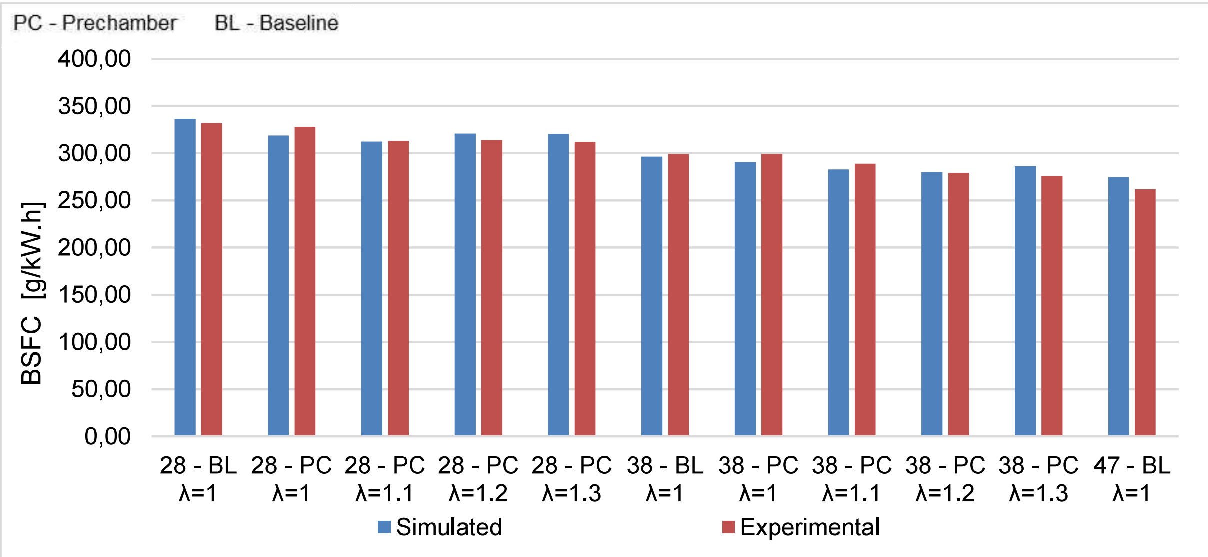

Figure 4.3 – Comparison of simulated BSFC values with experimental data at 2500 rpm. Source: Author

In the same way as for IMEP in Figure 4.1, we note that the simulated values are very close to the experimental ones, showing the accuracy of the model. Another piece of information worth highlighting is that there is an approximately linear reduction in specific fuel consumption that occurs both with increased engine load and with impoverished mixture, which is more efficient with the use of pre-chambers.

The Figure 4.4 shows the percentage error values between the simulated and experimental BSFC values results for all 11 simulated cases.

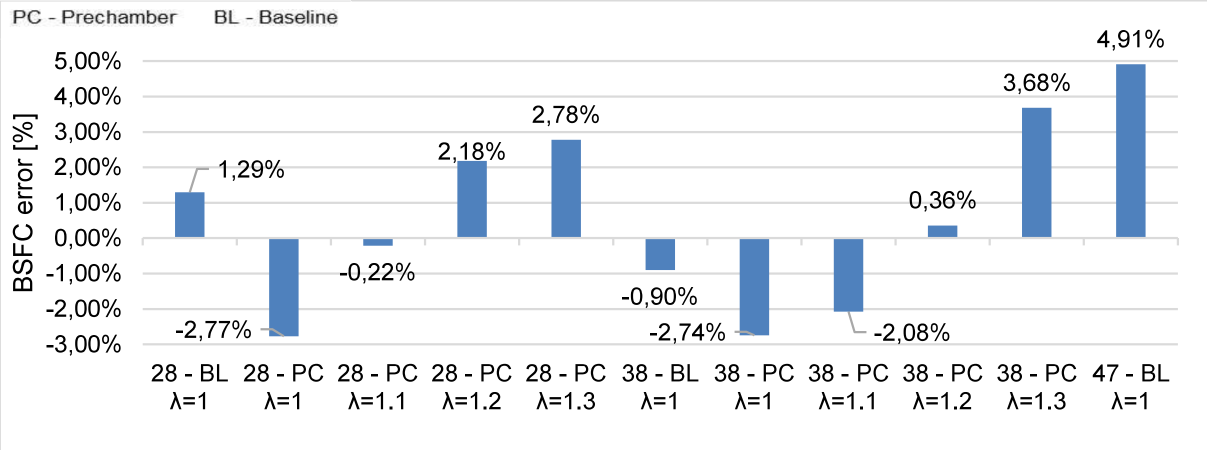

Figure 4.4 – Percentage error between the simulated and experimental BSFC values at 2500 rpm. Source: Author

The Table 4.1 presents the results of all evaluated parameters, for each of the eleven simulated cases containing for each of them the experimental data, the simulated values, and their respective percentage errors. Detailed results and pressure curves for all simulated cases are presented in Annex 1. Figures with comparisons between simulated and experimental values of torque, power, air flow and fuel flow are presented in Annex 2.

Table 4.1 – Summary of experimental data, simulated values, and their respective percentage errors. Source: Author

	28																	
	Baseline λ=1						With Pre-Chamber λ=1						With Pre-Chamber λ=1.1					
	BSFC [g/kW.h]	IMEP [bar]	Fuel Flow [kg/h]	Air Flow [kg/h]	Power [kW]	Torque [N.m]	BSFC [g/kW.h]	IMEP [bar]	Fuel Flow [kg/h]	Air Flow [kg/h]	Power [kW]	Torque [N.m]	BSFC [g/kW.h]	IMEP [bar]	Fuel Flow [kg/h]	Air Flow [kg/h]	Power [kW]	Torque [N.m]
Simulated	336,29	3,79	3,35	43,85	11,14	42,55	318,90	4,44	3,51	47,36	11,03	42,13	312,32	4,44	3,49	50,31	11,19	42,75
Experimental	332,00	3,66	3,42	45,30	11,52	43,98	328,00	4,46	3,41	45,20	11,53	44,04	313,00	4,23	3,33	48,50	11,77	44,96
Error	1,29%	3,55%	-2,02%	-3,20%	-3,30%	-3,25%	-2,77%	-0,34%	2,90%	4,78%	-4,34%	-4,34%	-0,22%	4,96%	4,96%	3,73%	-4,93%	-4,92%

	28												38					
	With Pre-Chamber λ=1.2						With Pre-Chamber λ=1.3						Baseline λ=1					
	BSFC [g/kW.h]	IMEP [bar]	Fuel Flow [kg/h]	Air Flow [kg/h]	Power [kW]	Torque [N.m]	BSFC [g/kW.h]	IMEP [bar]	Fuel Flow [kg/h]	Air Flow [kg/h]	Power [kW]	Torque [N.m]	BSFC [g/kW.h]	IMEP [bar]	Fuel Flow [kg/h]	Air Flow [kg/h]	Power [kW]	Torque [N.m]
Simulated	320,85	4,40	3,42	53,94	10,98	42,14	320,67	4,32	3,41	58,13	11,27	43,06	296,31	5,41	4,29	56,16	14,51	55,42
Experimental	314,00	4,52	3,27	51,40	11,53	44,23	312,00	4,14	3,26	55,50	11,62	44,38	299,00	5,20	4,11	54,50	14,63	58,53
Error	2,18%	-2,65%	4,75%	4,94%	-4,77%	-4,73%	2,78%	4,35%	4,60%	4,74%	-3,01%	-2,97%	-0,90%	4,08%	4,33%	3,05%	-0,82%	-5,31%

	38																	
	With Pre-Chamber λ=1						With Pre-Chamber λ=1.1						With Pre-Chamber λ=1.2					
	BSFC [g/kW.h]	IMEP [bar]	Fuel Flow [kg/h]	Air Flow [kg/h]	Power [kW]	Torque [N.m]	BSFC [g/kW.h]	IMEP [bar]	Fuel Flow [kg/h]	Air Flow [kg/h]	Power [kW]	Torque [N.m]	BSFC [g/kW.h]	IMEP [bar]	Fuel Flow [kg/h]	Air Flow [kg/h]	Power [kW]	Torque [N.m]
Simulated	290,80	5,55	4,24	57,15	14,59	55,73	283,00	5,73	4,29	62,04	15,18	57,97	280,00	5,62	4,14	64,89	14,80	56,56
Experimental	299,00	5,42	4,16	55,20	15,28	58,38	289,00	5,65	4,11	59,90	15,57	59,47	279,00	5,79	3,96	62,90	15,52	59,27
Error	-2,74%	2,40%	1,85%	3,53%	-4,52%	-4,54%	-2,08%	1,42%	4,46%	3,57%	-2,50%	-2,52%	0,36%	-2,94%	4,62%	3,16%	-4,64%	-4,57%

	38						47					
	With Pre-Chamber λ=1.3						Baseline λ=1					
	BSFC [g/kW.h]	IMEP [bar]	Fuel Flow [kg/h]	Air Flow [kg/h]	Power [kW]	Torque [N.m]	BSFC [g/kW.h]	IMEP [bar]	Fuel Flow [kg/h]	Air Flow [kg/h]	Power [kW]	Torque [N.m]
Simulated	286,16	5,34	4,12	70,87	14,74	56,35	274,87	6,47	5,08	66,65	18,58	70,71
Experimental	276,00	5,54	3,93	67,60	15,51	59,23	262,00	6,17	4,85	64,30	19,47	74,35
Error	3,68%	-3,61%	4,91%	4,84%	-4,96%	-4,86%	4,91%	4,86%	4,70%	3,65%	-4,57%	-4,90%

4.2 PERFORMANCE AND RESULTS ANALYSIS FOR PREDICTIVE MODELS

Two cases were simulated in a predictive way and the results are shown in this section. They are the model “28 with prechamber and lambda 1.10” and the model “38 with prechamber and lambda 1.10”. As previously mentioned, a predictive model has the main advantage that, after the model is created and calibrated, changes can be made to the geometry and points or parameters of engine operation without the need for experimental data for validation. In a first approach, the diameter of the prechamber hole was maintained at 6 mm and its volume was varied, according to the methodology illustrated in figure 3.8.

4.2.1 MODEL 28 WITH PRECHAMBER AND LAMBDA 1.10

The Table 4.2 shows a comparative result between the model and the experimental data for the model 28 with prechamber and lambda 1.10 and 2500 rpm. Even though the torque presented an error slightly higher than 5%, we can consider that the model describes the motor operation well, and in this case with the advantages of a predictive model, however with a longer computational simulation time.

Table 4.2 - Comparison of numerical x experimental results for the predictive model at 2500 rpm and λ=1.1. Source: Author

Predictive - λ=1.1 -2500 rpm	Numerical	Experimental	Error
Power [kW]	11.2887	11.77	4.26%
Torque [N.m]	42.746	44.96	5.18%
BSFC [g/kW.h]	316.06	313	0.97%
Fuel Flow [kg/h]	3.21	3.33	3.74%
Airflow [kg/h]	46.29	48.5	4.77%
IMEP [bar]	4.21	4.23	0.48%

After creating this model, changes to the hole diameter and prechamber volume were made. The Table 4.3 shows the volume variations made and the results of BSFC, fuel flow, air flow and IMEP for each of the simulated configurations.

Table 4.3 – Volume variation and results for predictive model 28 with prechamber and lambda 1.10 at 2500 rpm. Source: Author

28 with prechamber and lambda 1.10 - Volume variation					
V_PC/V_CC	Volume [cm³]	BSFC [g/kW.h]	Fuel flow [kg/h]	Air flow [kg/h]	IMEP [bar]
6,5%	2593	317,00	3,22	46,29	4,20
7,0%	2793	316,42	3,22	46,29	4,21
7,3%	2913	316,08	3,22	46,29	4,21
8,0%	3193	315,48	3,22	46,29	4,22
8,5%	3393	315,19	3,22	46,29	4,22

The Figure 4.5 shows the results of the cylinder pressure versus crankshaft angle curves for different pre-chamber volumes, keeping the pre-chamber orifice diameter at 6mm.

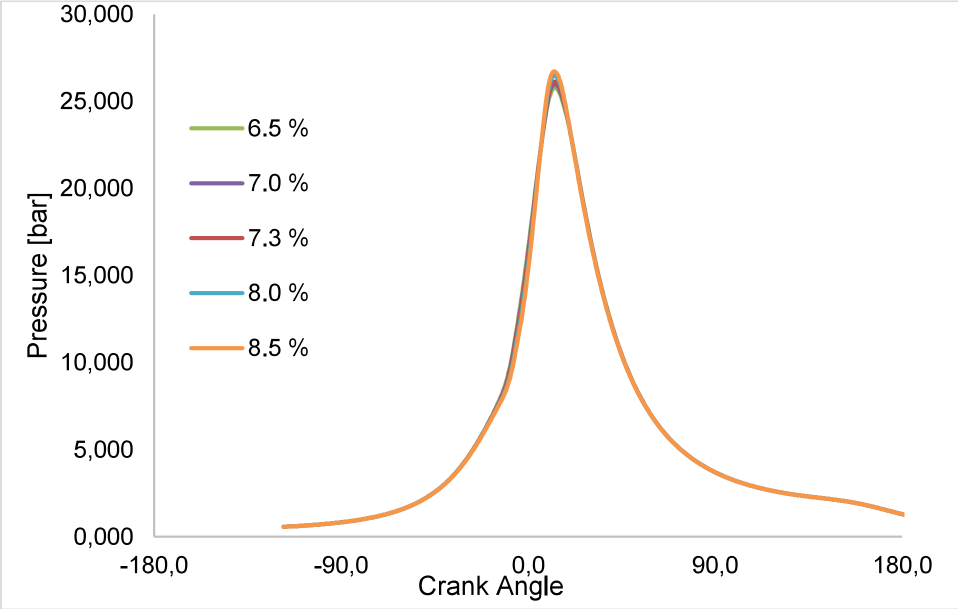

Figure 4.5 – Cylinder pressure curves as a function of crankshaft angle. Source: Author

It can be seen that the use of pre-chambers with a larger volume provided a peak pressure of around 3,5% higher compared to the pre-chamber with a smaller volume. The Figure 4.6 shows the cylinder pressure x volume curves for different prechamber volumes, keeping the prechamber orifice diameter at 6mm.

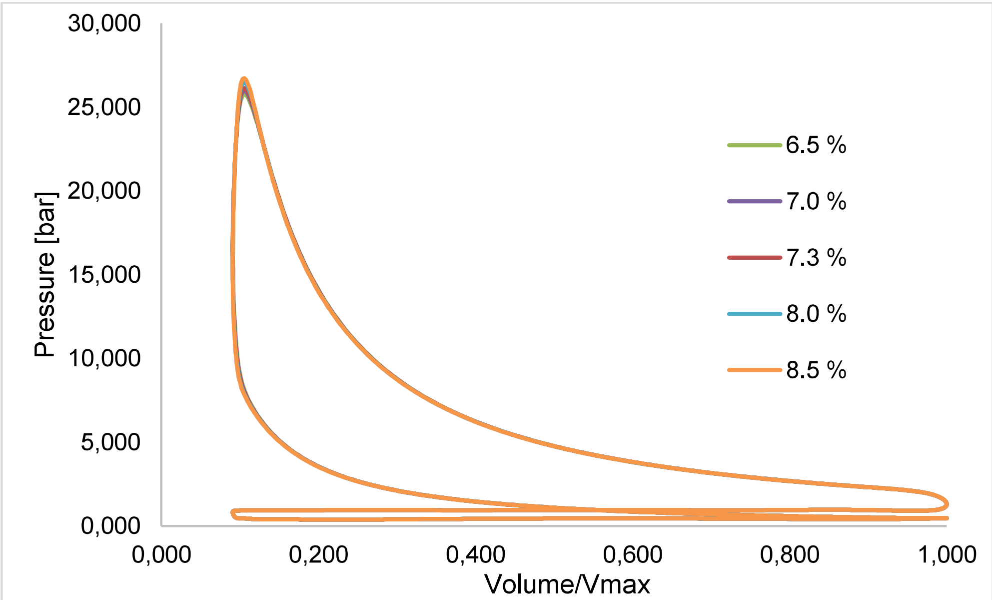

Figure 4.6 – Curves of Pressure x Volume for different prechamber volumes. Source: Author

The Table 4.4 shows the maximum pressure values for each of the different prechamber volumes. The maximum pressures have values very close to each other. This shows that variations in the volume of the pre-chamber have a smaller influence on the maximum pressure than variations in the diameter of the interconnection with the main chamber.

Table 4.4 – Maximum pressure for each different prechamber volume. Source: Author

Vpc/Vcc	Pressure [bar]
6,5%	25,4
7,0%	25,8
7,3%	25,9
8,0%	26,2
8,5%	26,4

Figure 4.7 shows the variation of IMEP and BSFC values as a function of pre-chamber volume variations. The specific consumption was affected by the increase in volume, having been reduced by around 0.6 %. In the same trend, the IMEP also improved, but this variation was in the range of 0.5%, a value that is much lower than the average of model errors. Therefore, it cannot be inferred that this will be the behavior of this indicator in the real case.

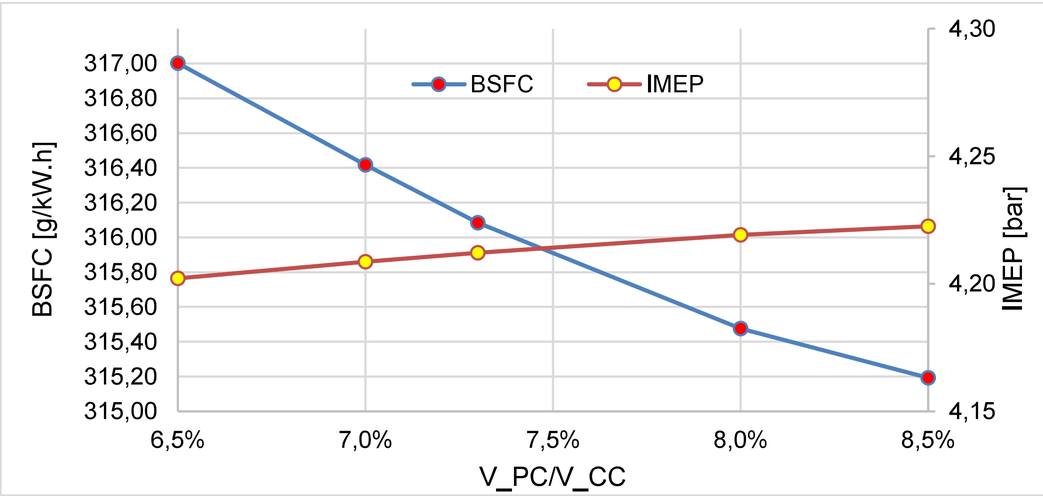

Figure 4.7 - Variation of IMEP and BSFC values as a function of pre-chamber volume. Source: Author

In a second approach, according to the methodology in figure 3.8, the diameter of the pre-chamber orifice was varied, maintaining a constant pre-chamber volume of 2,913 cm³, corresponding to 7.3% of the main chamber volume. The Table 4.5 shows the diameter variations made and the results of BSFC, fuel flow, air flow and IMEP for each of the simulated configurations.

Table 4.5 – Diameter variation and results for predictive model 28 with prechamber and lambda 1.10 at 2500 rpm. Source: Author

Predictive Combustion Simulation Results - 28 with PC - Lambda 1.10				
Diameter [mm]	BSFC [g/kW.h]	Fuel flow [kg/h]	Air flow [kg/h]	IMEP [bar]
4,00	313,20	3,22	46,29	4,25
5,00	313,72	3,22	46,29	4,24
6,00	316,06	3,22	46,29	4,21
7,00	318,58	3,22	46,29	4,18
8,00	321,33	3,21	46,29	4,16

The Figure 4.8 shows the results of the cylinder pressure versus crankshaft angle curves for different diameters at constant volume.

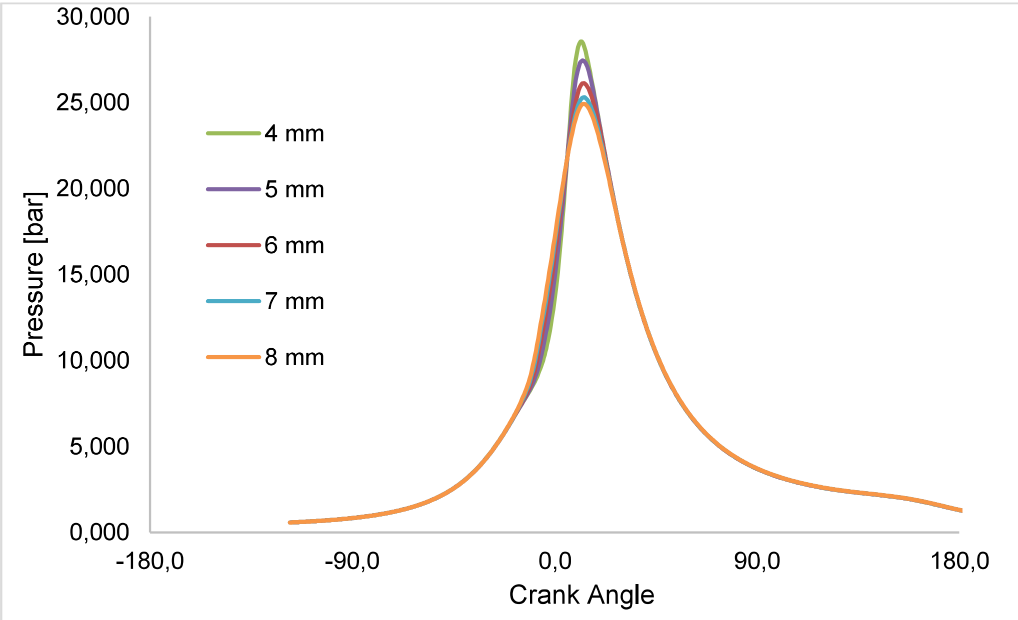

Figure 4.8 - Cylinder pressure curves versus crankshaft angle for different diameters. Source: Author

It can be noted that the use of pre-chambers with a smaller orifice diameter provided a peak pressure above 12.5% higher than that of the pre-chamber with a larger diameter. The Figure 4.9 shows the cylinder pressure x volume curves for different pre-chamber diameters, keeping the pre-chamber volume constant.

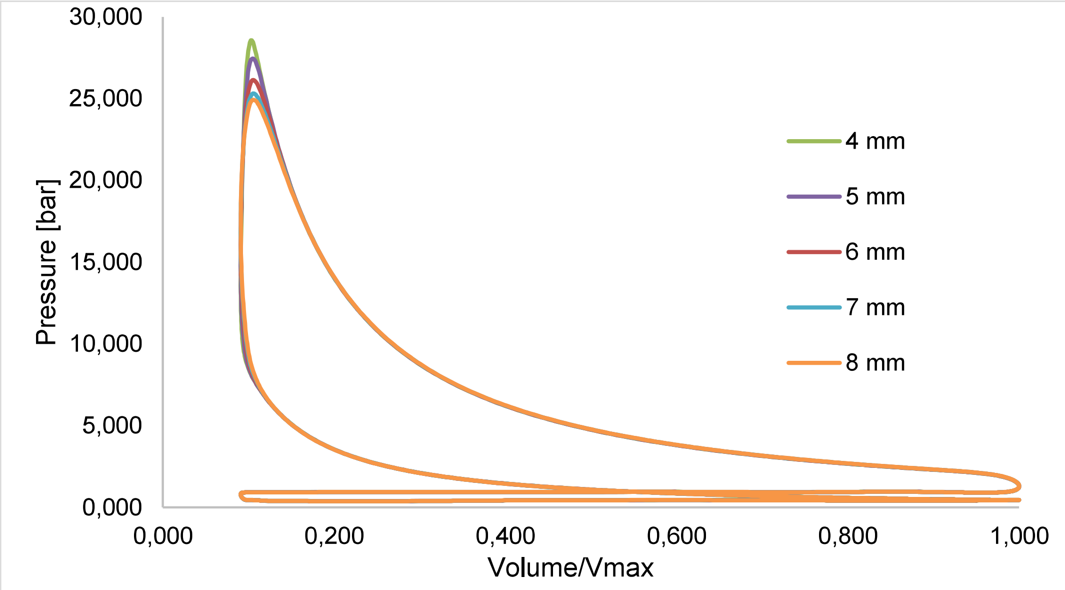

Figure 4.9 - Cylinder pressure x volume for different pre-chamber diameters, keeping the pre-chamber volume constant. Source: Author

Figure 4.10 shows the variation of IMEP and BSFC values as a function of variations in the pre-chamber orifice diameter. It appears that the specific consumption was more positively affected by the increase in diameter, having decreased by around 2.5%. On the other hand, the IMEP improved with the reduction in diameter, and this variation was around 2.0%.

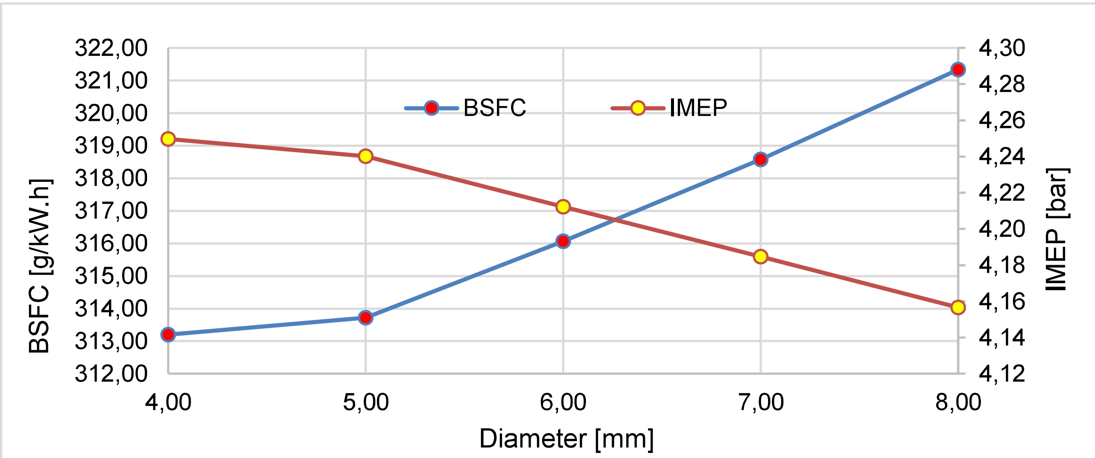

Figure 4.10 - Variation of IMEP and BSFC as a function of pre-chamber orifice diameter. Source: Author

When we compare Figures 4.5 and 4.6 with Figures 4.8 and 4.9, (variation in prechamber volume x variations in prechamber hole diameter), we can notice that the greatest variations in pressure peaks in the cylinder occur with variations in hole diameter. This result is essential to understand how the inclusion of an ignition pre-chamber influences the pressure dynamics inside the cylinder, which is a direct indication of combustion efficiency and, consequently, engine performance.

Typically, the pre-chamber is expected to promote faster and more efficient combustion, reflected in a rapid rise in pressure after the ignition point. Larger peaks may indicate more complete combustion, contributing to an increase in engine efficiency. Higher pressure values indicate a more significant energy release during combustion.

Variations in curves at different RPMs help to understand how the pre-chamber system behaves under different loads and engine speeds. This is crucial for evaluating the versatility and effectiveness of the prechamber system across a wide range of operating conditions.

As can be demonstrated, the performance parameters of the engine depend on both the volume of the prechamber and the diameter of its orifice. For this reason, a series of other simulations were carried out to obtain a trend map of engine performance as a function of both previously mentioned variables, diameter, and volume. The Table 4.6 shows the results of these multiple simulations with variations in volume and diameter in the prechamber.

Table 4.6 – Results of BSFC and IMEP for predictive model 28 with prechamber and lambda 1.10 at 2500 rpm. Source: Author

IMEP [bar]						
Volume		Diameter				
Volume [cm³]	V_pc/V_cc	4 mm	5 mm	6 mm	7 mm	8 mm
2593	6,50%	4,25	4,23	4,20	4,18	4,15
2793	7,00%	4,25	4,24	4,21	4,18	4,15
2993	7,50%	4,25	4,24	4,21	4,19	4,16
3193	8,00%	4,25	4,24	4,22	4,19	4,16
3393	8,50%	4,12	4,24	4,22	4,20	4,17
BSFC [g/kWh]						
Volume		Diameter				
Volume [cm³]	V_pc/V_cc	4 mm	5 mm	6 mm	7 mm	8 mm
2593	6,50%	313,02	314,28	317,01	319,37	321,86
2793	7,00%	313,03	313,89	316,40	318,85	321,59
2993	7,50%	313,31	313,64	315,87	318,35	321,17
3193	8,00%	313,58	313,56	315,49	317,88	320,72
3393	8,50%	326,21	313,64	315,20	317,52	320,38

The Figure 4.11 shows the IMEP results for each of the 25 combinations simulated using the predictive model.

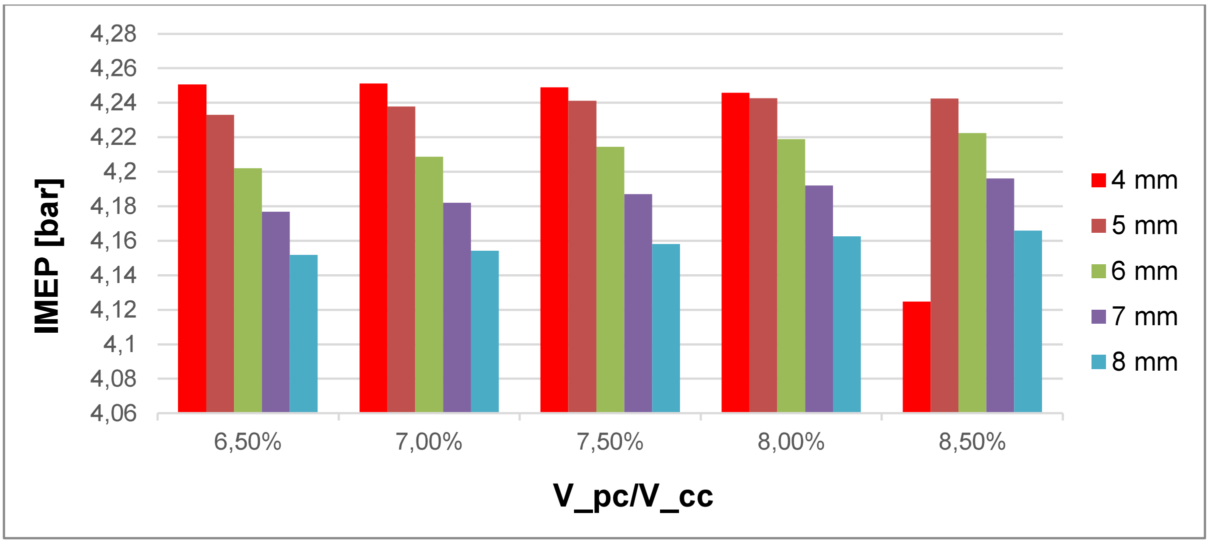

Figure 4.11 – IMEP results as a function on diameter and volume for predictive model 28 with prechamber and lambda 1.10 at 2500 rpm. Source: Author

Based on these results, Figure 4.12 was created, which shows a trend map of IMEP behavior as a function of variations in hole diameter and pre-chamber volume.

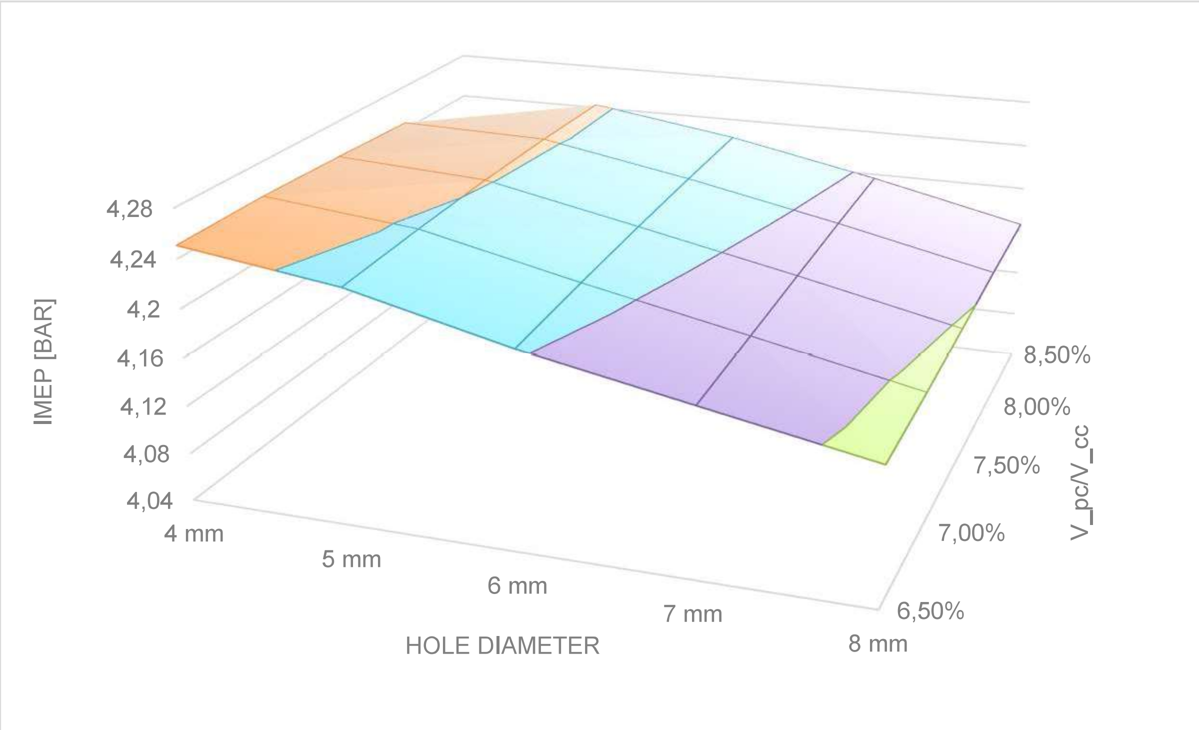

Figure 4.12 – Trend map of IMEP behavior as a function of hole diameter and pre-chamber volume for predictive model 28 with prechamber and lambda 1.10 at 2500 rpm. Source: Author

The Figure 4.13 shows the BSFC results for each of the 25 combinations simulated using the predictive model.

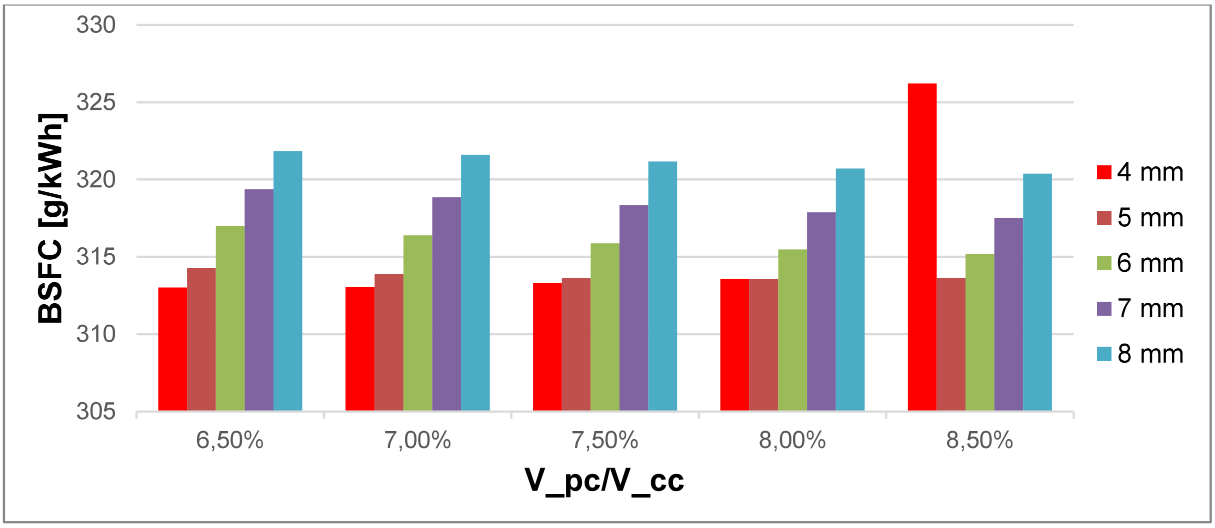

Figure 4.13 – BSFC results as a function on diameter and volume for predictive model 28 with prechamber and lambda 1.10 at 2500 rpm. Source: Author

Based on these results, Figure 4.14 was created, which shows a trend map of BSFC behavior as a function of variations in hole diameter and pre-chamber volume.

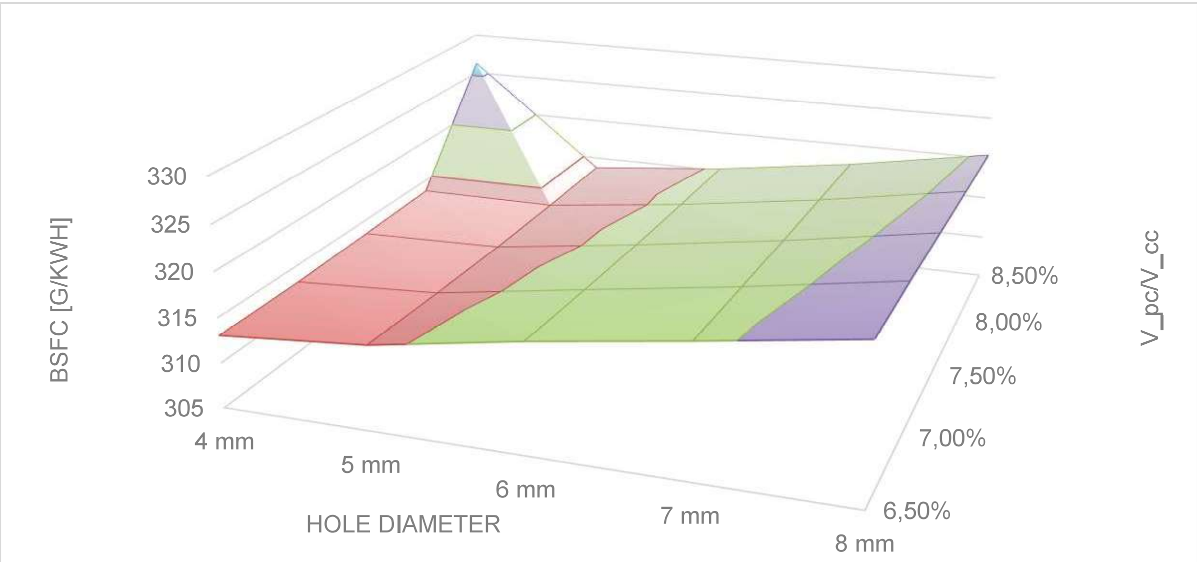

Figure 4.14 – Trend map of BSFC behavior as a function of hole diameter and pre-chamber volume for predictive model 28 with prechamber and lambda 1.10 at 2500 rpm. Source: Author

4.2.2 MODEL 38 WITH PRECHAMBER AND LAMBDA 1.10

After creating this model, changes to the hole diameter and prechamber volume were made. The Table 4.7 shows the volume variations made and the results of BSFC, fuel flow, air flow and IMEP for each of the simulated configurations.

Table 4.7 – Volume variation and results for predictive model 38 with prechamber and lambda 1.10 at 2500 rpm. Source: Author

38 with prechamber and lambda 1.10 - Volume variation					
Volume [cm³]	V_pc/V_cc	BSFC [g/kW.h]	Fuel flow [kg/h]	Air flow [kg/h]	IMEP [bar]
2593	6,50%	281,02	4,11	59,11	5,56
2793	7,00%	280,48	4,11	59,11	5,57
2993	7,50%	280,08	4,11	59,11	5,58
3193	8,00%	279,75	4,11	59,11	5,58
3393	8,50%	279,49	4,11	59,11	5,59

The Figure 4.15 shows the results of the cylinder pressure versus crankshaft angle curves for different pre-chamber volumes, keeping the pre-chamber orifice diameter at 6mm.

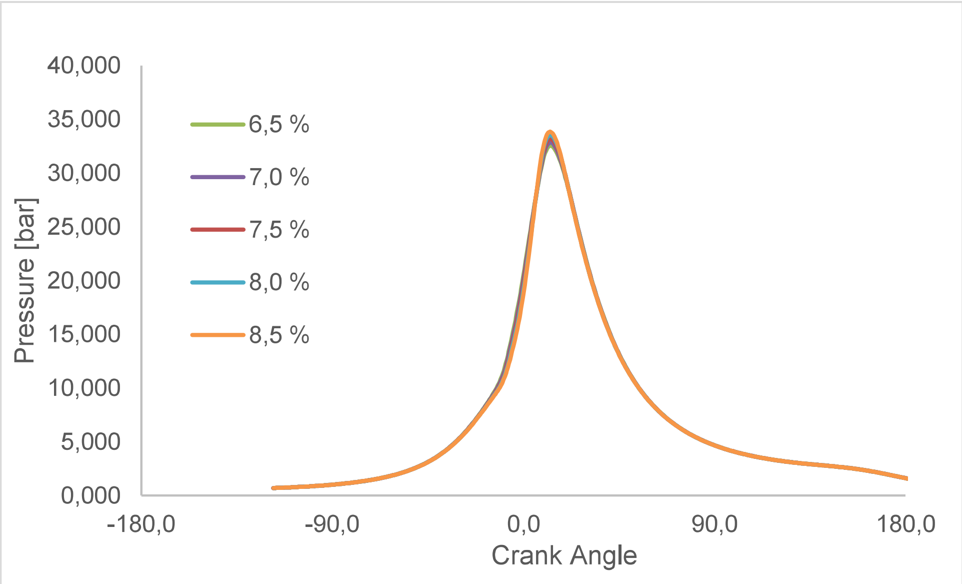

Figure 4.15 – Cylinder pressure curves as a function of crankshaft angle. Source: Author

It can be seen that the use of pre-chambers with a larger volume provided a peak pressure of around 4,0 % higher compared to the pre-chamber with a smaller volume. The

Figure 4.16 shows the cylinder pressure x volume curves for different prechamber volumes, keeping the prechamber orifice diameter at 6mm.

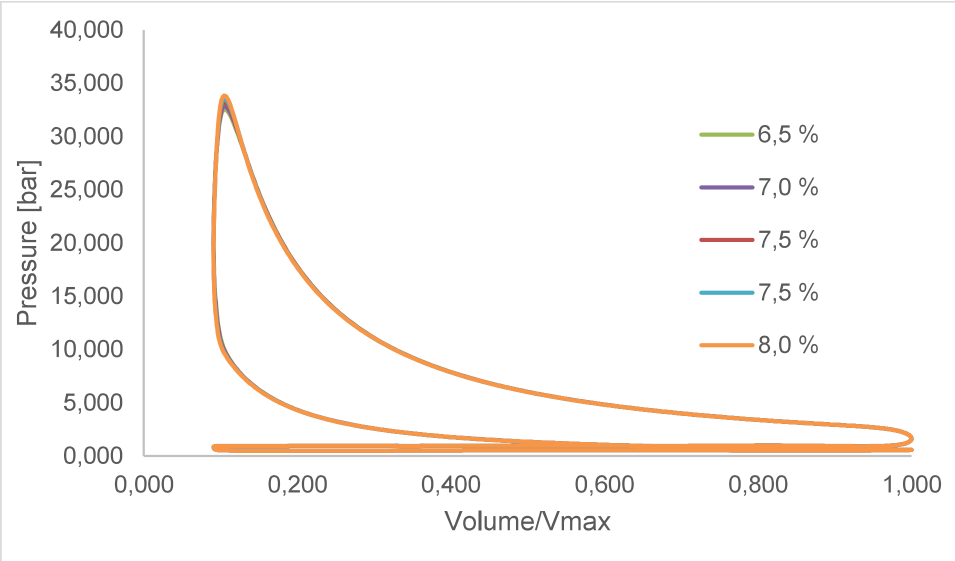

Figure 4.16 – Curves of Pressure x Volume for different prechamber volumes. Source: Author

The Table 4.8 shows the maximum pressure values for each of the different prechamber volumes. The maximum pressures have values very close to each other. This shows that variations in the volume of the pre-chamber have a smaller influence on the maximum pressure than variations in the diameter of the interconnection with the main chamber.

Table 4.8 – Maximum pressure for each different prechamber volume. Source: Author

Vpc/Vcc	Pressure [bar]
6,5%	32,55
7,0%	32,85
7,3%	33,18
8,0%	33,53
8,5%	33,85

Figure 4.17 shows the variation of IMEP and BSFC values as a function of pre-chamber volume variations. The specific consumption was affected by the increase in volume, having been reduced by around 0.5 %. In the same trend, the IMEP also improved, but this variation

was in the range of 0.6%, a value that is much lower than the average of model errors. Therefore, it cannot be inferred that this will be the behavior of this indicator in the real case.

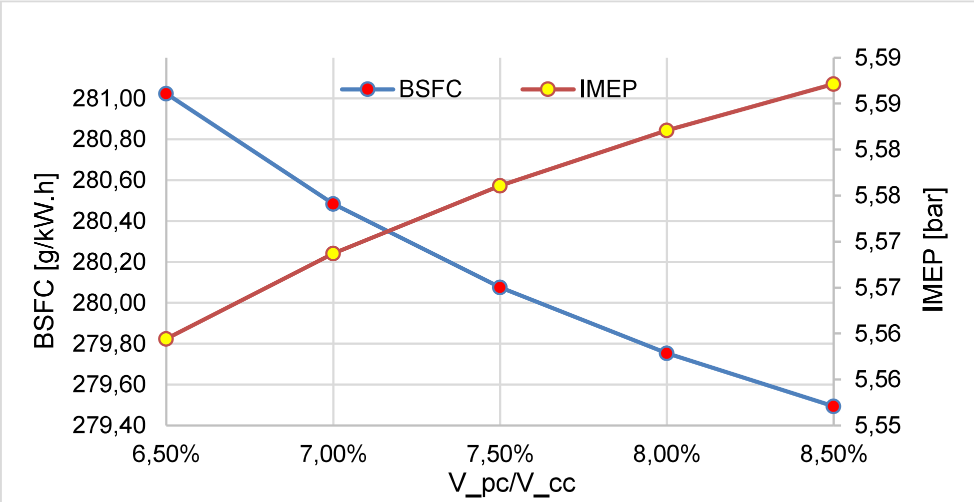

Figure 4.17 - Variation of IMEP and BSFC values as a function of pre-chamber volume. Source: Author

In a second approach, according to the methodology in figure 3.8, the diameter of the pre-chamber orifice was varied, maintaining a constant pre-chamber volume of 2,913 cm³, corresponding to 7.3% of the main chamber volume. The Table 4.9 shows the diameter variations made and the results of BSFC, fuel flow, air flow and IMEP for each of the simulated configurations.

Table 4.9 – Diameter variation and results for predictive model 28 with prechamber and lambda 1.10 at 2500 rpm. Source: Author

38 with prechamber and lambda 1.10 - Diameter variation				
Diameter [mm]	BSFC [g/kW.h]	Fuel flow [kg/h]	Air flow [kg/h]	IMEP [bar]
4,00	278,36	4,11	59,11	5,62
5,00	278,47	4,11	59,11	5,61
6,00	280,08	4,11	59,11	5,58
7,00	282,36	4,11	59,11	5,54
8,00	283,65	4,11	59,11	5,51

The Figure 4.18 shows the results of the cylinder pressure versus crankshaft angle curves for different diameters at constant volume.

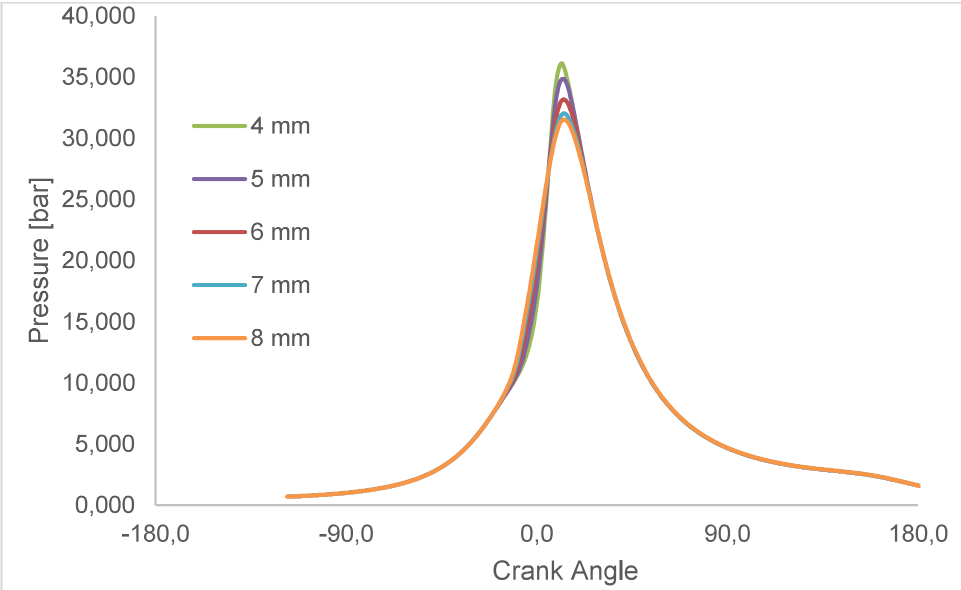

Figure 4.18 - Cylinder pressure curves versus crankshaft angle for different diameters. Source: Author

It can be noted that the use of pre-chambers with a 4 mm orifice diameter provided a peak pressure above 13 % higher than that of the pre-chamber with a 8 mm diameter. The Figure 4.19 shows the cylinder pressure x volume curves for different pre-chamber diameters, keeping the pre-chamber volume constant.

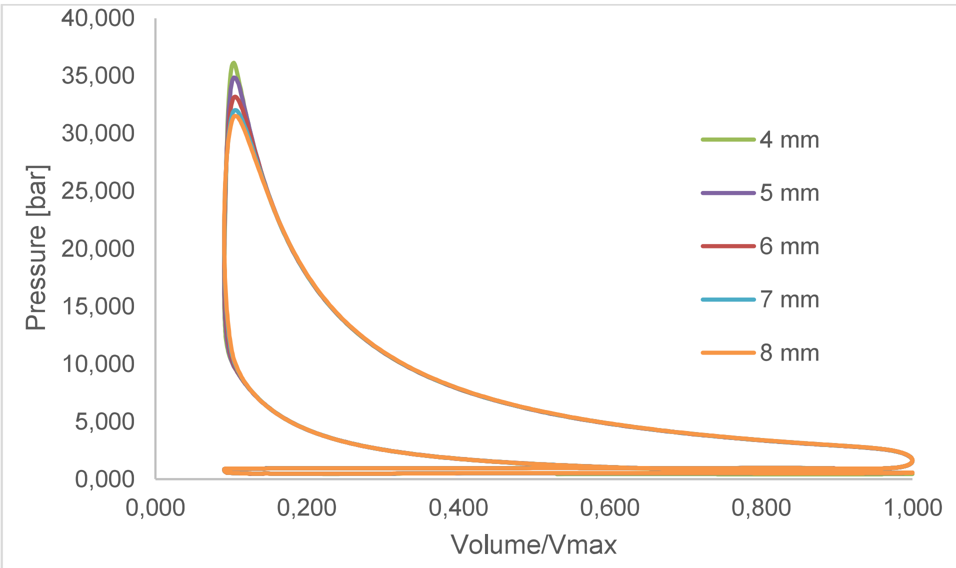

Figure 4.19 - Cylinder pressure x volume for different pre-chamber diameters, keeping the pre-chamber volume constant. Source: Author

Figure 4.20 shows the variation of IMEP and BSFC values as a function of variations in the pre-chamber orifice diameter. It appears that the specific consumption was more positively affected by the increase in diameter, having decreased by around 2.5%. On the other hand, the IMEP improved with the reduction in diameter, and this variation was around 2.0%.

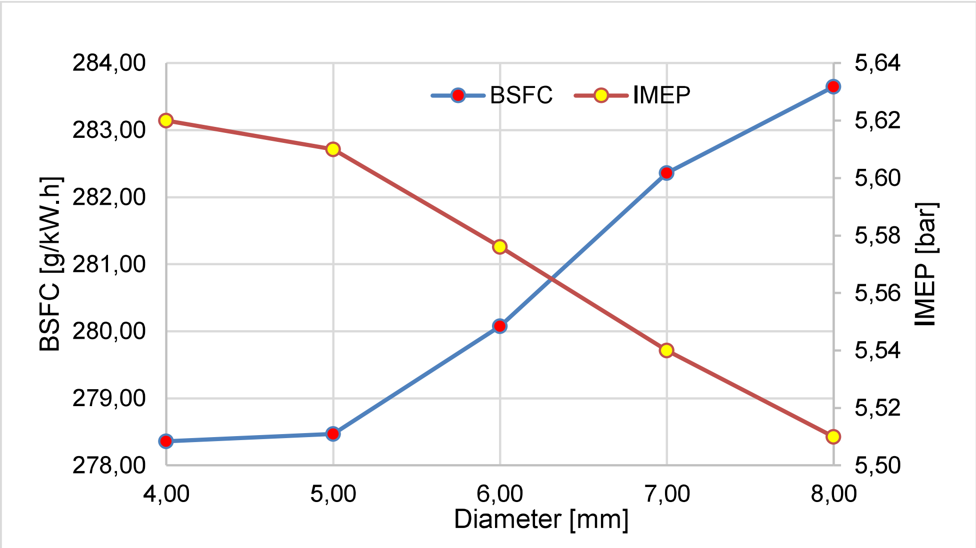

Figure 4.20 - Variation of IMEP and BSFC as a function of pre-chamber orifice diameter.
Source: Author

As can be demonstrated, the performance parameters of the engine depend on both the volume of the prechamber and the diameter of its orifice. For this reason, a series of other simulations were carried out to obtain a trend map of engine performance as a function of both previously mentioned variables, diameter, and volume. In a similar way to the previous section, we can note that the greatest variations in pressure peaks in the cylinder occur with variations in hole diameter. The results of these multiple simulations with variations in volume and diameter in the prechamber are summarized in Table 4.10.

Table 4.10 – Summary of results for predictive model 38 with prechamber and lambda 1.10 at 2500 rpm. Source: Author

IMEP [bar]						
Volume		Diameter				
Volume [cm³]	V_pc/V_cc	4 mm	5 mm	6 mm	7 mm	8 mm
2593	6,50%	5,62	5,60	5,56	5,52	5,51
2793	7,00%	5,62	5,60	5,57	5,53	5,51
2993	7,50%	5,62	5,61	5,58	5,54	5,51
3193	8,00%	5,46	5,61	5,58	5,54	5,52
3393	8,50%	5,45	5,61	5,59	5,55	5,52
BSFC [g/kWh]						
Volume		Diameter				
Volume [cm³]	V_pc/V_cc	4 mm	5 mm	6 mm	7 mm	8 mm
2593	6,50%	278,12	278,85	281,02	283,07	284,11
2793	7,00%	278,18	278,60	280,48	282,70	283,87
2993	7,50%	278,36	278,47	280,08	282,33	283,65
3193	8,00%	288,59	278,45	279,75	281,95	283,49
3393	8,50%	289,10	278,54	279,49	281,59	283,36

The Figure 4.21 shows the IMEP results for each of the 25 combinations simulated using the predictive model.

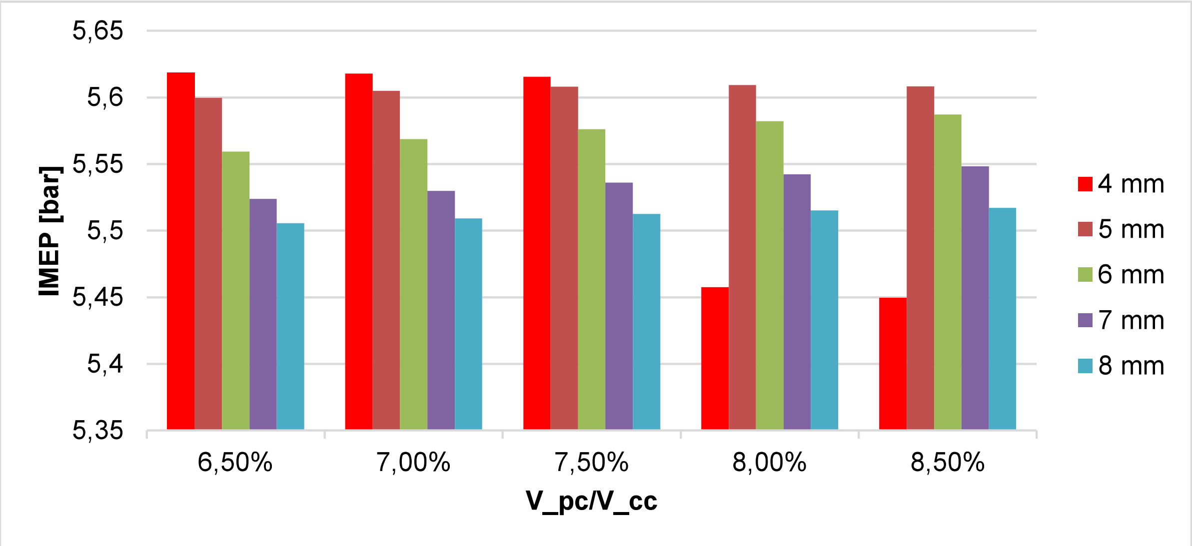

Figure 4.21 – IMEP results as a function on diameter and volume for predictive model 38 with prechamber and lambda 1.10 at 2500 rpm. Source: Author

Based on these results the Figure 4.22 was created, which shows a trend map of IMEP behavior as a function of variations in hole diameter and pre-chamber volume.

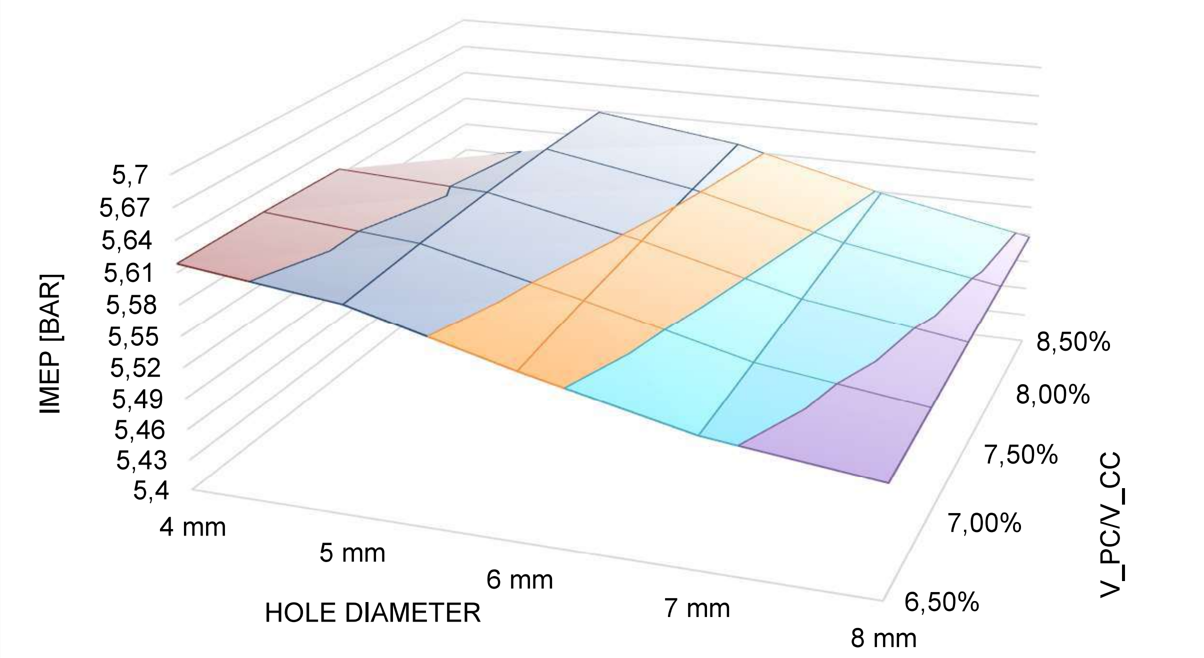

Figure 4.22 – Trend map of IMEP behavior as a function of hole diameter and pre-chamber volume for predictive model 38 with prechamber and lambda 1.10 at 2500 rpm. Source: Author

The Figure 4.23 shows the BSFC results for each of the 25 combinations simulated using the predictive model.

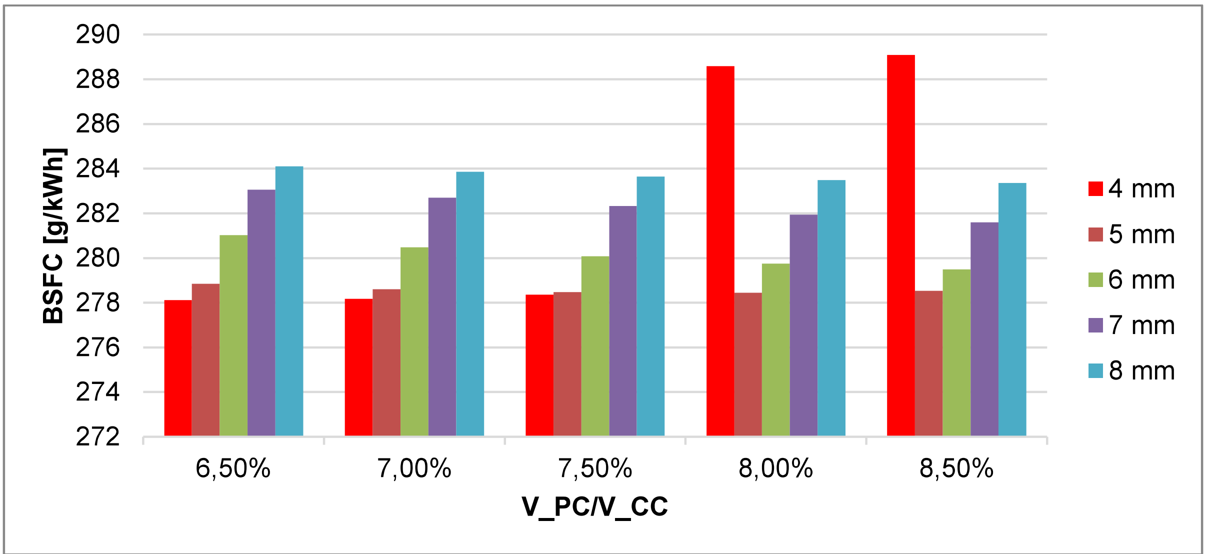

Figure 4.23 – BSFC results as a function on diameter and volume for predictive model 38 with prechamber and lambda 1.10 at 2500 rpm. Source: Author

Based on these results the Figure 4.24 was created, which shows a trend map of BSFC behavior as a function of variations in hole diameter and pre-chamber volume.

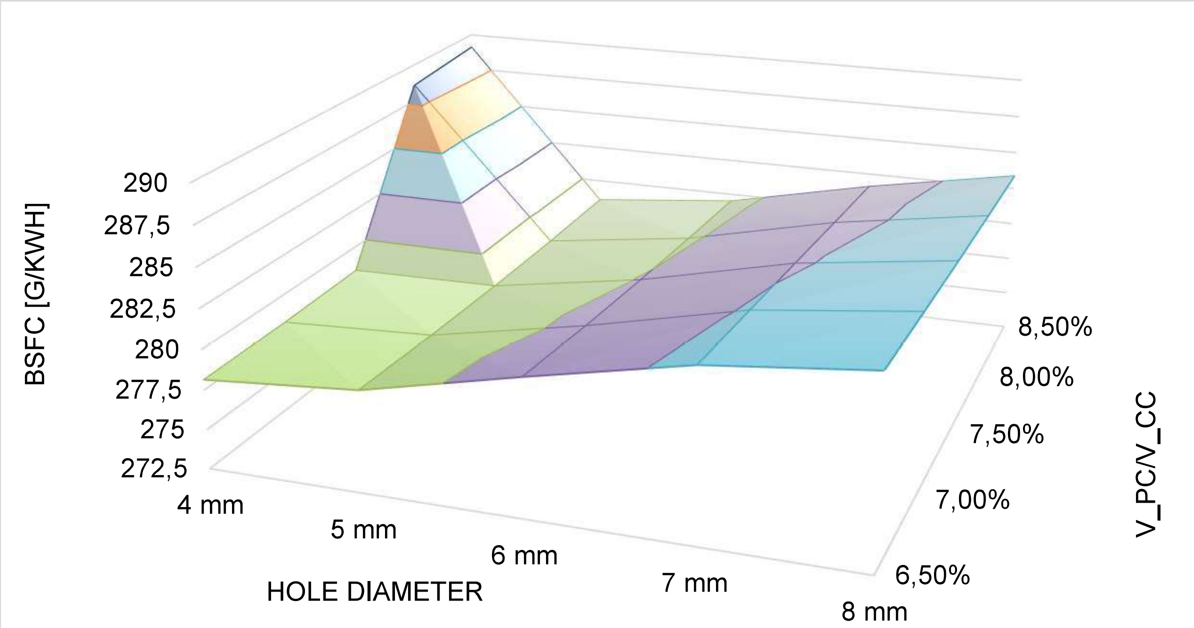

Figure 4.24 – Trend map of BSFC behavior as a function of hole diameter and pre-chamber volume for predictive model 38 with prechamber and lambda 1.10 at 2500 rpm.
Source: Author

4.2.3 ANALYSIS AND FINAL CONSIDERATIONS ON THE RESULTS

It was possible to verify that the non-predictive models after their calibration obtained percentage errors of less than 5.0% for all evaluated parameters, which shows a good convergence of the numerical results compared to the experimental data. As verified by several works mentioned in the literature review, it was possible to see that the use of prechambers tends to improve the performance of engines compared to baseline engines. It was also possible to verify that the use of prechambers allows working with leaner mixtures and keeping the engine's performance and fuel consumption parameters constant.

As in the case of the non-predictive model, the predictive models presented a convergent result and with an error below 5.0%. After the multiple simulations carried out for both predictive cases, it was possible to verify that for all evaluated parameters the engine is more sensitive to variations in the diameter of the pre-chamber hole than to variations in its volume. It was also observed, for all simulated volumes, a trend towards an increase in power, torque and IMEP and a reduction in specific fuel consumption as the diameter of the pre-chamber orifice was reduced.

However, a break in the trend that occurred for cases combining the largest volume prechambers with the smallest orifice diameters was noted. In other words, in these cases, the reduction in diameter caused an increase in fuel consumption and a reduction in power, torque and IMEP. Table 4.11 shows the cases that presented this change in the trend of results.

Table 4.11 – Cases that presented this change in the trend of predictive results. Source: Author

Case	Volume [V_pc/V_cc]	Diameter [mm]
28 with prechamber and lambda 1.10	8,50%	4
38 with prechamber and lambda 1.10	8,0 % and 8,5 %	4

In order to verify the possible reasons for this change in trend in the simulation results, we sought to verify the influence of pressures inside the prechamber and the exit velocities of the burned gases from the prechamber to the main chamber. As can be seen in Figure 4.25 and Figure 4.26, the exit velocity of the burned gases between the prechamber and the main combustion chamber is strongly dependent on the prechamber orifice diameter and increases as this diameter decreases. It is also noted that the increase in prechamber volume also causes an increase in this exit speed.

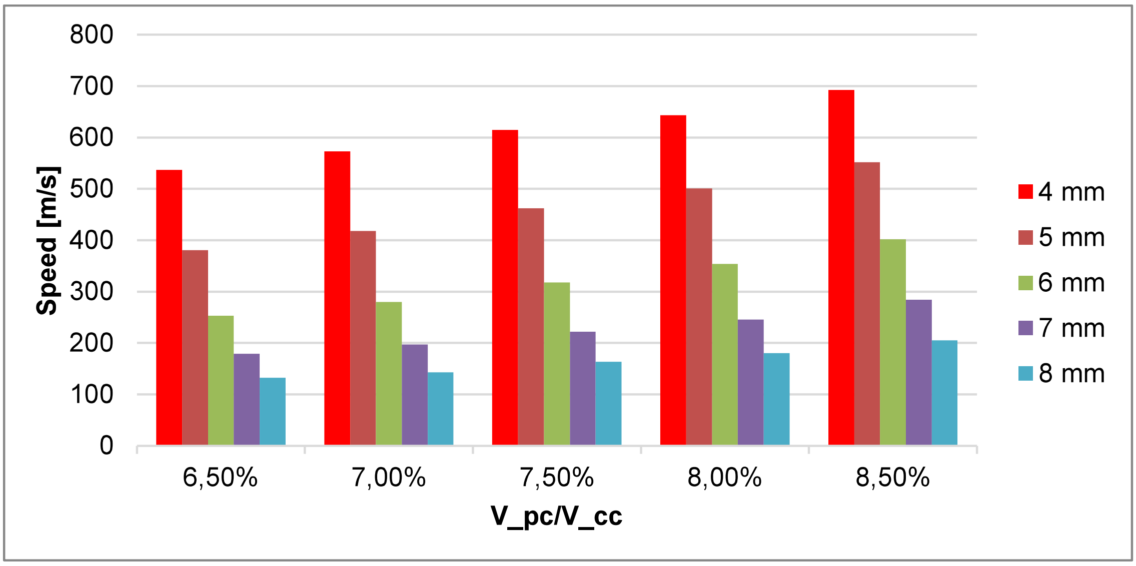

Figure 4.25 – Exit speed of gases from the prechamber to the main chamber for model 28 with prechamber and lambda 1.10. Source: Author

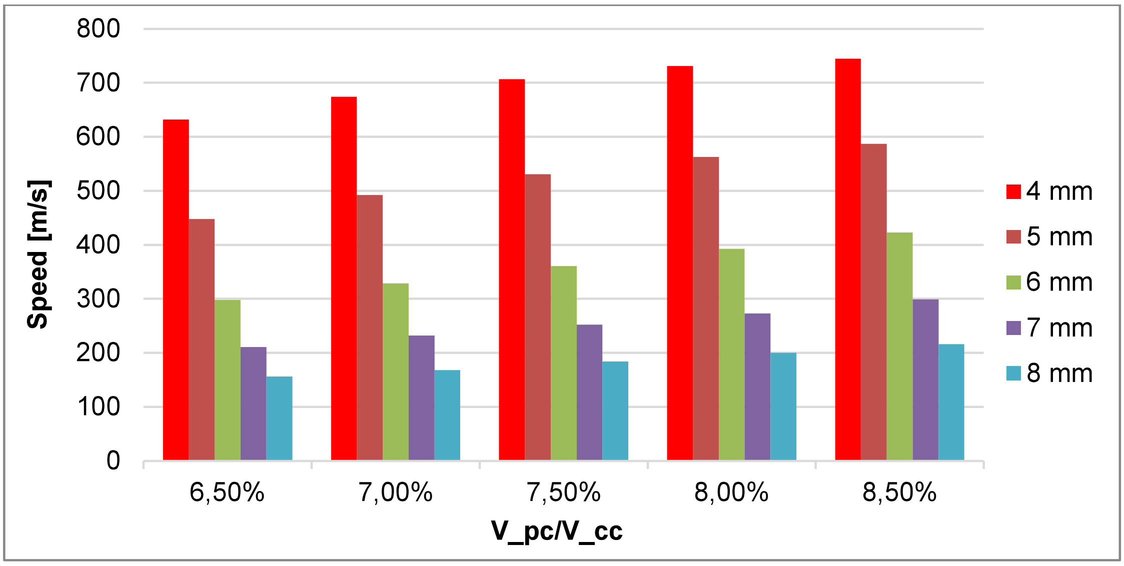

Figure 4.26 – Exit speed of gases from the prechamber to the main chamber for model 38 with prechamber and lambda 1.10. Source: Author

In Figure 4.27 and Figure 4.28 it can be seen that pressure is also affected by hole diameter and prechamber volume in a similar way as speed.

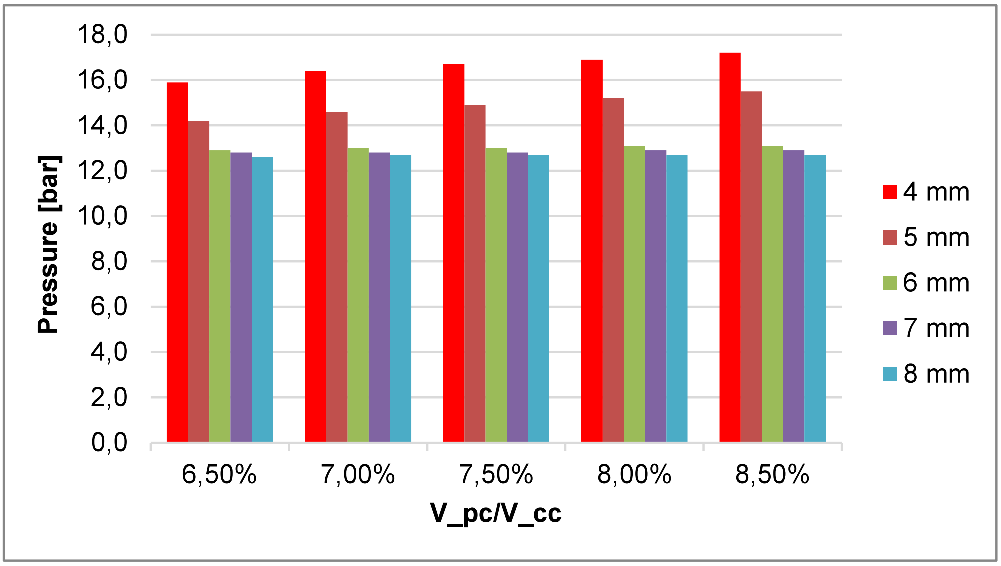

Figure 4.27 - Pressure inside the prechamber as a function of its hole diameter and volume for model 28 with prechamber and lambda 1.10. Source: Author

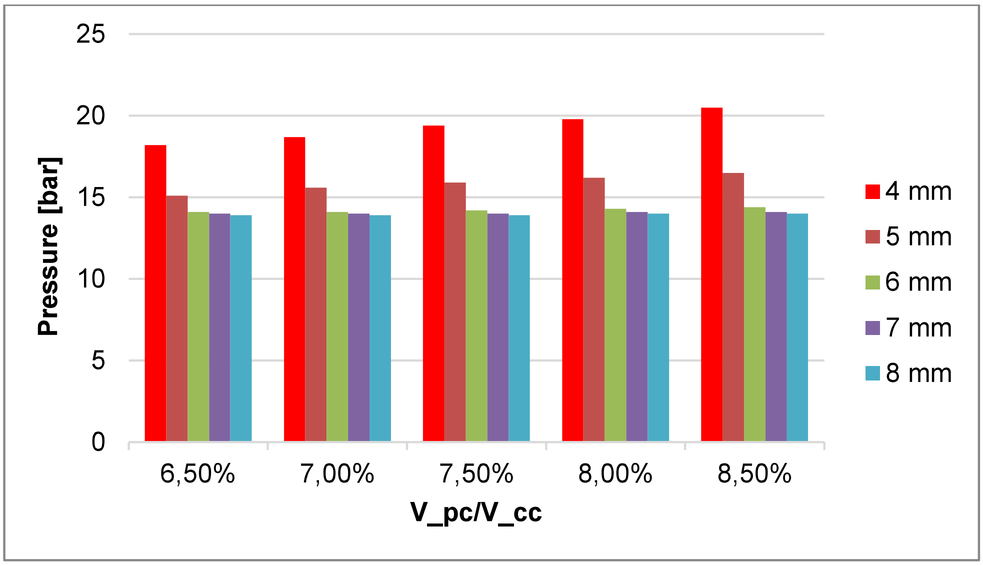

Figure 4.28 - Pressure inside the prechamber as a function of its hole diameter and volume for model 38 with prechamber and lambda 1.10. Source: Author

Based on the simulated information on the temperature inside the prechamber and the composition of the burned gases that exit through its orifice, the speed of sound in this environment was calculated for each of the simulated conditions. The result of calculating these speeds is shown in Table 4.12 and Table 4.13. Furthermore, these tables relate the prechamber exit velocities in each case with their respective speed of sound.

Table 4.12 – Speed of sound for the 25 combinations simulated using the predictive model 28 with prechamber and lambda 1.10. Source: Author

Volume		Diameter														
		4 mm			5 mm			6 mm			7 mm			8 mm		
Volume [cm³]	V_pc / V_cc	Speed [m/s]	Speed of Sound [m/s]	Mach	Speed [m/s]	Speed of Sound [m/s]	Mach	Speed [m/s]	Speed of Sound [m/s]	Mach	Speed [m/s]	Speed of Sound [m/s]	Mach	Speed [m/s]	Speed of Sound [m/s]	Mach
2593	6,5%	537	719	0,75	381	698	0,55	253	725	0,35	179	713	0,25	133	733	0,18
2793	7,0%	573	737	0,78	418	714	0,59	280	724	0,39	197	724	0,27	143	748	0,19
2993	7,5%	615	745	0,83	462	722	0,64	318	729	0,44	222	732	0,30	164	761	0,22
3193	8,0%	643	745	0,86	501	741	0,68	354	731	0,48	246	739	0,33	180	758	0,24
3393	8,5%	694	759	0,91	552	740	0,75	402	737	0,55	284	744	0,38	205	773	0,27

Table 4.13 – Speed of sound for the 25 combinations simulated using the predictive model 38 with prechamber and lambda 1.10. Source: Author

Volume		Diameter														
		4 mm			5 mm			6 mm			7 mm			8 mm		
Volume [cm³]	V_pc / V_cc	Speed [m/s]	Speed of Sound [m/s]	Mach	Speed [m/s]	Speed of Sound [m/s]	Mach	Speed [m/s]	Speed of Sound [m/s]	Mach	Speed [m/s]	Speed of Sound [m/s]	Mach	Speed [m/s]	Speed of Sound [m/s]	Mach
2593	6,5%	632	765	0,83	448	759	0,59	298	766	0,39	211	784	0,27	156	788	0,20
2793	7,0%	674	776	0,87	492	768	0,64	329	767	0,43	232	787	0,29	168	813	0,21
2993	7,5%	707	786	0,90	531	777	0,68	361	775	0,47	252	795	0,32	184	812	0,23
3193	8,0%	731	796	0,92	563	786	0,72	393	778	0,50	273	795	0,34	200	813	0,25
3393	8,5%	745	803	0,93	587	794	0,74	423	782	0,54	299	797	0,37	216	814	0,27

Based on the exit speed of the burned gases from the prechamber to the main chamber and the speed of sound for each simulated case, Figure 4.29 and Figure 4.30 relate these velocities for each of the simulated points. It can be noted that for all Cases that presented this change in trend, shown in Table 4.11, the exit velocities of the burned gases from the pre-chamber to the main chamber are very close to the respective speed of sound for this case.

Taking into account the ranges covered by the 5.0% margin of error that was considered for the previous calibration of the models, we can state that a possible cause of the change in the trend of the simulated results was that the speed of sound was reached in these scenarios, and therefore an increase in the volume of the pre-chamber or a reduction in the diameter of its orifice cannot bring more benefits to engine's performance, as in previous cases.

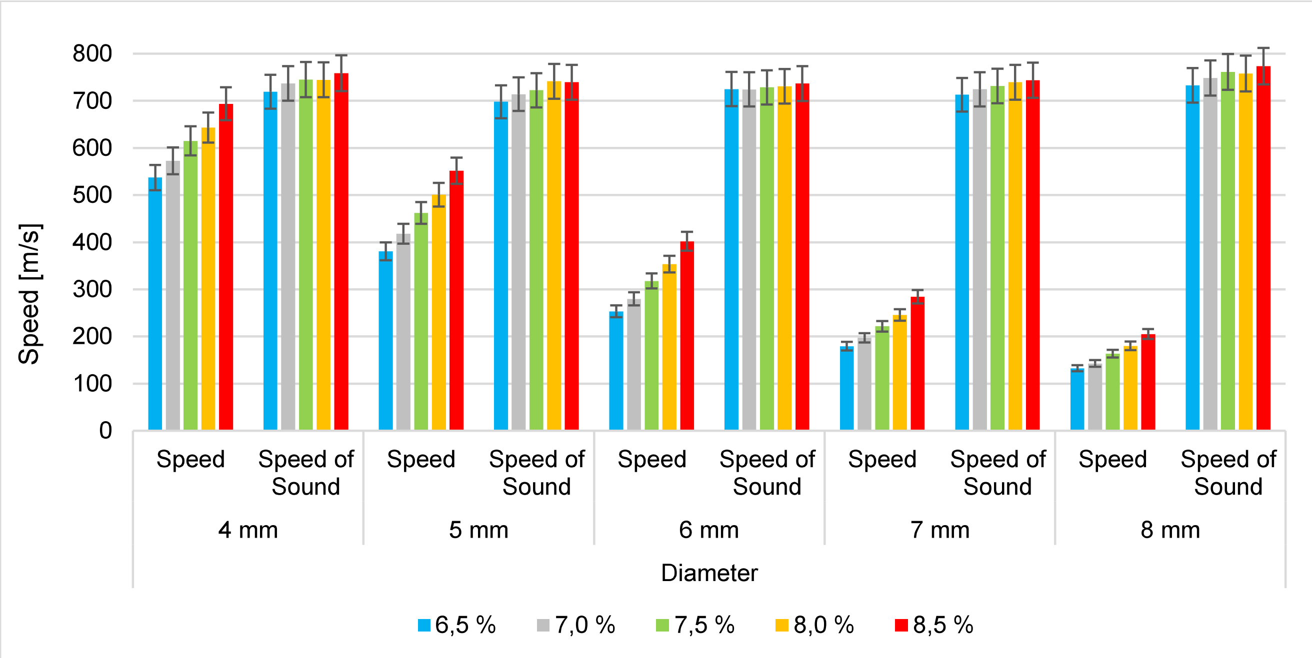

Figure 4.29 – Comparison between the exit velocity from the prechamber to the main chamber and the speed of sound for each case using the predictive model 28 with prechamber and lambda 1.10. Source: Author

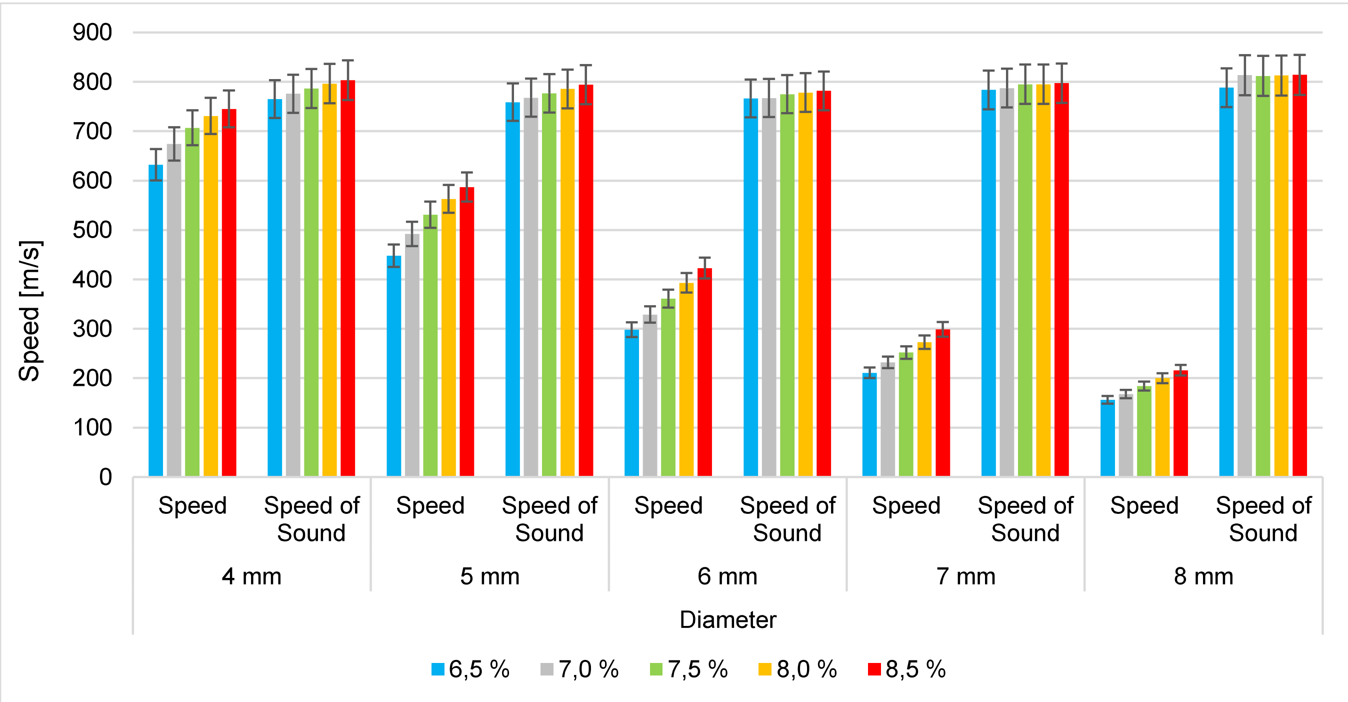

Figure 4.30 – Comparison between the exit velocity from the prechamber to the main chamber and the speed of sound for each case using the predictive model 38 with prechamber and lambda 1.10. Source: Author

From the results of the predictive models, discussed in this section, it can be inferred that there must be a pair of bore diameter and prechamber volume that offers the best performance to the engine, and it can also be seen that these parameters can be interfered by the load at which the engine operates.

It was also noted that the reduction in the diameter of the prechamber hole caused an increase in pressure inside it, however this increase in pressure does not convert into an increase in the exit speed of hot gases from this to the main chamber, as these gases end up being held back by the reduced diameter and also by not being able to exceed the speed of sound in these conditions of temperature and pressure.

To better understand this phenomenon, one-dimensional models are limited, and the use of three-dimensional modeling and computational fluid dynamics are more appropriate. Furthermore, mapping these critical points through predictive simulations can be useful in directing studies that evaluate them experimentally.

5 CONCLUSIONS AND SUGGESTIONS FOR FUTURE WORK

This chapter presents the main discussions and conclusions regarding the results obtained throughout this research and, based on the results obtained, some possible guidelines for continuing studies are suggested, in order to improve understanding of the topics covered.

5.1 CONCLUSIONS

The main objectives established at the beginning of the work were achieved, both general and specific objectives.

With the need to mitigate greenhouse gas emissions caused by engines without compromising their performance and flexibility, the use prechambers of combustion has a lot to contribute to this objective. In this regard computer simulations play an essential role, as they can reduce the cost and time of research and can be used together with experimental research.

The models simulated by the non-predictive method proved to be effective in simulating performance parameters and specific fuel consumption, requiring low computational effort. On the other hand, this methodology depends on providing pressure data inside the cylinder among other experimental data, a fact that requires expensive measuring equipment and a large mass of data for calibration and validation of the model. The effectiveness of the applied numerical method is evidenced by the low percentage errors found in the results, all below 5.0%, and as mentioned in the literature review, these numerical errors are consistent with expectations.

As for the models simulated by the predictive method, their results proved to be very useful for understanding the behavior of the pre-chambers in scenarios not analyzed experimentally. Despite the advantages, predictive simulations also present some errors and are much more expensive from the point of view of computational effort.

Compared to non-predictive models, predictive models proved to be very useful because they allowed, after calibration, the simulation of geometric variations that had not been tested on the bench and were therefore able to predict the operation of engines under these conditions. This use of predictive models, together with experimental studies, demonstrates great potential to contribute to technological and scientific development with the advantage of reducing costs related to experimental studies.

The literature review gave evidence that smaller prechamber hole diameters tend to present better performance and efficiency results. In this context, the main conclusion that could be drawn from the variations in volume and diameter of the prechamber orifice, made possible by the use of the predictive model, is that this reduction in diameter cannot be done indefinitely and that there is an optimum point beyond which any reduction in diameter causes more harm than good to the engine's performance. There are also other effects of reducing diameters that certainly interfere with engine performance and that were not evaluated in this work, including air inlet, and scavenging of burnt gases from the prechamber during its operation.

It was evident based on the predictive results that for each engine load there will be an optimal combination of diameter and volume of the pre-chambers that will enable better equipment performance. For this reason, more in-depth studies must be carried out to determine these conditions for each type of engine, vehicle and conditions of use, combined with the use in conjunction with other engineering solutions such as the CVT transmission, which allows for better control of the operating range of vehicle engines and can facilitate the commercial application of pre-chambers.

5.2 SUGGESTIONS FOR FURTHER WORK

Based on the results obtained in this work and its analysis, it was possible to prepare proposals for future work that will contribute to the development of the research theme carried out, and they are:

- Replication of the work carried out, using the same proposed model, with other fuels: ethanol, natural gas, etc.

- Improvement of simulations in regions close to the optimal geometric limits using the numerical data generated in the present work to define new pre-chamber geometries and configurations of interconnection holes to be subsequently tested experimentally.

- Creation of a predictive model for combustion in the prechamber.

6 BIBLIOGRAPHIC REFERENCES

ANFAVEA. **Anuário da Indústria Automobilística Brasileira**. São Paulo: [s.n.]. Disponível em: <https://anfavea.com.br/anuario2021/anuario.pdf>. Acesso em: 25 de abril de 2022.

ANP - Anuário Estatístico 2020 - Dados Abertos. Disponível em: <https://www.gov.br/anp/pt-br/centrais-de-conteudo/dados-abertos/anuario-estatistico-2020-dados-abertos>. Acesso em: 1 out. 2023.

AVELAR, Fausto Torres Magalhães. Desenvolvimento de um modelo unidimensional para simulação de desempenho e emissões de um motor ciclo Otto Ford Sigma 1.6 16V. Pós-Graduação em Engenharia da Energia, Centro Federal de Educação Tecnológica de Minas Gerais, 2018, 117p.

BAETA, J. G. C. Metodologia experimental para maximização do desempenho de um motor multi-combustível turboalimentado sem prejuízo à eficiência energética global. Tese de Doutorado. Programa de Pós-graduação em Engenharia Mecânica - UFMG. Belo Horizonte - MG. 2006, 202 p.

EMBRAPA. Balanço de emissões de CO2 por biocombustíveis no Brasil: histórico e perspectivas. - Portal Embrapa. Disponível em: <https://www.embrapa.br/busca-de-publicacoes/-/publicacao/987401/balanco-de-emissoes-de-co2-por-biocombustiveis-no-brasil-historico-e-perspectivas>. Acesso em: 1 out. 2023.

BENAJES, Jesús et al. Evaluation of the passive pre-chamber ignition concept for future high compression ratio turbocharged spark-ignition engines. **Applied Energy**, v. 248, p. 576-588, 2019.

BENAJES, Jesús et al. Computational assessment towards understanding the energy conversion and combustion process of lean mixtures in passive pre-chamber ignited engines. **Applied Thermal Engineerin**g, v. 178, p. 115501, 2020.

BP GROUP. Statistical Review of World Energy 2021. London: [s.n.]. Disponível em: <https://www.bp.com/content/dam/bp/business-sites/en/global/corporate/pdfs/energy-economics/statistical-review/bp-stats-review-2021-full-report.pdf>. Acesso em: 24 de abril de 2022.

BURESHAID, K. et al. Experimental Studies of the Effect of Ethanol Auxiliary Fueled Turbulent Jet Ignition in an Optical Engine. **Source: SAE International Journal of Engines**, v. 12, n. 4, p. 387–400, 2019a.

BURESHAID, K. et al. Combustion and emissions of gasoline, anhydrous ethanol, and wet ethanol in an optical engine with a turbulent jet ignition system. **Proceedings of the Institution of Mechanical Engineers, Part D: Journal of Automobile Engineering**, v. 233, n. 13, p. 3528–3537, 1 nov. 2019b.

BURKARDT, Patrick; WOUTERS, Christian; PISCHINGER, Stefan. Potential of alcohol fuels in active and passive pre-chamber applications in a passenger car spark-ignition engine. **International Journal of Engine Research**, p. 14680874211053168, 2021.

CHEN, L. et al. Optical experiments on the effect of turbulent jet ignition on lean burning and engine knocking. **Fuel**, v. 307, 1 jan. 2022.

CHINNATHAMBI, Prasanna. Performance metrics for fueled and unfueled turbulent jet igniters in a rapid compression machine. **Applyed Thermal Engeneering**, v. 182, p. 115893, 2021.

CRUZ, C. H. DE B. et al. **Universidades e empresas: 40 anos de ciência e tecnologia para o etanol brasileiro**. São Paulo: Editora Edgard Blücher Ltda, 2016a.

CRUZ, I. W. S. L. et al. Zero-dimensional mathematical model of the torch ignited engine. **Applied Thermal Engineering**, v. 103, p. 1237–1250, 25 jun. 2016b.

Duan, W., Huang, Z., Chen, H., Tang, P., Wang, L., & Chen, W. (2021). Effects of passive pre-chamber jet ignition on combustion and emission at gasoline engine. Advances in Mechanical Engineering, 13(12). https://doi.org/10.1177/16878140211067148

GAMMA TECHNOLOGIES. GT-SUITE: Engine Performance Tutorials. Gamma Technologies, 2022. Version 7.6. Access in: 15 Jun. 2023

GAMMA TECHNOLOGIES. GT-SUITE: Flow Theory Manual. Gamma Technologies, 2022.Version 7.6. Access in: 15 Jun 2023

HEYWOOD, John B. Internal Combustion Engine Fundamentals. 1 ed. New York McGraw-Hill, Inc., 1998. 930 p.

HEYWOOD, John. B. Internal Combustion Engine Fundamentals. McGraw-Hill Education. 2ed, 2018.

HILOIDHARI, M. et al. Life cycle energy–carbon–water footprints of sugar, ethanol and electricity from sugarcane. Bioresource technology, v. 330, n. 125012, p. 125012, 2021.

HUA, Jianxiong et al. Effects on cycle-to-cycle variations and knocking combustion of turbulent jet ignition (TJI) with a small volume pre-chamber. **SAE Technical Paper**, 2020.

HUA, Jianxiong et al. Influence of pre-chamber structure and injection parameters on engine performance and combustion characteristics in a turbulent jet ignition (TJI) engine. **Fuel**, v. 283, p. 119236, 2021a.

INMETRO – Instituto Nacional de Metrologia (2019) Qualidade e Tecnologia: Programa Brasileiro de Etiquetagem: Tabela de consumo e eficiência energética. http://www.inmetro.gov.br/consu midor /pbe/veicu los_leves 2018.pdf. Accessed 1 Mar 2019

JANKOWSKI, A.; KOWALSKI, M. Environmental pollution caused by a direct injection engine. **Journal of KONES Powertrain and Transport**, v. 22, n. 4, p. 133–138, 2015.

KHEYROLLAHI, Javad et al. Improvement of performance and emission in a lean-burn gas fueled spark ignition engine by using a new pre-chamber. **Environmental Progress & Sustainable Energy**, v. 40, n. 5, p. e13637, 2021.

LIMA, B. S. Modelagem Tridimensional da Combustão em um Motor Adaptado com Pré-câmara. Pós-Graduação em Engenharia Mecânica, Universidade Federal de Minas Gerais, 2018

MALAQUIAS, A. C. T.; NETTO, N. A. D., RODRIGUES FILHO, F. A.; COSTA, R. B. R.; LANGEANI, M.; BAETA, J. G. C. "The misleading total replacement of internal combustion engines by electric motors and a study of the Brazilian ethanol importance for the sustainable future of mobility: a review," J. Brazilian Soc. Mech. Sci. Eng., vol. 41, no. 12, p. 567, 2019.

MASERATI - EUROPEAN PATENT SPECIFICATION - 2019. Gasoline internal combustion engine, with a combustion pre-chamber and two spark plugs. Benzinverbrennungsmotor mit einer verbrennungsvorkammer und zwei zündkerzen moteur à combustion interne à essence, comprenant une préchambre de combustion et deux bougies d'allumage. https://data.epo.org/publication-server/document?iDocId=6063079&iFormat=2

ONOFRIO, Gessica et al. Combustion sensitivity to the nozzle hole size in an active pre-chamber ultra-lean heavy-duty natural gas engine. **Energy**, v. 235, p. 121298, 2021.

QIAO, Li. Ignition of ultra-lean premixed H2/air using multiple hot turbulent jets generated by pre-chamber combustion. **Applied Thermal Engeneering**, v. 132, p 102-114, 2018.

Reitz, R. D., Ogawa, H., Payri, R., Fansler, T., Kokjohn, S., Moriyoshi, Y., Agarwal, A. K., Arcoumanis, D., Assanis, D., Bae, C., Boulouchos, K., Canakci, M., Curran, S., Denbratt, I., Gavaises, M., Guenthner, M., Hasse, C., Huang, Z., Ishiyama, T., … Zhao, H. (2020). IJER editorial: The future of the internal combustion engine. In International Journal of Engine Research (V. 21, Issue 1, pp. 3-10). SAGE Publications Ltd. https://doi.org/10.1177/1468087419877990

RODRIGUES FILHO, F. A. 2014. Projeto, construção e caracterização do desempenho de um motor de combustão interna provido de um sistema de ignição por lança chamas de carga estratificada. Belo Horizonte. Pós-Graduação em Engenharia Mecânica, Universidade Federal de Minas Gerais, 2014.

RODRIGUES FILHO, F. BAETA, J. TEIXEIRA, A. VALLE, R. SOUZA, J. E25 stratified torch ignition engine emissions and combustion analysis. Energy Conversion and Management. v. 121, 2016.

ROSO, Vinícius Rückert et al. Evaluation of a stratified prechamber ignition concept for vehicular applications in real world and standardized driving cycles. **Applied Energy**, v. 254, p. 113691, 2019.

SANDOVAL, M. Humberto Barrientos. 2018. Análise numérica da combustão em um motor de ignição por centelha com pré-câmaras de diferentes geometrias operado com etanol. Belo Horizonte. Pós-Graduação em Engenharia Mecânica, Universidade Federal de Minas Gerais, 2018.

SANTOS, NATHÁLIA DUARTE SOUZA ALVARENGA. 2023. Development and characterization of a stratified turbulent jet ignition system using a dedicated pre-chamber with a focus on reducing fuel consumption using alcohol fuels. Belo Horizonte. Pós-Graduação em Engenharia Mecânica, Universidade Federal de Minas Gerais, 2023.

SENS, Marc; BINDER, Emanuel. Pre-chamber ignition as a key technology for future powertrain fleets. **MTZ worldwide**, v. 80, n. 2, p. 44-51, 2019.

SILVA, Mickael et al. Effects of geometry on passive pre-chamber combustion characteristics. **SAE Technical Paper**, 2020.

TANG, Qinglong, et al. Study on the effects of narrow-throat pre-chamber geometry on the pre-chamber jet velocity using dual formaldehyde PLIF imaging. **Combustion and Flame**, v. 240, p. 111987, 2022

VERA-TUDELA, Walter; BARRO, Christophe; BOULOUCHOS, Konstantinos. Investigations on spark pre-chamber ignition and subsequent turbulent jet main chamber ignition in a novel optically accessible test rig. **International Journal of Engine Research**, p. 14680874211019849,2021.

WOSCHNI, G. "A Universally Applicable Equation for the Instantaneous Heat Transfer Coefficient in the Internal Combustion Engine". SAE paper # 670931, 1967.

ZHOU, L. et al. Effects of different hole structures of pre-chamber with turbulent jet ignition on the flame propagation and lean combustion performance of a single-cylinder engine. **Fuel**, v. 308, 15 jan. 2022.

ANNEX 1 – RESULT TABLES AND PRESSURE CURVES

This annex presents the P x V diagrams, pressure curves and results table for all simulated non-predictive models. Compared to experimental data used for model calibration. Such experimental results were produced by Rodrigues Filho, 2014, and used with permission.

28 – Baseline with lambda 1,00

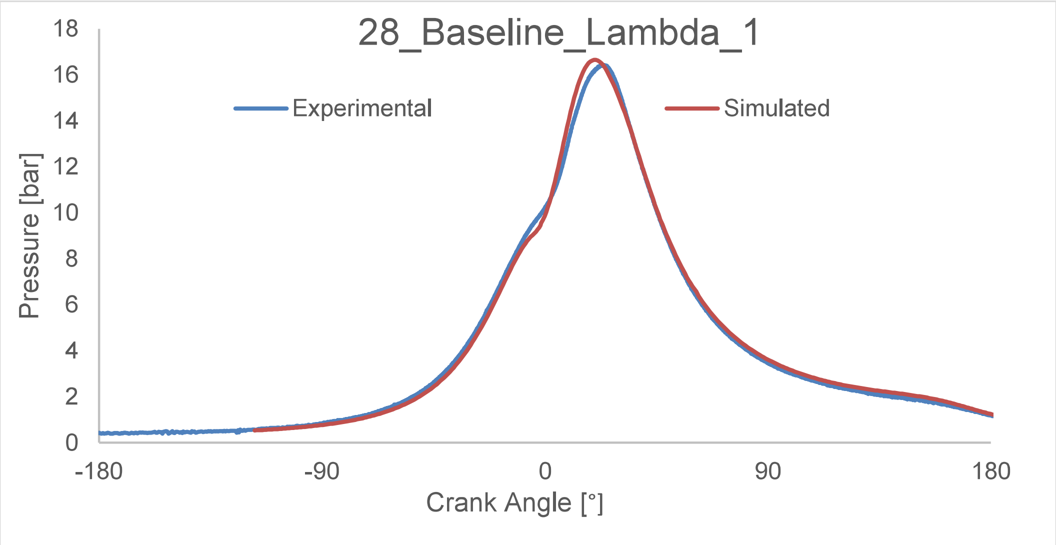

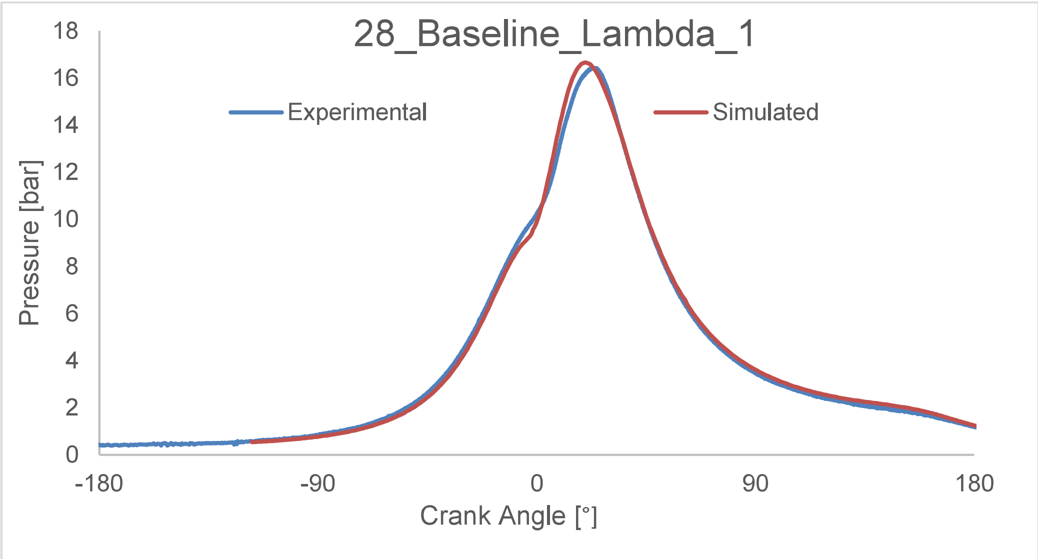

Simulated					
Power [kW]	Torque [N.m]	BSFC [g/kW.h]	Fuel Flow [kg/h]	Air Flow [kg/h]	IMEP [bar]
11,14	42,55	336,29	3,35	43,85	3,79

Experimental					
Power [kW]	Torque [N.m]	BSFC [g/kW.h]	Fuel Flow [kg/h]	Air Flow [kg/h]	IMEP [bar]
11,52	43,98	332	3,419	45,3	3,66

Error					
Power [kW]	Torque [N.m]	BSFC [g/kW.h]	Fuel Flow [kg/h]	Air Flow [kg/h]	IMEP [bar]
-3,30%	-3,25%	1,29%	-2,02%	-3,20%	3,55%

28 – With prechamber and lambda 1,00

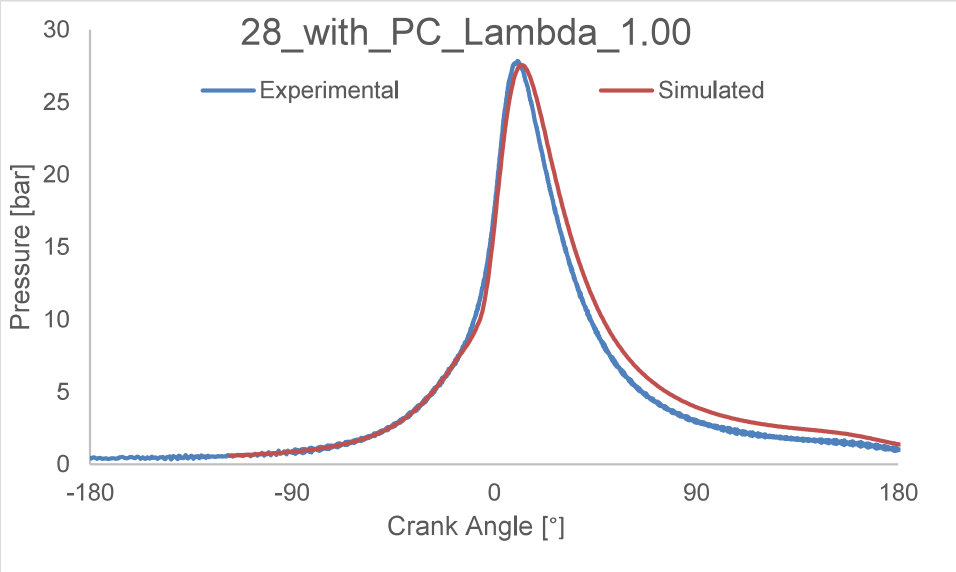

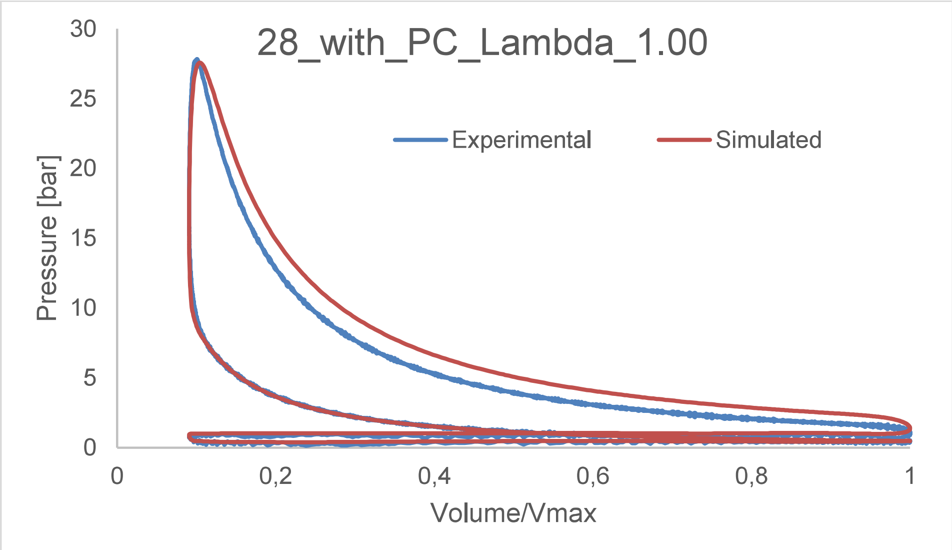

Simulated					
Power [kW]	Torque [N.m]	BSFC [g/kW.h]	Fuel Flow [kg/h]	Air Flow [kg/h]	IMEP [bar]
11,03	42,13	318,9	3,51	47,36	4,44

Experimental					
Power [kW]	Torque [N.m]	BSFC [g/kW.h]	Fuel Flow [kg/h]	Air Flow [kg/h]	IMEP [bar]
11,53	44,04	328	3,411	45,2	4,4550049

Erro					
Power [kW]	Torque [N.m]	BSFC [g/kW.h]	Fuel Flow [kg/h]	Air Flow [kg/h]	IMEP [bar]
-4,34%	-4,34%	-2,77%	2,90%	4,78%	-0,34%

28 – With prechamber and lambda 1,10

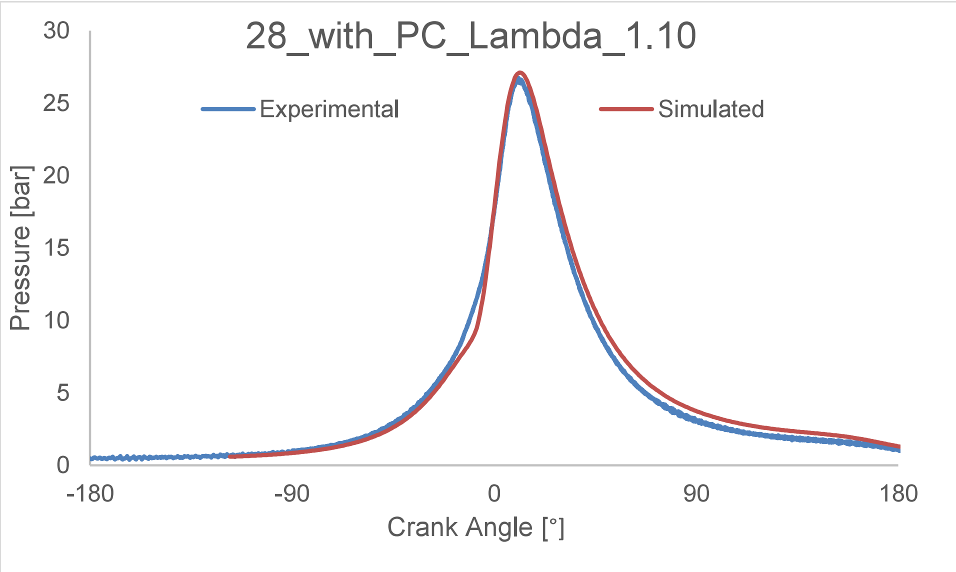

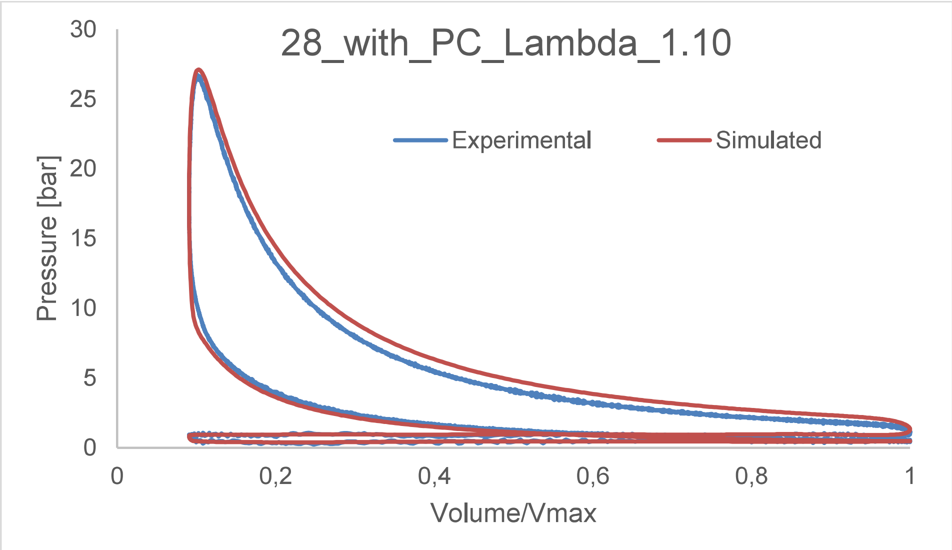

Simulated					
Power [kW]	Torque [N.m]	BSFC [g/kW.h]	Fuel Flow [kg/h]	Air Flow [kg/h]	IMEP [bar]
11,19	42,75	312,32	3,49	50,31	4,44

Experimental					
Power [kW]	Torque [N.m]	BSFC [g/kW.h]	Fuel Flow [kg/h]	Air Flow [kg/h]	IMEP [bar]
11,77	44,96	313	3,325	48,5	4,23

Error					
Power [kW]	Torque [N.m]	BSFC [g/kW.h]	Fuel Flow [kg/h]	Air Flow [kg/h]	IMEP [bar]
-4,93%	-4,92%	-0,22%	4,96%	3,73%	4,88%

28 – With prechamber and lambda 1,20

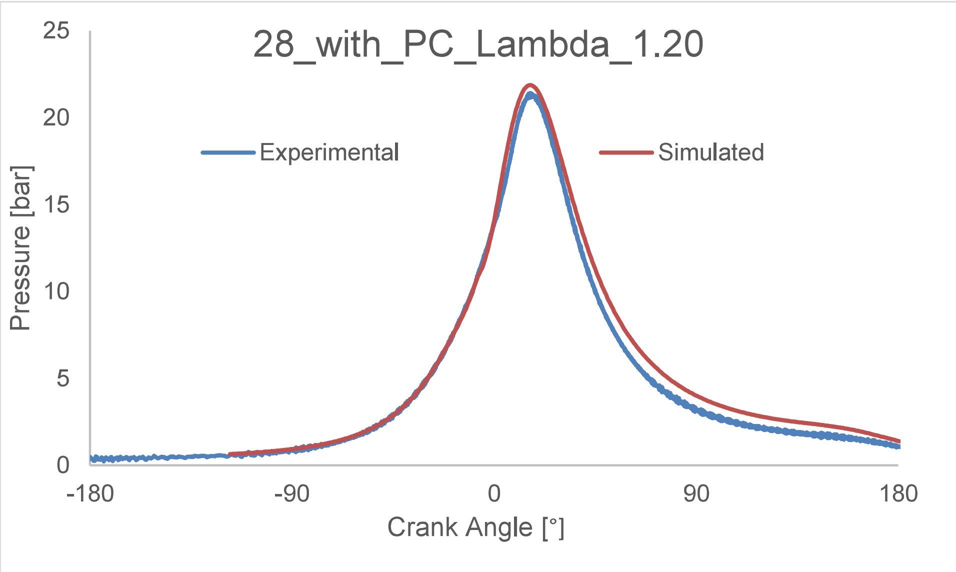

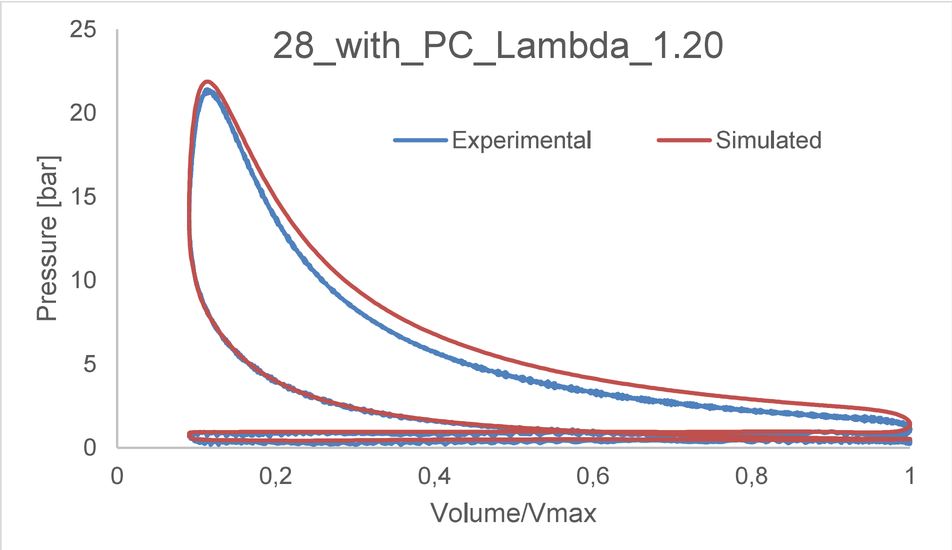

Simulated					
Power [kW]	Torque [N.m]	BSFC [g/kW.h]	Fuel Flow [kg/h]	Air Flow [kg/h]	IMEP [bar]
10,98	42,14	320,85	3,42	53,94	4,4

Experimental					
Power [kW]	Torque [N.m]	BSFC [g/kW.h]	Fuel Flow [kg/h]	Air Flow [kg/h]	IMEP [bar]
11,53	44,23	314	3,265	51,4	4,5268115

Error					
Power [kW]	Torque [N.m]	BSFC [g/kW.h]	Fuel Flow [kg/h]	Air Flow [kg/h]	IMEP [bar]
-4,77%	-4,73%	2,18%	4,75%	4,94%	-2,80%

28 – With prechamber and lambda 1,30

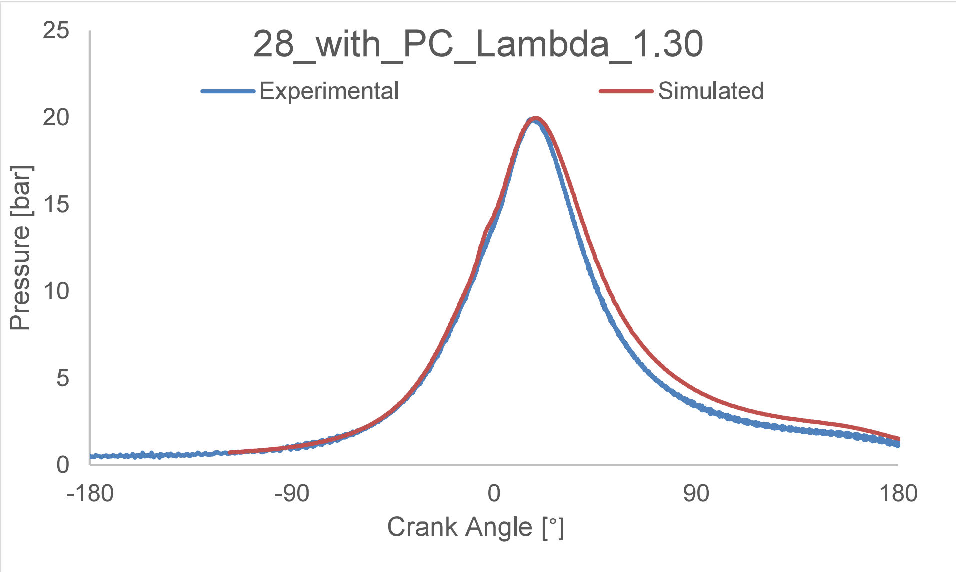

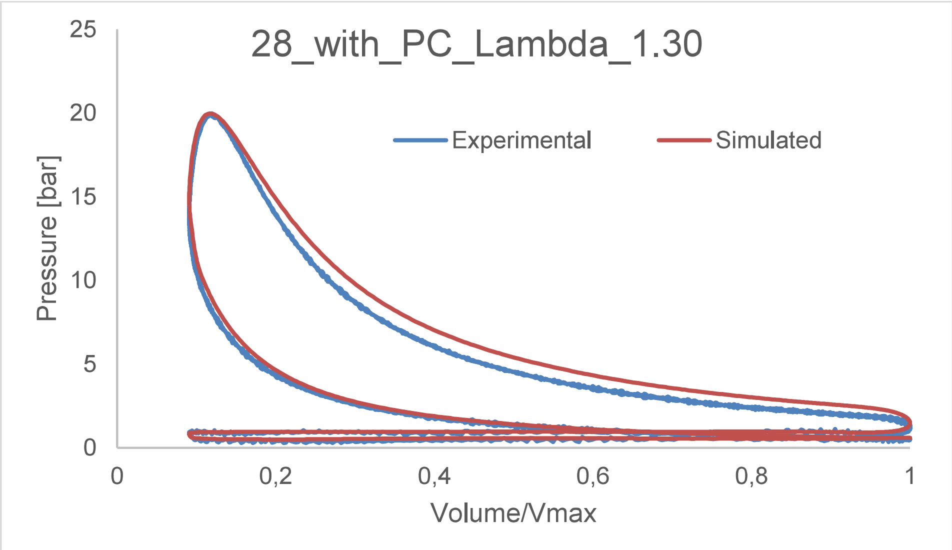

Simulated					
Power [kW]	Torque [N.m]	BSFC [g/kW.h]	Fuel Flow [kg/h]	Air Flow [kg/h]	IMEP [bar]
11,27	43,06	320,67	3,41	58,13	4,32

Experimental					
Power [kW]	Torque [N.m]	BSFC [g/kW.h]	Fuel Flow [kg/h]	Air Flow [kg/h]	IMEP [bar]
11,62	44,38	312	3,26	55,6	4,1369724

Erro					
Potência	Torque	BSFC	Vazão comb.	Vazão Ar	IMEP
-3,01%	-2,97%	2,78%	4,60%	4,55%	4,42%

38 – Baseline with lambda 1,00

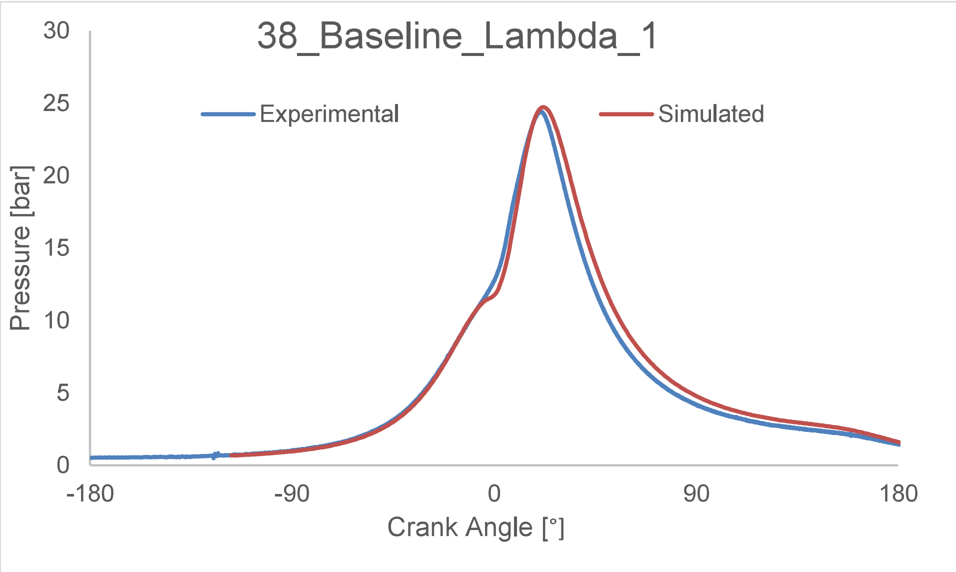

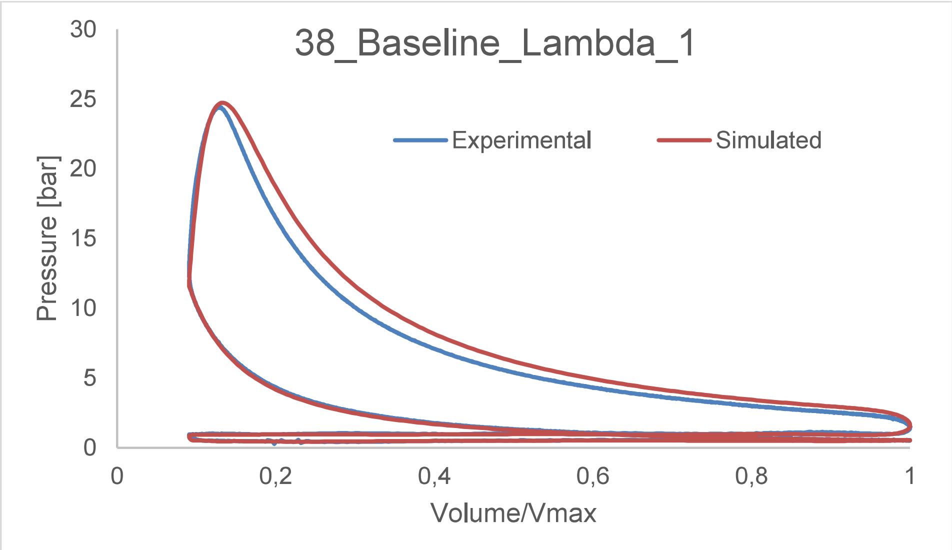

Simulated					
Power [kW]	Torque [N.m]	BSFC [g/kW.h]	Fuel Flow [kg/h]	Air Flow [kg/h]	IMEP [bar]
14,51	55,42	296,31	4,29	56,16	5,41

Experimental					
Power [kW]	Torque [N.m]	BSFC [g/kW.h]	Fuel Flow [kg/h]	Air Flow [kg/h]	IMEP [bar]
14,63	58,53	299	4,112	54,5	5,1986731

Error					
Power [kW]	Torque [N.m]	BSFC [g/kW.h]	Fuel Flow [kg/h]	Air Flow [kg/h]	IMEP [bar]
-0,82%	-5,31%	-0,90%	4,33%	3,05%	4,07%

38 – With prechamber and lambda 1,00

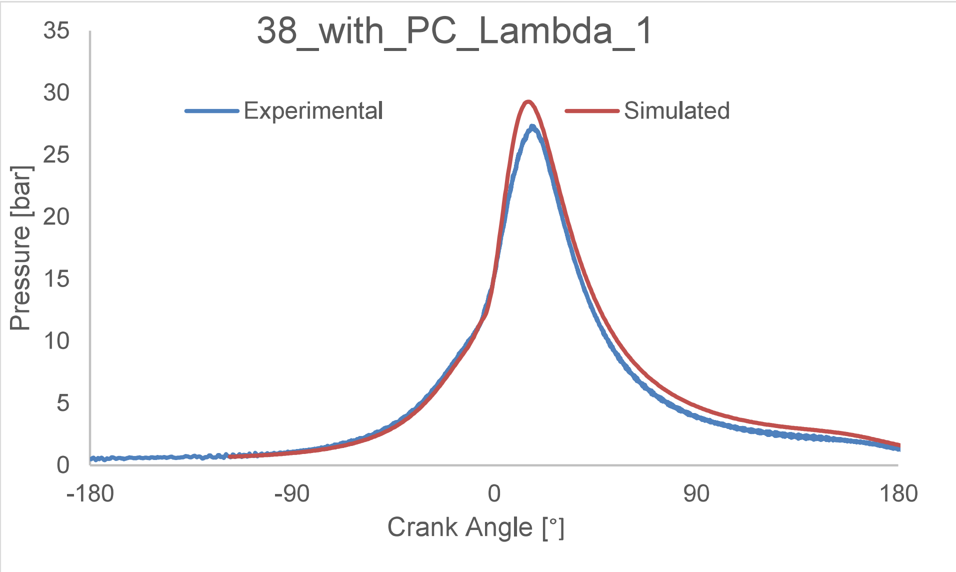

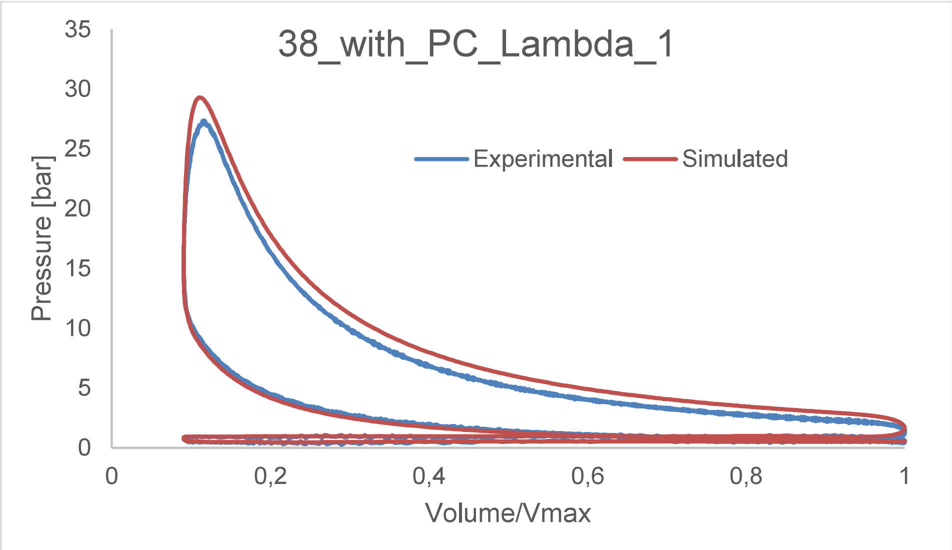

Simulated					
Power [kW]	Torque [N.m]	BSFC [g/kW.h]	Fuel Flow [kg/h]	Air Flow [kg/h]	IMEP [bar]
14,59	55,73	290,8	4,24	57,15	5,55

Experimental					
Power [kW]	Torque [N.m]	BSFC [g/kW.h]	Fuel Flow [kg/h]	Air Flow [kg/h]	IMEP [bar]
15,28	58,38	299	4,163	55,2	5,42

Error					
Power [kW]	Torque [N.m]	BSFC [g/kW.h]	Fuel Flow [kg/h]	Air Flow [kg/h]	IMEP [bar]
-4,52%	-4,54%	-2,74%	1,85%	3,53%	2,40%

38 – With prechamber and lambda 1,10

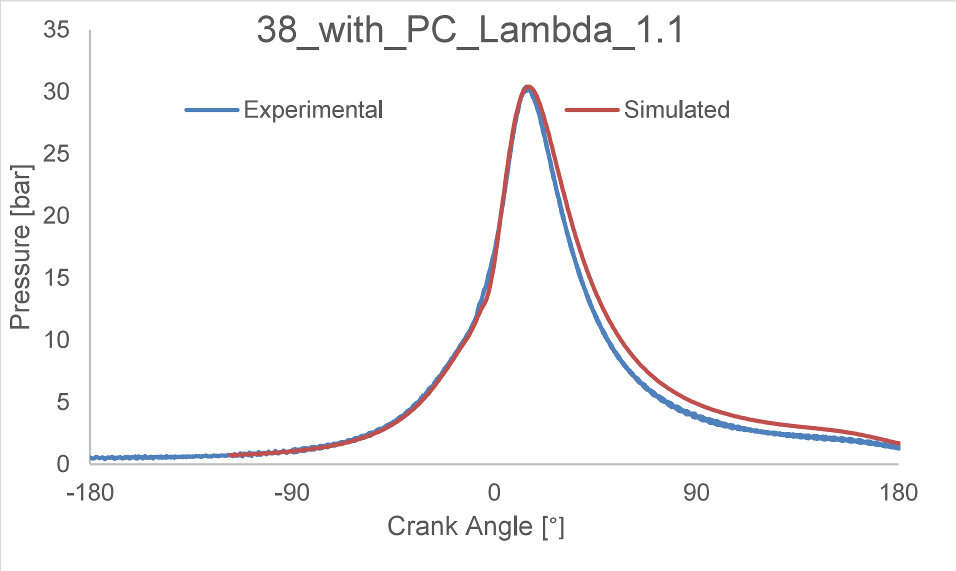

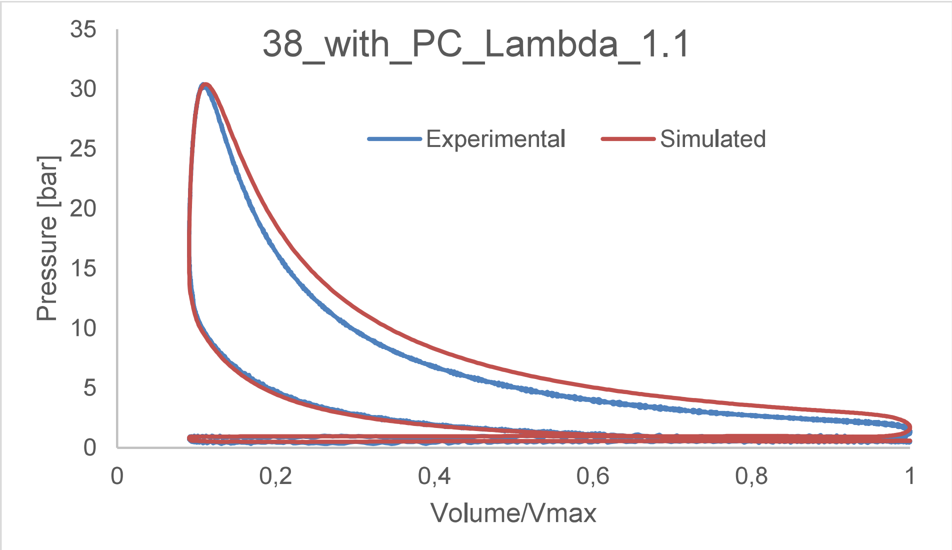

Simulated					
Power [kW]	Torque [N.m]	BSFC [g/kW.h]	Fuel Flow [kg/h]	Air Flow [kg/h]	IMEP [bar]
15,18	57,97	283	4,29	62,04	5,73

Experimental					
Power [kW]	Torque [N.m]	BSFC [g/kW.h]	Fuel Flow [kg/h]	Air Flow [kg/h]	IMEP [bar]
15,57	59,47	289	4,107	59,9	5,65

Error					
Power [kW]	Torque [N.m]	BSFC [g/kW.h]	Fuel Flow [kg/h]	Air Flow [kg/h]	IMEP [bar]
-2,50%	-2,52%	-2,08%	4,46%	3,57%	1,42%

38 – With prechamber and lambda 1,20

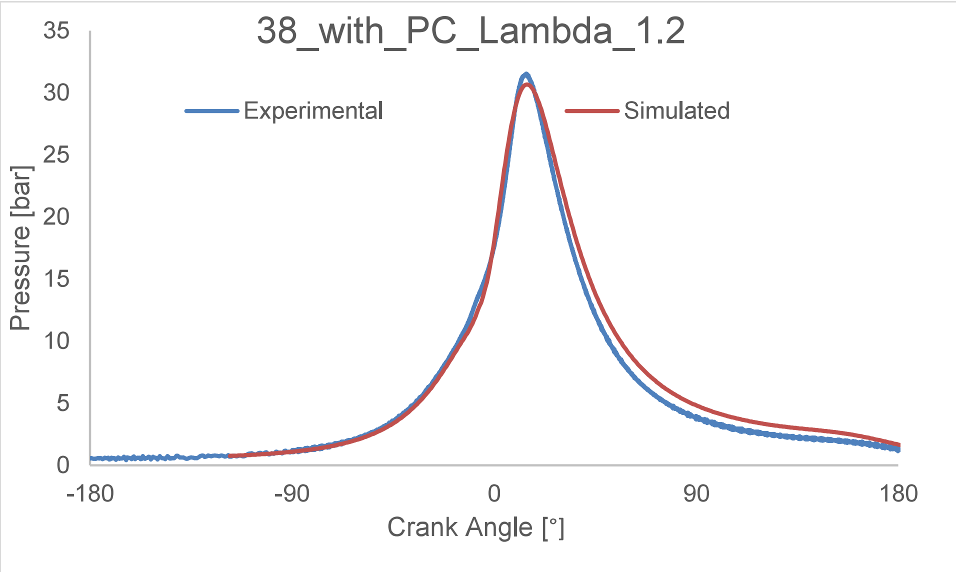

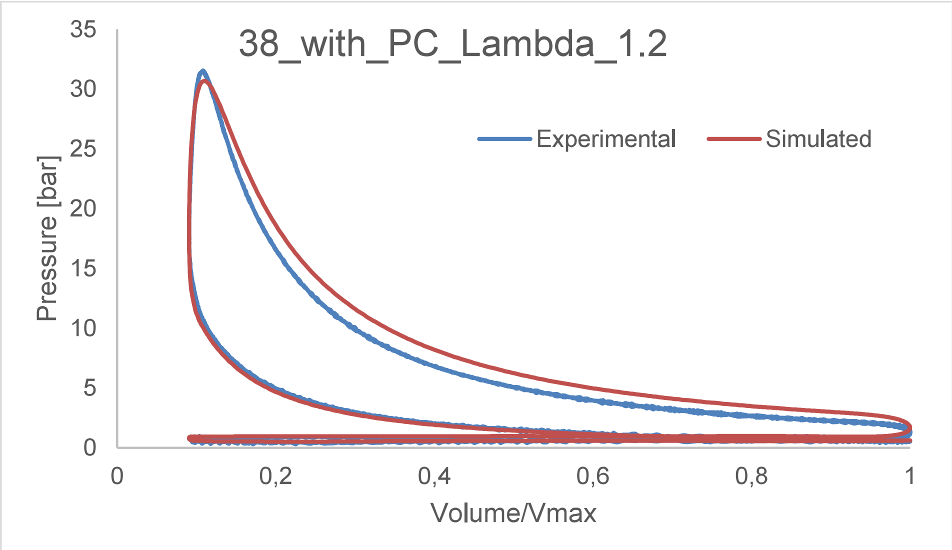

Simulated					
Power [kW]	Torque [N.m]	BSFC [g/kW.h]	Fuel Flow [kg/h]	Air Flow [kg/h]	IMEP [bar]
14,8	56,56	280	4,14	64,89	5,62

Experimental					
Power [kW]	Torque [N.m]	BSFC [g/kW.h]	Fuel Flow [kg/h]	Air Flow [kg/h]	IMEP [bar]
15,52	59,27	279	3,957	62,9	5,79

Error					
Power [kW]	Torque [N.m]	BSFC [g/kW.h]	Fuel Flow [kg/h]	Air Flow [kg/h]	IMEP [bar]
-4,64%	-4,57%	0,36%	4,62%	3,16%	-2,94%

38 – With prechamber and lambda 1,30

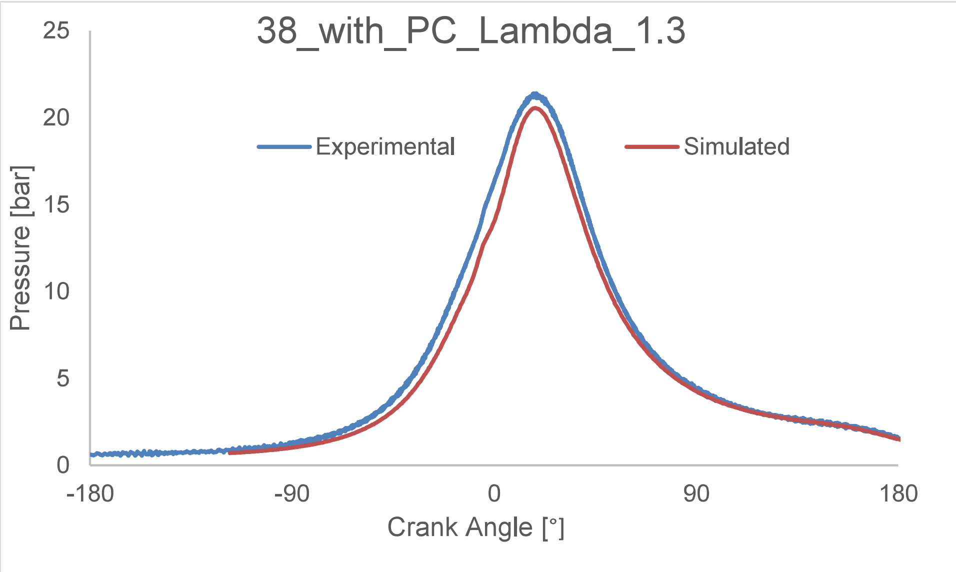

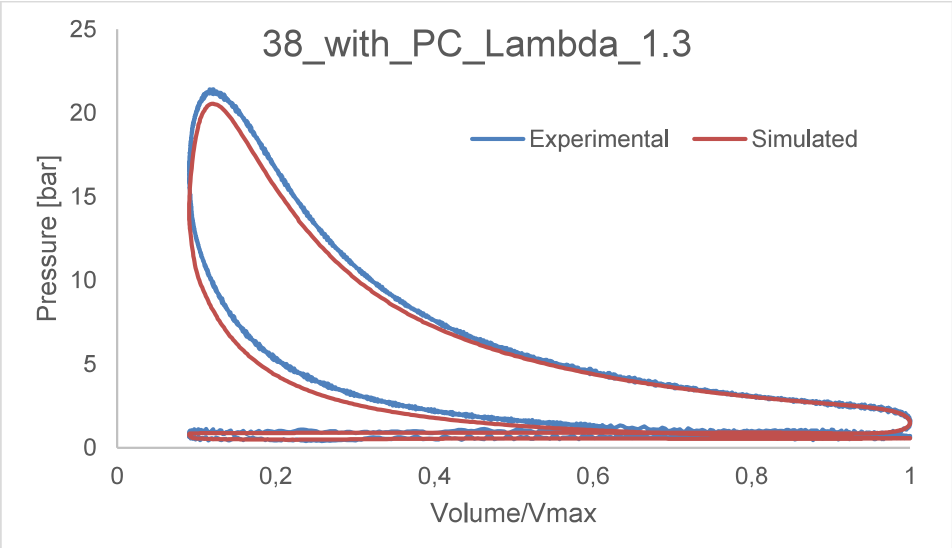

Simulated					
Power [kW]	Torque [N.m]	BSFC [g/kW.h]	Fuel Flow [kg/h]	Air Flow [kg/h]	IMEP [bar]
14,74	56,35	286,16	4,12	70,87	5,34

Experimental					
Power [kW]	Torque [N.m]	BSFC [g/kW.h]	Fuel Flow [kg/h]	Air Flow [kg/h]	IMEP [bar]
15,51	59,23	276	3,927	67,6	5,54

Error					
Power [kW]	Torque [N.m]	BSFC [g/kW.h]	Fuel Flow [kg/h]	Air Flow [kg/h]	IMEP [bar]
-4,96%	-4,86%	3,68%	4,91%	4,84%	-3,61%

47 – Baseline with lambda 1,00

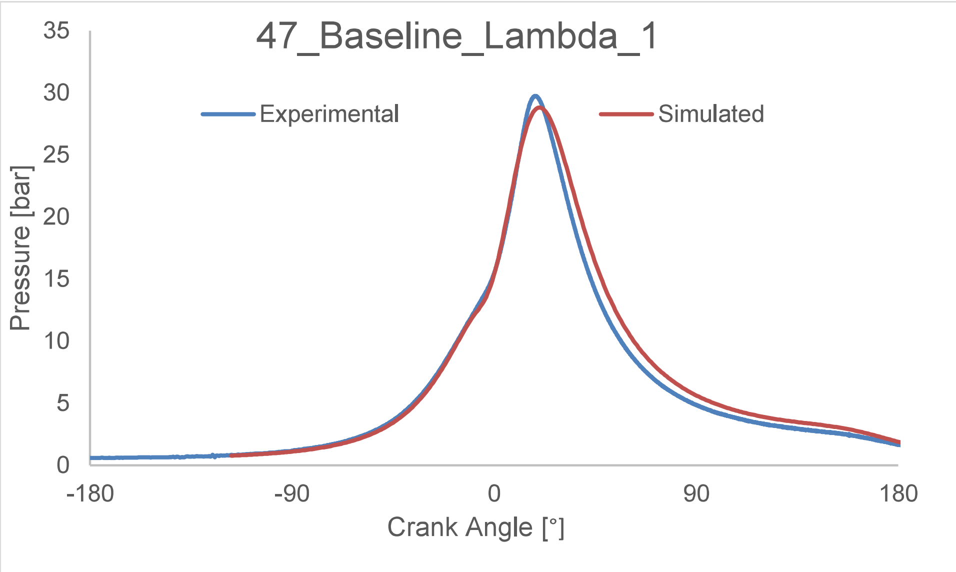

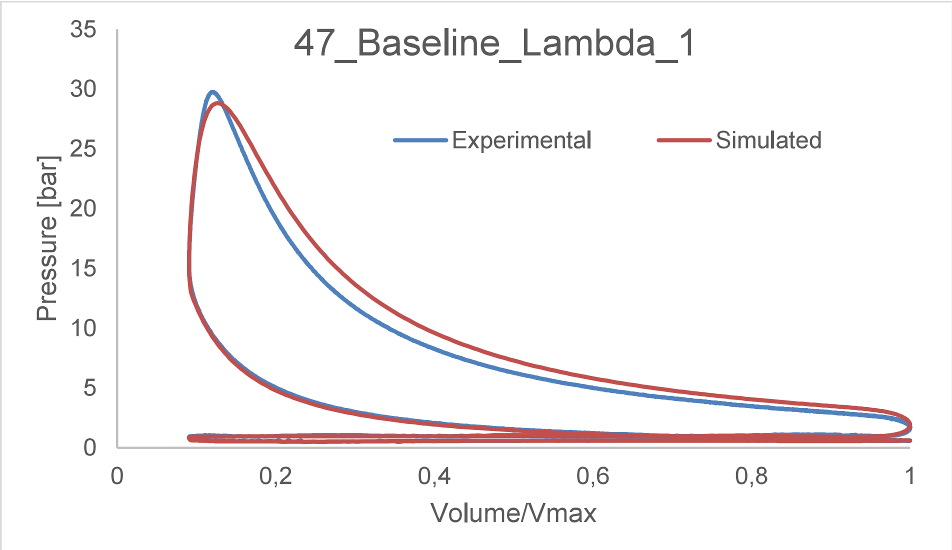

Simulated					
Power [kW]	Torque [N.m]	BSFC [g/kW.h]	Fuel Flow [kg/h]	Air Flow [kg/h]	IMEP [bar]
18,58	70,71	274,87	5,08	66,65	6,47

Experimental					
Power [kW]	Torque [N.m]	BSFC [g/kW.h]	Fuel Flow [kg/h]	Air Flow [kg/h]	IMEP [bar]
19,47	74,35	262	4,852	64,3	6,17

Error					
Power [kW]	Torque [N.m]	BSFC [g/kW.h]	Fuel Flow [kg/h]	Air Flow [kg/h]	IMEP [bar]
-4,57%	-4,90%	4,91%	4,70%	3,65%	4,86%

ANNEX 2 – RESULT FIGURES AND TREND MAPS

This annex presents the results of power, torque, air flow and fuel flow, comparing the simulation results with the experimental results used to calibrate the models. Such experimental results were produced by Rodrigues Filho, 2014, and used with permission.

This annex also presents the torque and power results for the predictive models, as well as their respective trend maps as a function of hole diameter and pre-chamber volume.

The next figure shows the comparison of simulated fuel flow values with experimental data for all 11 simulated cases.

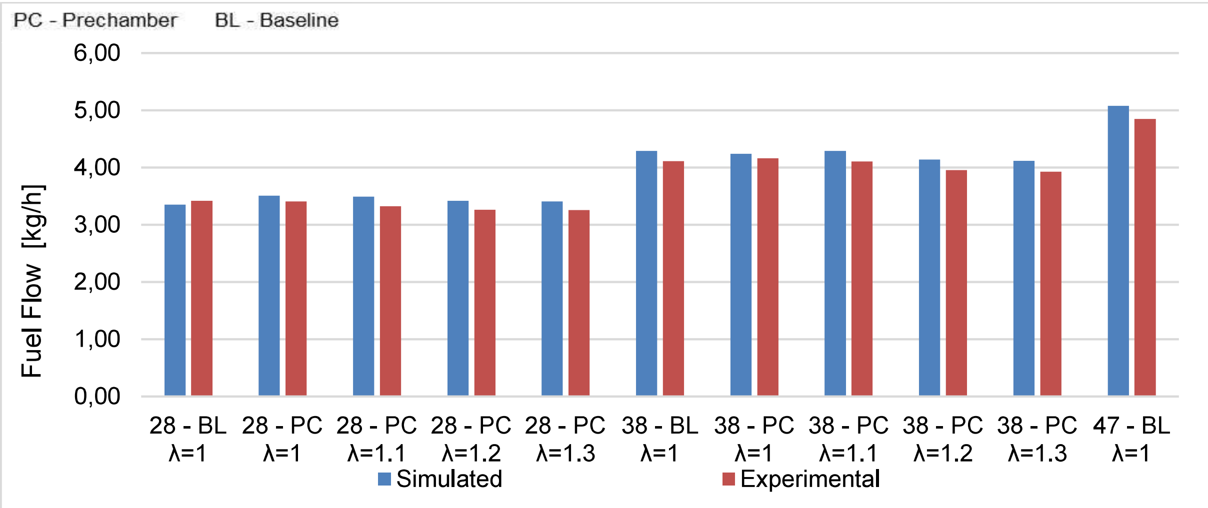

Comparison of simulated fuel flow values with experimental data at 2500 rpm. Source: Author

The next figure shows the percentage error values between the simulated and experimental fuel flow values results for all 11 simulated cases.

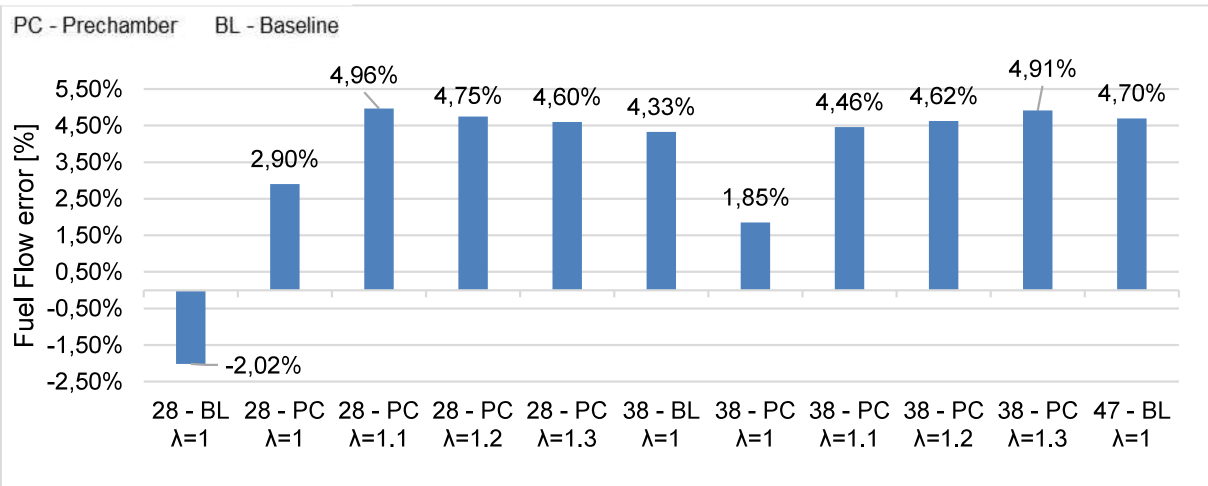

Percentage error between the simulated and experimental fuel flow values at 2500 rpm. Source: Author

The next figure shows the comparison of simulated air flow values with experimental data for all 11 simulated cases.

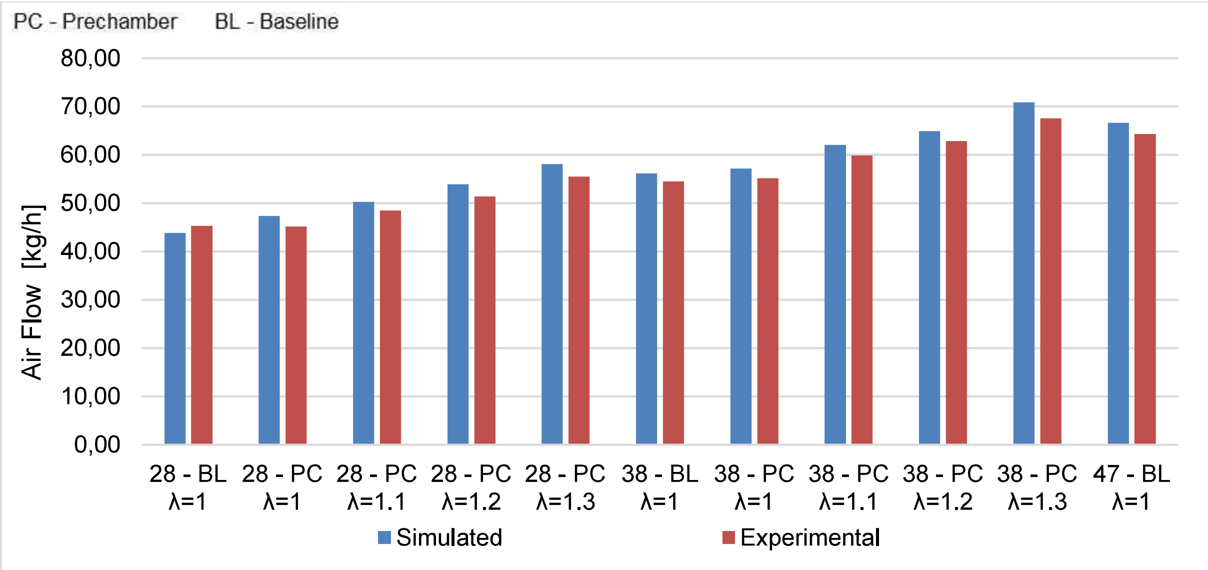

Comparison of simulated air flow values with experimental data at 2500 rpm. Source: Author

The next figure shows the percentage error values between the simulated and experimental air flow values results for all 11 simulated cases.

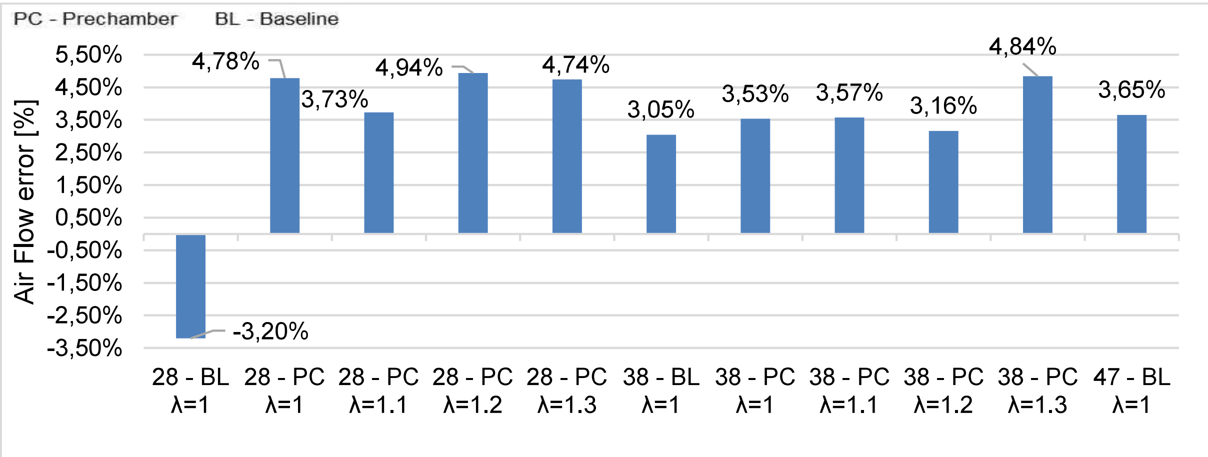

Percentage error between the simulated and experimental air flow values at 2500 rpm.

Source: Author

The next figure shows the comparison of simulated power values with experimental data for all 11 simulated cases.

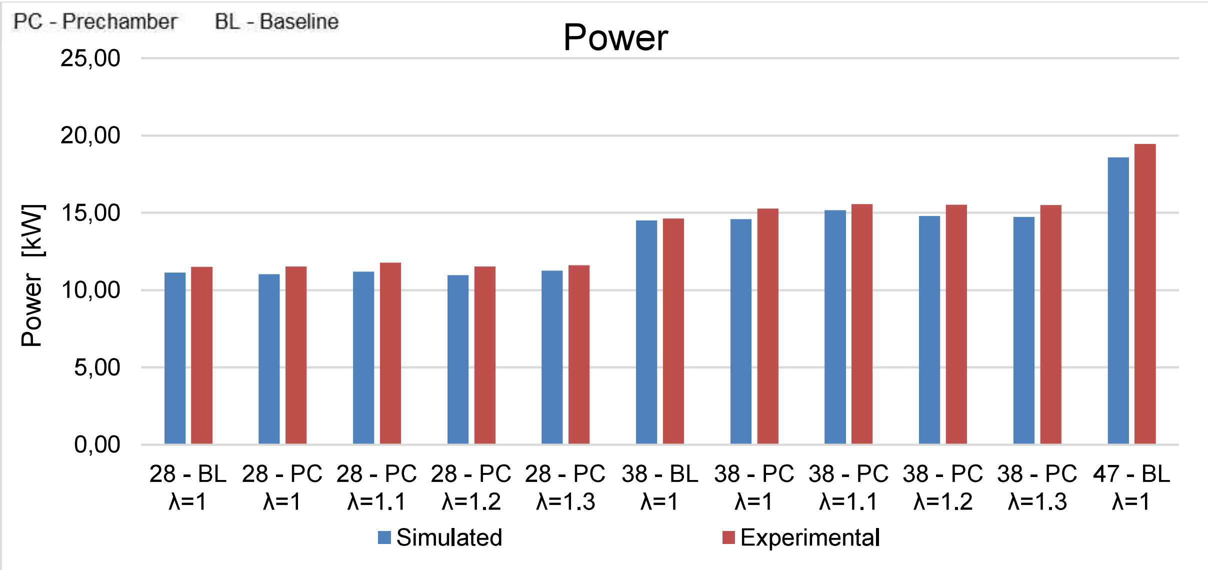

Comparison of simulated power values with experimental data at 2500 rpm. Source: Author

The next figure shows the percentage error values between the simulated and experimental power values results for all 11 simulated cases.

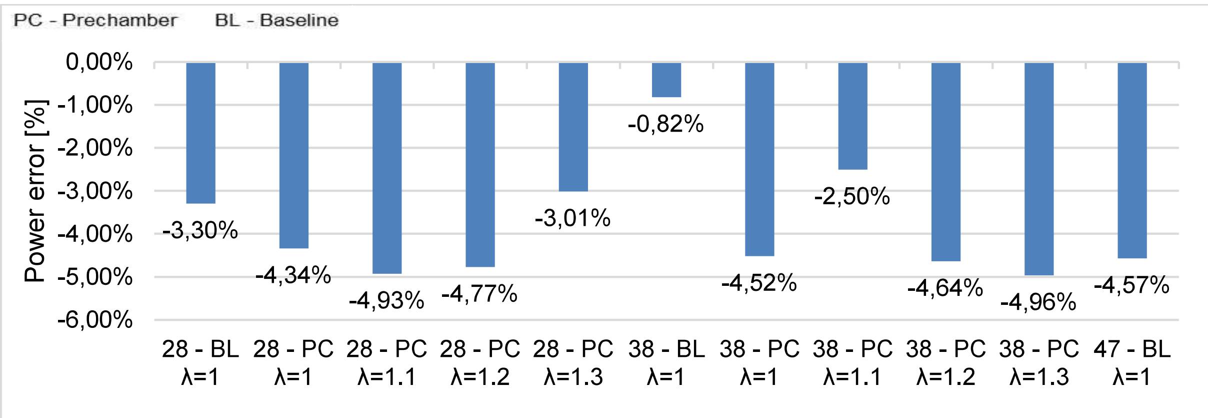

Percentage error between the simulated and experimental power values at 2500 rpm. Source: Author

The next figure shows the comparison of simulated torque values with experimental data for all 11 simulated cases.

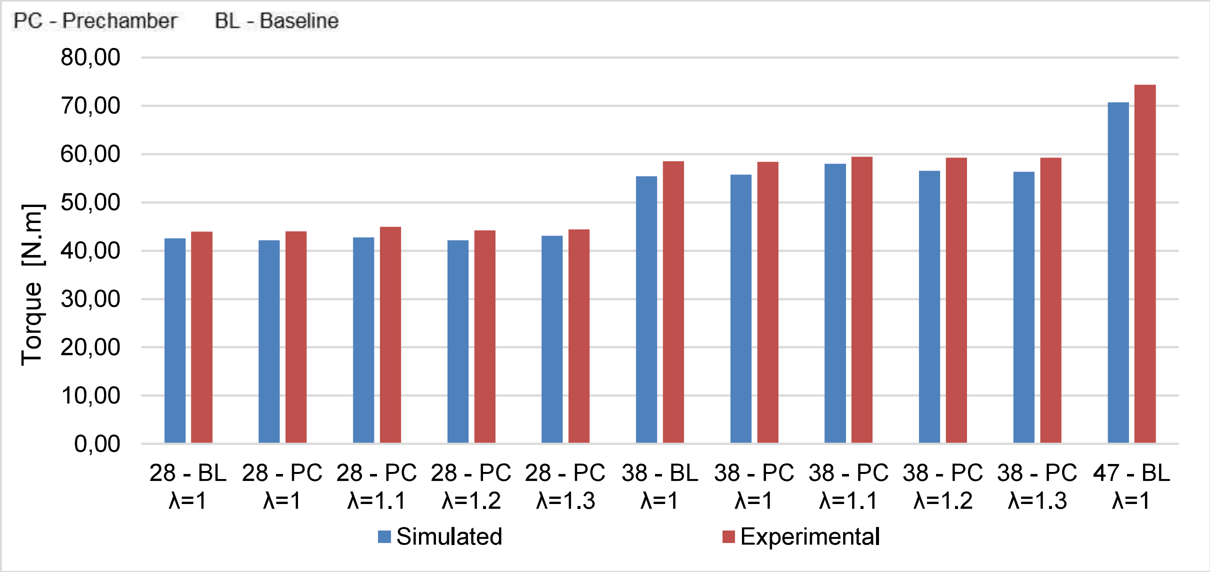

Comparison of simulated power values with experimental data at 2500 rpm. Source: Author

The next figure shows the percentage error values between the simulated and experimental power values results for all 11 simulated cases.

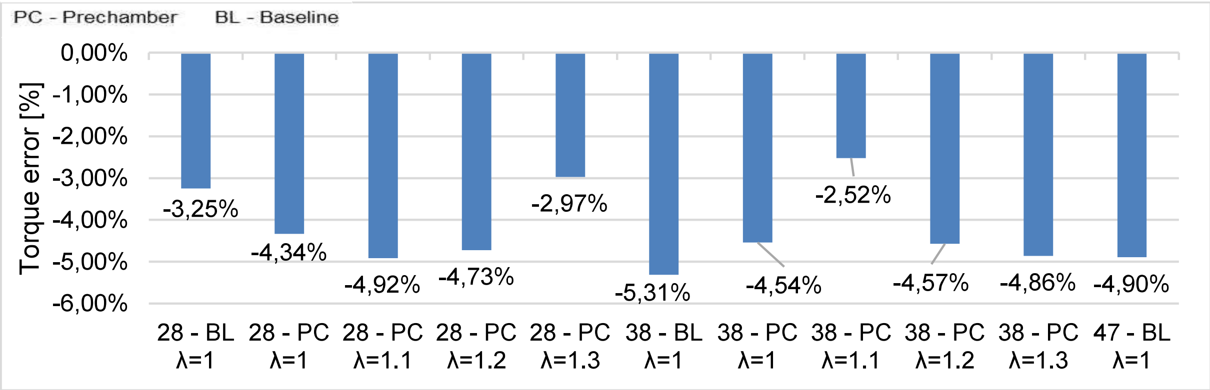

Percentage error between the simulated and experimental torque values at 2500 rpm. Source: Author

All results for predictive model 28 with prechamber and lambda 1.10 at 2500 rpm.

Source: Author

IMEP [bar]						
Volume		Diameter				
Volume [cm³]	V_pc/V_cc	4 mm	5 mm	6 mm	7 mm	8 mm
2593	6,50%	4,25	4,23	4,20	4,18	4,15
2793	7,00%	4,25	4,24	4,21	4,18	4,15
2993	7,50%	4,25	4,24	4,21	4,19	4,16
3193	8,00%	4,25	4,24	4,22	4,19	4,16
3393	8,50%	4,12	4,24	4,22	4,20	4,17
Torque [N.m]						
Volume		Diameter				
Volume [cm³]	V_pc/V_cc	4 mm	5 mm	6 mm	7 mm	8 mm
2593	6,50%	39,26	39,09	38,75	38,46	38,15
2793	7,00%	39,26	39,14	38,82	38,52	38,18
2993	7,50%	39,23	39,17	38,89	38,58	38,23
3193	8,00%	39,19	39,18	38,93	38,63	38,29
3393	8,50%	37,65	39,17	38,97	38,68	38,32
BSFC [g/kWh]						
Volume		Diameter				
Volume [cm³]	V_pc/V_cc	4 mm	5 mm	6 mm	7 mm	8 mm
2593	6,50%	313,02	314,28	317,01	319,37	321,86
2793	7,00%	313,03	313,89	316,40	318,85	321,59
2993	7,50%	313,31	313,64	315,87	318,35	321,17
3193	8,00%	313,58	313,56	315,49	317,88	320,72
3393	8,50%	326,21	313,64	315,20	317,52	320,38
Power [kW]						
Volume		Diameter				
Volume [cm³]	V_pc/V_cc	4 mm	5 mm	6 mm	7 mm	8 mm
2593	6,50%	10,28	10,23	10,14	10,07	9,99
2793	7,00%	10,28	10,25	10,16	10,08	10,00
2993	7,50%	10,27	10,26	10,18	10,10	10,01
3193	8,00%	10,26	10,26	10,19	10,11	10,02
3393	8,50%	9,86	10,26	10,20	10,13	10,03

The next figure shows the power results for each of the 25 combinations simulated using the predictive model.

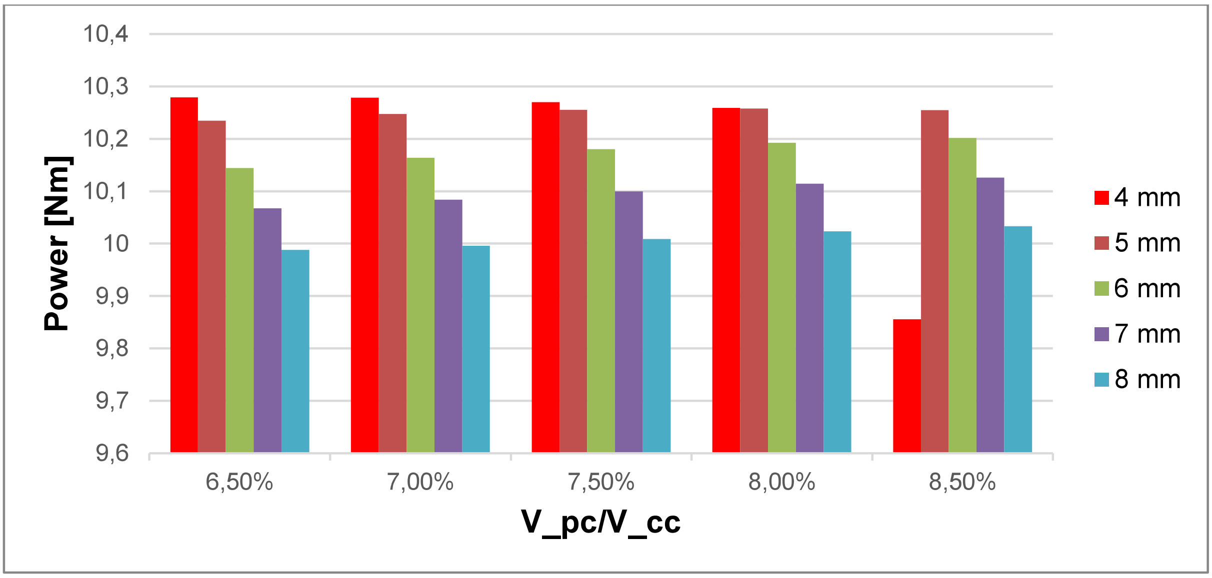

Power results as a function on diameter and volume for predictive model 28 with prechamber and lambda 1.10 at 2500 rpm. Source: Author

Based on previous figure, the next results figure was created, which shows a trend map of power behavior as a function of variations in hole diameter and pre-chamber volume.

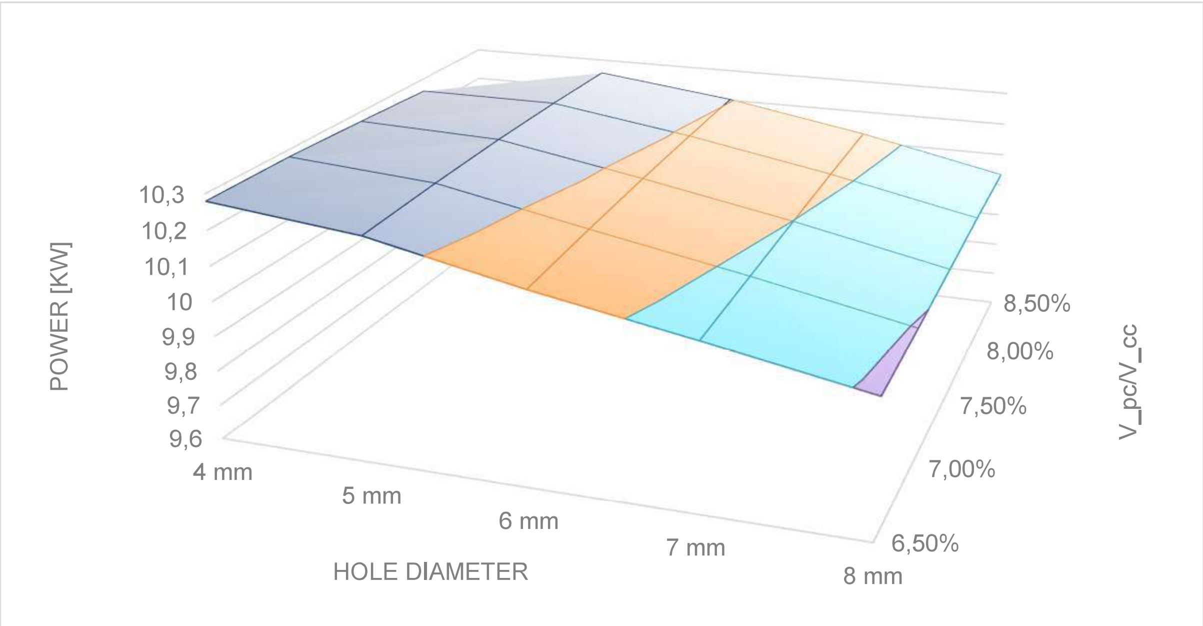

Trend map of power behavior as a function of hole diameter and pre-chamber volume for predictive model 28 with prechamber and lambda 1.10 at 2500 rpm. Source: Author

The next figure shows the torque results for each of the 25 combinations simulated using the predictive model.

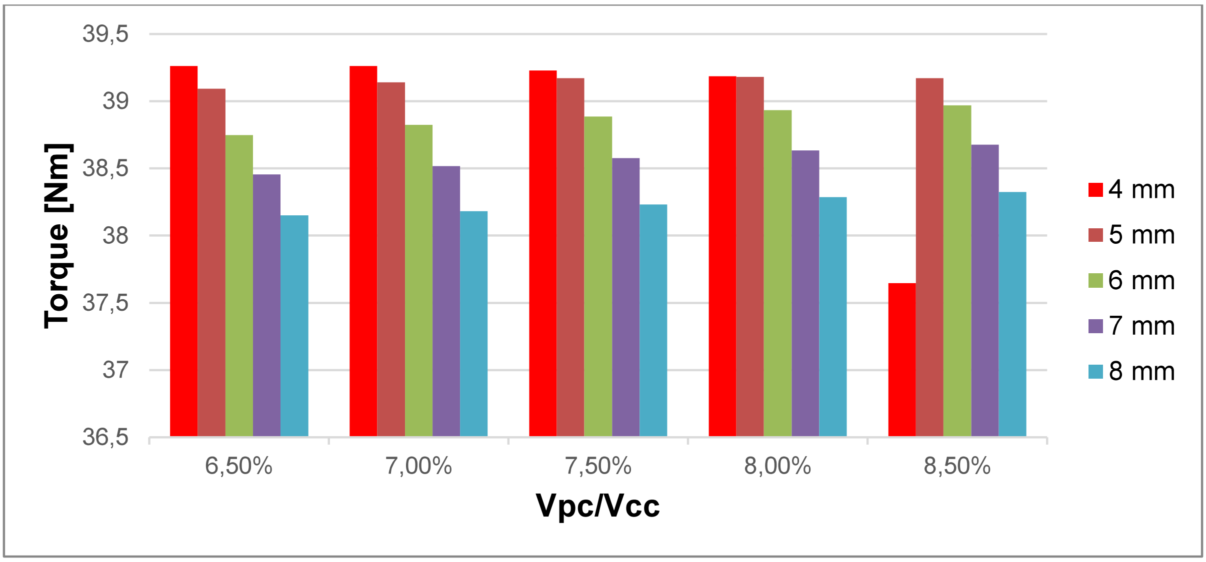

Torque results as a function on diameter and volume for predictive model 28 with prechamber and lambda 1.10 at 2500 rpm. Source: Author

Based on previous figure, the next results figure was created, which shows a trend map of torque behavior as a function of variations in hole diameter and pre-chamber volume.

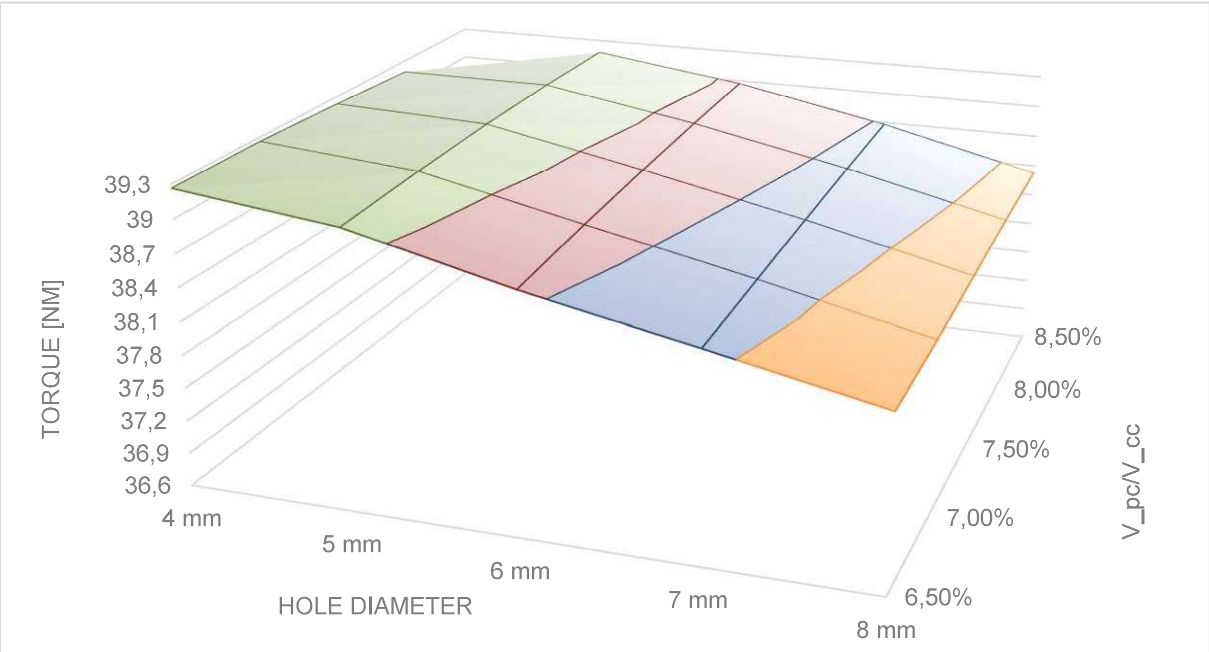

Trend map of torque behavior as a function of hole diameter and pre-chamber volume for predictive model 28 with prechamber and lambda 1.10 at 2500 rpm. Source: Author

All results for predictive model 38 with prechamber and lambda 1.10 at 2500 rpm.

Source: Author

IMEP [bar]						
Volume		Diameter				
Volume [cm³]	V_pc/V_cc	4 mm	5 mm	6 mm	7 mm	8 mm
2593	6,50%	5,62	5,60	5,56	5,52	5,51
2793	7,00%	5,62	5,60	5,57	5,53	5,51
2993	7,50%	5,62	5,61	5,58	5,54	5,51
3193	8,00%	5,46	5,61	5,58	5,54	5,52
3393	8,50%	5,45	5,61	5,59	5,55	5,52
Torque [Nm]						
Volume		Diameter				
Volume [cm³]	V_pc/V_cc	4 mm	5 mm	6 mm	7 mm	8 mm
2593	6,50%	56,28	56,11	55,66	55,25	55,03
2793	7,00%	56,26	56,16	55,76	55,32	55,08
2993	7,50%	56,22	56,18	55,84	55,39	55,12
3193	8,00%	54,21	56,18	55,91	55,46	55,15
3393	8,50%	54,11	56,16	55,96	55,53	55,17
BSFC [g/kWh]						
Volume		Diameter				
Volume [cm³]	V_pc/V_cc	4 mm	5 mm	6 mm	7 mm	8 mm
2593	6,50%	278,12	278,85	281,02	283,07	284,11
2793	7,00%	278,18	278,60	280,48	282,70	283,87
2993	7,50%	278,36	278,47	280,08	282,33	283,65
3193	8,00%	288,59	278,45	279,75	281,95	283,49
3393	8,50%	289,10	278,54	279,49	281,59	283,36
Power [kW]						
Volume		Diameter				
2593	V_pc/V_cc	4 mm	5 mm	6 mm	7 mm	8 mm
2793	6,50%	14,73	14,69	14,57	14,46	14,41
2993	7,00%	14,73	14,70	14,60	14,48	14,42
3193	7,50%	14,72	14,71	14,62	14,50	14,43
3393	8,00%	14,19	14,71	14,64	14,52	14,44
3393	8,50%	14,17	14,70	14,65	14,54	14,44

The next figure shows the power results for each of the 25 combinations simulated using the predictive model.

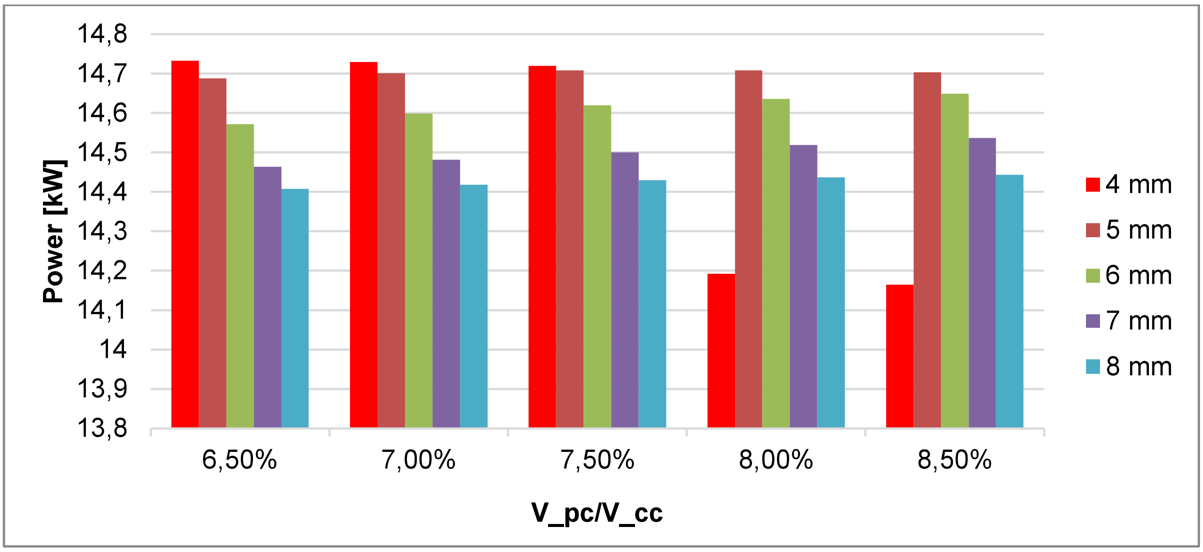

Power results as a function on diameter and volume for predictive model 38 with prechamber and lambda 1.10 at 2500 rpm. Source: Author

Based on previous figure, the next results figure was created, which shows a trend map of power behavior as a function of variations in hole diameter and pre-chamber volume.

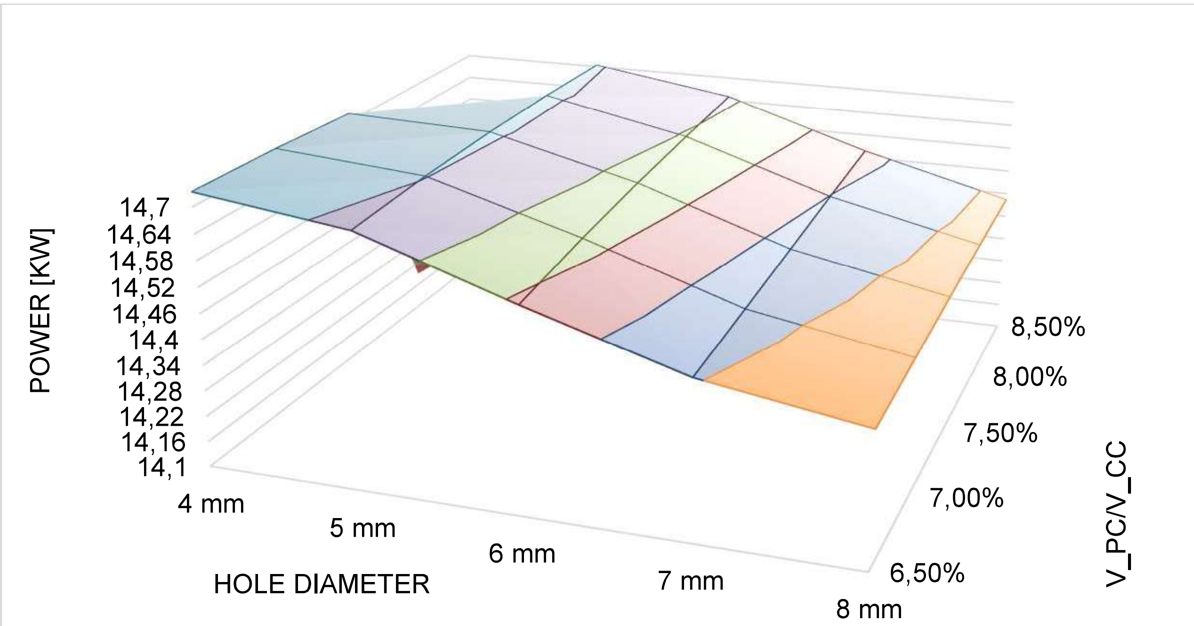

Trend map of power behavior as a function of hole diameter and pre-chamber volume for predictive model 38 with prechamber and lambda 1.10 at 2500 rpm. Source: Author

The next figure shows the torque results for each of the 25 combinations simulated using the predictive model.

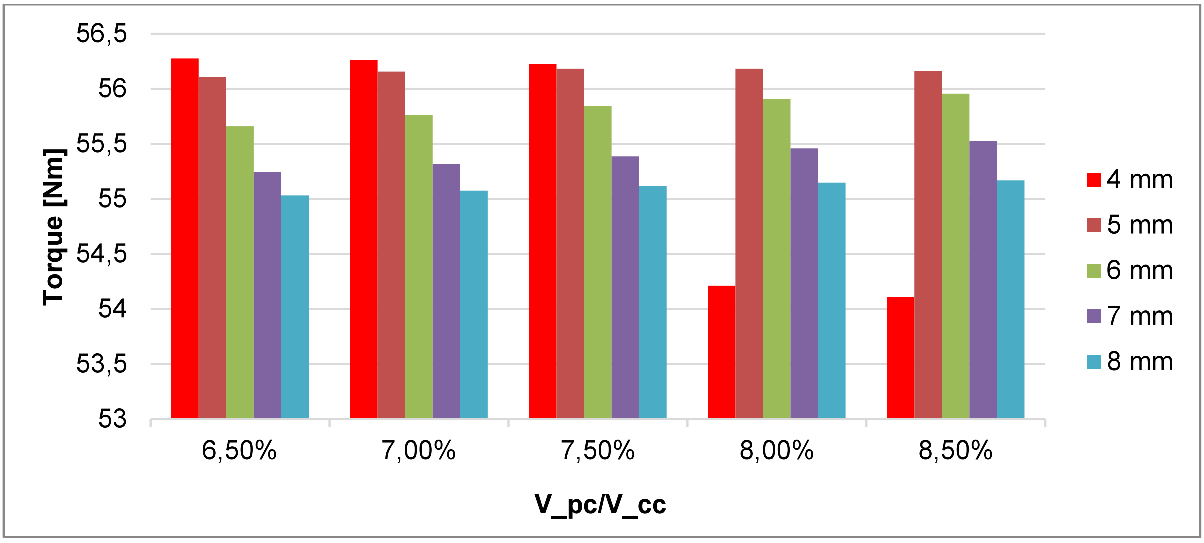

Torque results as a function on diameter and volume for predictive model 38 with prechamber and lambda 1.10 at 2500 rpm. Source: Author

Based on previous figure, the next results figure was created, which shows a trend map of torque behavior as a function of variations in hole diameter and pre-chamber volume.

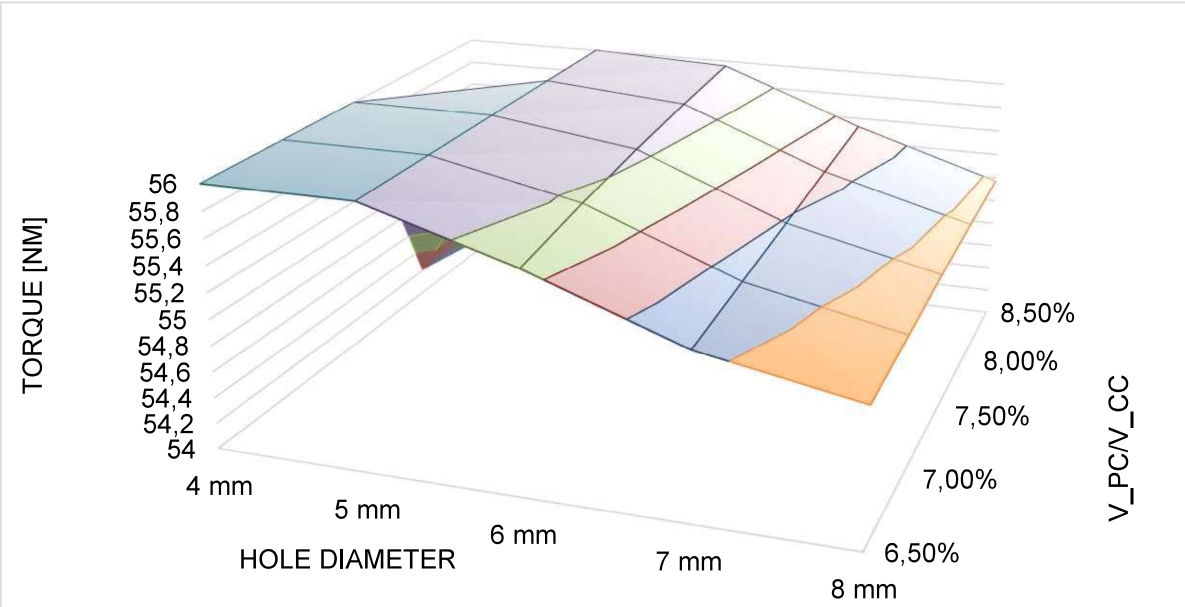

Trend map of torque behavior as a function of hole diameter and pre-chamber volume for predictive model 38 with prechamber and lambda 1.10 at 2500 rpm. Source: Author